Design of DC-DC Converters using Tunable Piezoelectric Transformers

Mudit Khanna

Thesis submitted to the faculty of the Virginia Polytechnic Institute and State University in partial fulfillment of the requirements for the degree of

Master of Science
In
Electrical Engineering

Rolando Burgos
Khai D.T. Ngo
Shashank Priya

May 9th, 2017
Blacksburg, Virginia

Keywords: Piezoelectric Transformers, Tunable Piezoelectric Transformers, DC-DC Converters, Resonant Converters

Design of DC-DC Converters using Tunable Piezoelectric Transformers

Mudit Khanna

ABSTRACT
(Academic)

This thesis introduces the ‘tunable’ piezoelectric transformers (TPT) which provide an extra control terminal, used in this case, to regulate the output voltage. A detailed mathematical analysis is done on the electrical equivalent circuit of the TPT to understand the effect of control terminal loading on the circuit performance. Based on this analysis, a variable capacitor connected across the control terminal is proposed to regulate the output voltage for line and load variations is suggested. The concept of ‘tunability’ in a TPT is introduced and mathematical conditions are derived to achieve the required ‘tunability’. This analysis can help a TPT designer to design the TPT for a specific application and predict the load and line regulations limits for a given design.

A circuit implementation of the variable capacitor, intended for control, is presented. With the proposed control circuit design, the effective value of a fixe capacitor can be controlled by controlling the duty cycle of a switch. Hence, this enables pulse width modulated (PWM) control for the TPT based converter operating at a constant frequency. Fixed frequency operation enables a high efficiency operation of TPT near its resonant frequency and the complete secondary control requires no isolation in the voltage feedback and control circuit. This prevents any ‘cross-talk’ between primary and secondary terminals and reduces the component count. The design of series input inductor for achieving zero voltage switching (ZVS) in the inverter switches for the new control is also discussed.

Experimental results for two different TPT designs are presented. Their differences in structure and its effect on the circuit performance has been discussed to support the mathematical analysis.

Design of DC-DC Converters using Tunable Piezoelectric Transformers

Mudit Khanna

ABSTRACT

(General audience)

Piezoelectric transformers (PTs) are electromechanical devices which can transfer electrical energy by using acoustic coupling. Piezoelectricity is a phenomenon where certain crystalline materials develop electric potential across their surface when subjected to a mechanical stress (transducer). This can also occur in inverse i.e. an electric field inside such a material can produce a mechanical strain inside them (actuator). These direct and indirect piezoelectric effects are used to make a PT which has a transducer and an actuator coupled together to transfer electrical energy.

Power electronics is a rapidly growing field which relies heavily on conventional electromagnetics to store energy (inductors), step-down and step-up voltage (magnetic transformers) and to act as band pass circuits (resonant converter topologies) etc. to enable power conversion. Piezoelectric transformers behave as band pass circuits as such they resonate at a certain frequency and hence allow only a narrow range of frequencies to pass through them. Owing to their light weight, high power density and automated manufacturing capability, they are seen as a potential replacement for electromagnetic transformers in power converters.

This thesis introduces a new structure of PTs, namely the tunable piezoelectric transformers, which allow for better control techniques as compared to standard PTs. Using the extra ‘control’ terminal provided in such a structure the design of a DC-DC converter using TPT is discussed in detail. Mathematical analysis to support the design is presented and the two hardware prototypes, with distinctive designs, are developed to verify the results.

Acknowledgement

This thesis was done as a part of a research work supported by Defense Advanced Research Projects Agency (DARPA) under the grant number 11874492. I would like to thank DARPA and all the supporting organizations part of this project for the opportunity provided to me to conduct research for this thesis.

I would like to take this opportunity to thank everyone who has helped during my time at Virginia Tech.

I would like to start by thanking my advisors Dr. Rolando Burgos, Dr. Khai D.T. Ngo and Dr. Shashank Priya for their advice and support during this work. Working under their guidance, I could pursue my work in right direction and improve my technical skills. I would also like to thank professors Dr. Qiang Li and Dr. Fred C. Lee from whom I have learnt a lot through their courses.

It has been an immense pleasure to work with all the CPES staff and without whose support it would have been very difficult to complete this work. I thank everyone for all his/her help and support. I would also like to thank all my friends and colleagues in CPES and Virginia Tech. I have received utmost help and support from them in my thick and thin. Along with deep knowledge in power electronics, I will be taking back a lot of fond memories of this place.

Special thanks to Mr. Alfredo Vazquez Carazo from Micromechatronics, Inc. for his endless help and guidance. The hour-long calls and valuable discussions we had on piezoelectric transformers have helped me immensely in my research.

Finally, I would like to thank my parents, my family and my friends in India for their constant encouragement and belief in me. This would not have been possible without their love and support.

Table of Contents

List of Figures

List of Tables

Chapter 1

Introduction

1.1 Background

Power electronics has seen rapid developments in the past two decades. The need for more efficient and compact technologies has grown with the increase in energy demand. Magnetics is an essential cog in the wheel of power electronics and still, are one of the bulkiest components in most of the power electronic devices. Therefore, extensive research is ongoing to miniaturize magnetics and reduces losses in order to increase the efficiency of the system.

In the early 1950s, Charles A Rosen came up with a Piezoelectric Transformer (PT) design [1]. Named after him, 'Rosen-Type' PT was used for their capability to produce DC-DC converters with high output voltage. In the past 50 years, PT technology has grown and various other types of PT structures have been developed for different applications. Piezoelectric transformers are now seen as a potential replacement for traditional magnetic transformers. In comparison with magnetic transformers, PTs have the potential to be lighter, have higher power density, have proven to be suitable for automated manufacturing, as well as work in the presence of the high magnetic fields [2],[3]. This makes them very useful for environments with high ambient magnetic fields such as MRI machines where the magnetic field presence can affect the working of a normal magnetic transformer [4].

Even with promising characteristics, piezoelectric transformers have not been able to enjoy commercial success. High voltage, low power PTs for use in electronic lamp ballasts have been the only noticeable success story for PT based converters [5]. Some of the issues with the technology including power limitation, efficiency, and efficient driving technologies have impeded its growth [6]. With respect to the driving technology, limited range of frequency operation in PTs for enabling ZVS in the inverter circuit and achieving optimum operation of PT have been an issue. Recently, inductor-less driving

scheme with ZVS in the inverter switches have been extensively researched [7],[9],[8],[10],[11].

Radial Mode PTs were developed and patented by Face Electronics in 1996 [12],[13]. This technology promised high power density, and high efficiency compared to its counterparts. This structure is also suitable for low voltage high current step – down applications. Thus, it has found applications in electronics lamp ballasts and AC/DC adapter [14],[15],[16],[17].

Based on the radial mode design, a new structure has been proposed recently, namely the tunable piezoelectric transformers (TPTs). In the proposed TPT structure, a new 'control' section is added to a radial mode piezoelectric transformer, which makes the tunable PT a three-terminal device with input, output and control. Prior to this, a similar structure has been proposed but the 'control' terminal in that PT was used for sensing and control [18].

1.2 Motivation

The motivation behind this work is to explore the capabilities of a tunable piezoelectric transformer. With an additional control section available, a whole set of new possibilities open up in terms of design and its application. This thesis explores the use of tunable piezoelectric transformers in DC-DC converter applications.

Due to the band pass nature of the PTs with high quality factor, PTs have been used in resonant converter topologies to enable power conversion. The electrical equivalent circuit of a PT resembles a LCC tank circuit with an extra input capacitor. Hence, the gain characteristics of the PT are highly dependent on load and frequency. To regulate the output voltage a traditional pulse frequency control has been adopted in most control schemes [19]. However, PTs have been found to be most efficient when operated near its fundamental mode of resonance [20]. Hence, it is desirable to run the PT in a narrow band of frequencies. This has led to some challenges in the design of load and line regulated converters [6],[21]. The proposed control scheme with TPTs can alleviate some of these issues and gives a PT based DC-DC converter some exciting characteristics which have been explored in this work.

1.3 Scope and Objective

This research focuses mostly on the implementation of a tunable piezoelectric transformer in a DC-DC converter based application. With the addition of a control section, the resonant frequency of the TPT can be altered by changing the loading conditions at the control terminal. None of the work done in the past has used this concept to control DC-DC converter and that is one of the objectives of this thesis. More focus has been given to a practical implementation of such a device and to demonstrate a working prototype based on this concept. Device modeling and 'lumped' electrical equivalent circuit derivation is not considered within the scope of this work. However, to verify the efficacy of the given electrical model, certain tests have been conducted and are presented in the body of work. Beyond any such verification, the authors have considered the provided electrical equivalent circuit for each device to be accurate and has used the circuit analysis as a tool to analyze the properties of a TPT.

The following bullet points list out some of the main objectives of this research.

- To understand the operation of the new tunable piezoelectric transformers.
- To review the existing literature on PTs, understand their drawbacks, and propose improvements with the new structure.
- To propose methods which use the control section of the TPT as a means to regulate the output voltage.
- To propose a control scheme, which enable line and load regulation of a DC-DC converter based on tunable piezoelectric transformer.
- To implement a closed loop controlled TPT based DC-DC converter on hardware and build a working prototype.

1.4 Dissertation Outline and Major Results

This thesis is composed of six chapters and references. Summary of each chapter and the major results obtained from this work are briefly discussed below.

Chapter 2 reviews the concept of piezoelectric transformers. Basic principle of operation and some of the important characteristics of a standard PT are discussed. The chapter also reviews some of the significant work done in this field to provide a foundation for the operation of tunable piezoelectric transformers.

Chapter 3 introduces the concept of tunable piezoelectric transformers. The difference in the physical structure of a TPT from a PT is discussed briefly without going into the details of a TPT design. An exhaustive analysis of the electrical equivalent circuit of a TPT has been done to understand its behavior in the circuit. The chapter also proposes a way to regulate the TPT based DC-DC converter using the control terminal. This led to the introduction of the concept of 'Tunability' and is discussed in detail.

Chapter 4 addresses the design of DC-DC converters using the analysis done on TPTs. Achieving ZVS in the inverter switches is an essential feature of resonant converters which gives them high efficiency. The design concept behind achieving ZVS for tunable piezoelectric transformers based converters has been discussed. Circuit implementation of a variable capacitor at the control terminals to regulate the output voltage has been presented. Using this concept, a simple voltage mode PWM control of output voltage has been implemented on the converter.

Chapter 5 discusses two design examples of TPT based DC-DC converters. Design with two different structures of TPT has been discussed and the effect of the physical structure on the converter performance has been outlined. Major experimental results from the two designs have been presented.

Chapter 6 summarizes the major results of this work and proposes future work which can be done in this field.

Chapter 2

An Overview of Piezoelectric Transformers

2.1 Introduction

Piezoelectric transformers transfer electrical energy via acoustic coupling whereas magnetic transformers use magnetic coupling to transfer the electrical energy. The mechanical vibrations inside a PT are of the largest magnitude at the resonance point. Since, PTs are widely used for electrical energy transfer, an electrical circuit representation of their characteristics becomes very important.

The electromechanical nature of piezoelectric transformers has caused the development of both electrical and mechanical models for PTs. Derivation of electrical equivalent circuit model makes the design of circuits using PTs much simpler. The electrical equivalent circuit of a piezoelectric transformer represents a band pass tank circuit with a high-quality factor. An accurate model enables a circuit designer to predict the behavior of PTs and use precise design techniques to develop a product. Hence, a lot of work has been done to derive a good electrical model for PTs [7],[9],[22].

Based on the direction of vibration and electric field inside a PT actuator and transducer, PTs can be classified into various types such as longitudinal mode, thickness mode, Radial mode etc. [2]. A physics based equivalent circuit was developed using the wave equations for longitudinal mode PT [23],[24], radial mode PT [7],[25] and thickness mode PT [22]. These are 1-d models of the corresponding PT structure. Physics based models give a good understanding of the PT operation and help relate the physical parameters of a PT to the electrical circuit parameters. To improve the accuracy of these models, experimental measurement and parameter extraction techniques using impedance analyzers have been proposed [26]. Finite element analysis techniques have also been suggested which help in parameter extraction of PTs [27].

To capture the operation of PT at frequencies far away from the fundamental resonant frequency, researchers have proposed techniques which add LC branches to the existing model to include other points of resonance [7]. However, this is a complicated model and unless there is a need to operate a PT far away from its resonant frequency, such models provide little advantage over simpler 1-D models.

This chapter briefly reviews the basics of piezoelectricity, types of piezoelectric transformers and the basic equations governing the operation of PTs. Radial mode PTs, which are used to develop tunable piezoelectric transformers, are then discussed more elaborately. This chapter reviews some of the modeling work for radial mode PTs to help understand tunable piezoelectric transformers. The chapter also discusses the basic electrical properties of the PTs using electrical equivalent circuit analyses.

2.2 Piezoelectricity

Piezoelectricity is the ability of certain crystalline materials to generate an electrical charge when a mechanical stress is applied on them. This could also occur in reverse where a mechanical stress is created in a material when an electrical charge is applied on it. Thus, a mechanical vibration at a certain frequency can generate alternating voltage in the piezoelectric material. Both of the above mentioned, direct and inverse, piezoelectric effects are used to develop piezoelectric transformers [28].

Materials commonly used for PTs are PZT, combinations of lead zirconate/lead titanate etc. [28]. Due to non-uniformity in the crystal structure, such materials consists of domains which have a dipole moment in a specific direction. For an un-polarized piezoelectric material, the dipoles inside a material are random and hence the net dipole of the material is zero. These materials have to undergo a process called poling to impart piezoelectric characteristics to it. In poling, the material is subjected to a high electric filed, which aligns its internal electrical dipoles in the direction of the electric field. Most dipoles retain their alignment after the electric field is removed and the material has a unique direction of poling. This direction can, however, be disturbed if a field in the opposite direction is applied or the material is exposed to curie temperatures [28]. **Error!**

Reference source not found. shows the effect of poling on the internal electric dipoles of a piezoelectric material.

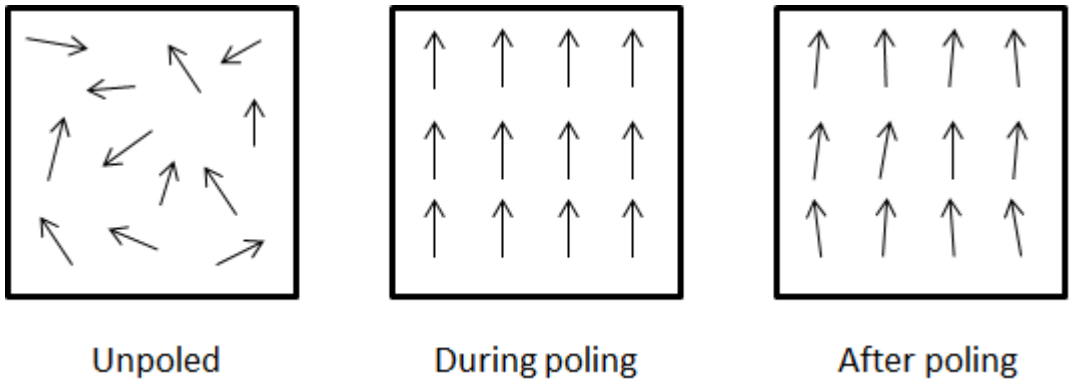

Fig. 2.1. The alignment of domains inside a piezoelectric material before poling, during poling and after poling. The domains retain their alignment after the poling process is over.

For a piezoelectric transformer, two such poled piezoelectric devices, which exhibit direct and inverse piezoelectric effect, are coupled mechanically together. In magnetic technologies, the electrical energy is transferred from the output to the input by inductive coupling. The input electrical energy is converted into magnetic field which gets coupled to the secondary side and gets transformed back to electrical energy. For Piezoelectric Transformers (PTs), the basic principle remains the same. However, the transfer of electrical energy occurs with the help of acoustic coupling. The piezoelectric actuator converts an input electrical wave into mechanical standing waves inside the piezoelectric material (inverse piezoelectric effect). These waves are coupled to a piezoelectric transducer, which converts the mechanical energy back to electric energy (direct piezoelectric effect).

2.3 Types of Piezoelectric Transformers

A piezoelectric transformer is a combination of a piezoelectric transducer and a piezoelectric actuator. Based on the direction of vibration and poling, four major structures of piezoelectric transformers have been developed.

- *Rosen Type PT*: A Rosen type PT, shown in Fig. 2.2, has a longitudinal type piezoelectric element and a transverse vibration type PT mechanically coupled together. An electrical AC signal input to the transverse piezoelectric element produces a mechanical vibration along the length of the ceramic element. This mechanical stress is coupled to the longitudinal mode type piezoelectric element, which in turn produces an output electrical signal. When the crystal vibrates near its mechanical resonance, vibrations of largest magnitude are produced [29]. The original structure proposed by Charles A. Rosen consisted of a single ceramic layer for the input and output sections [1]. This structure can produce high voltage gains. With further research on materials and manufacturing technologies, input and output sections made up of multiple layers co-fired together were developed to match the output impedance characteristics of the load [30].

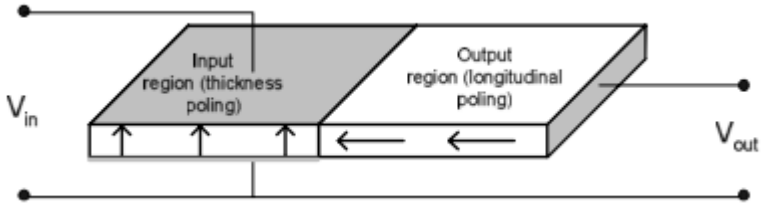

Fig. 2.2. A Rosen-Type PT structure showing the vibration modes in the input and output sections [6].

Due to high voltage gains and larger output impedance, this transformer structure was suitable for high output voltage, step-up applications [30],[31]. Owing to their light weight, high voltage gains compared to magnetic transformers and with the development in materials/driving technology, Rosen type PTs were employed in the cold cathode fluorescent lamps (CCFLs) for LCD backlighting applications [32],[33].

Owing to the structural design, Rosen type PTs were, however, unsuitable for higher power, step down applications. The power densities for a typical Rosen type PT is around 5-10 W/cm3 with power levels ranging from 5 - 8 W [2].

- *Radial PT*: Radial Type PTs, Trasoner® PTs, were first developed by Face electronics in 1996 [12],[13]. Shown in Fig. 2.3, a radial mode PT is made up of radial discs which are poled in thickness direction and the mechanical stress occurs in the radial direction. An input AC electrical signal creates vibration in the radial direction of the PT which is coupled to the output sections and produces a transformed AC voltage at the output. Multiple layer designs for the input and output section are used to create the desired step down/step up voltage levels for the PT [34]. Since lower output impedances can be achieved by careful design of the output section, these transformers are suitable for step down applications [35],[36]. The circular design of the ceramic plates help in avoiding vibrations in the spurious modes increasing the efficiency of the PT [13]. Due to higher electromechanical coupling factors, higher power densities in the order of 30-40W/cm^3 can be achieved using this structure [3]. Researches have been done which have proposed designs above 100 W power levels with the ability to go beyond [6].

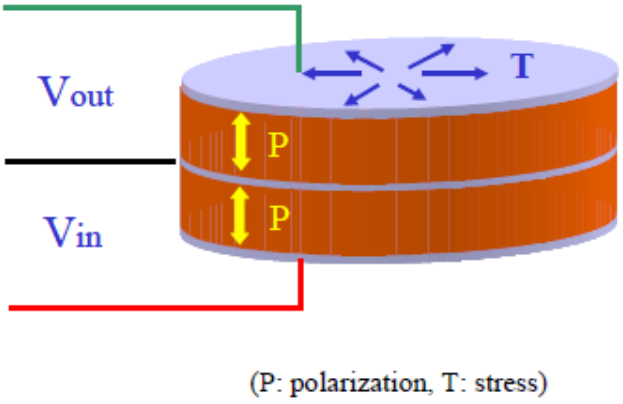

Fig. 2.3. A Radial mode piezoelectric transformer [14].

Radial mode PTs have been deployed in various applications such as electronic lamp ballasts [15], AC-DC adapter applications [3] etc. showing high levels of efficiency. This research uses the radial structure extensively to explore

a new class of transformers called the ‘Tunable Piezoelectric Transformers’. This will be further discussed in Chapter 3 of this thesis.

- *Thickness vibration mode PT*: Developed by Zaitsu et al [37], the mechanical vibrations in the thickness mode PTs occur in the direction of poling i.e. in the thickness direction. This is possible when the electrical signal applied to the input of the transformer resonates the thickness mode mechanical resonance of the PT instead of the longitudinal mode. Fig. 2.4 shows the direction of poling and the input and output connections for a conventional thickness mode vibration PT.

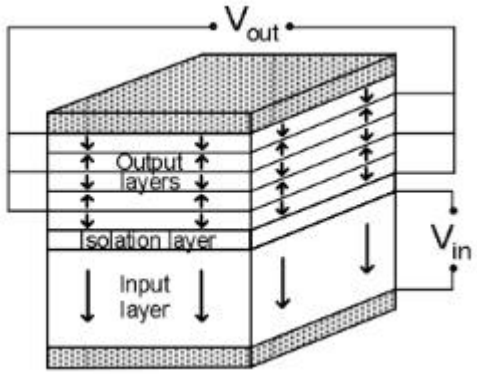

Fig. 2.4. Thickness extension mode piezoelectric transformer [6].

The voltage gain is a function of the ratio of input layer thickness to the output layer thickness [22]. Due to lower output impedance, this structure can be used for lower output voltage step-down applications. Higher power densities are possible due to good electromechanical coupling in the thickness direction. Vibrations in the thickness direction (which is generally small in dimension) gives a high resonant frequency to the structure. PTs with resonant frequency of up to 2 MHz have been proposed [38], [37]. Recently, Noliac came up with a ring type structure which shows higher power densities of 50W/cm3 and high efficiencies of up to 98% [17], [39].

- *Thickness – Shear vibration mode PT*: The mechanical stress developed in this type of PT is perpendicular to the poling direction for both input and output sections of the PT. Fig. 2.5 shows one of the structures proposed by Du et al [40].

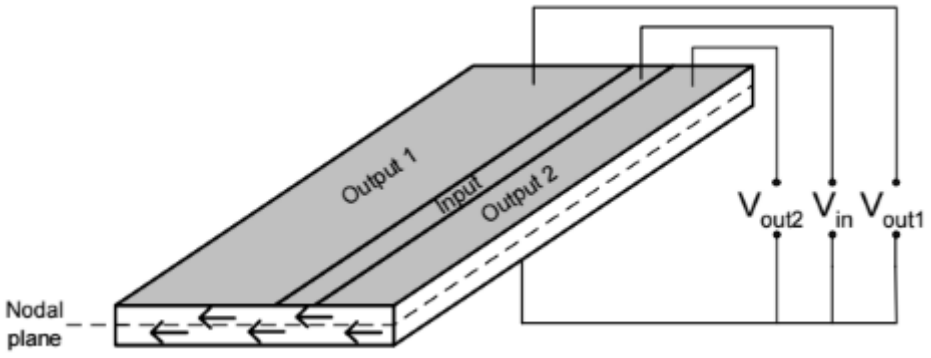

Fig. 2.5. A thickness-shear vibration mode PT [6].

An input electrical signal produces a mechanical shear strain in the input sections of the PT which is coupled to the output section with the shear electromechanical coupling factor. The transformed output voltage appears across the output electrodes of the PT. The use of such structures has been fairly limited compared to the Rosen type PT and the radial mode PTs. The design proposed in [40] has been able to demonstrate the structure for use in step down applications with a total power of 169.9 W and efficiency of 90%.

2.4 Modeling of Piezoelectric Transformers

Fig. 2.6 shows the structure of a Radial mode PT with circular discs. Using the fundamental equations of piezoelectric operation, a physics based model for the radial mode piezoelectric transformer can be derived.

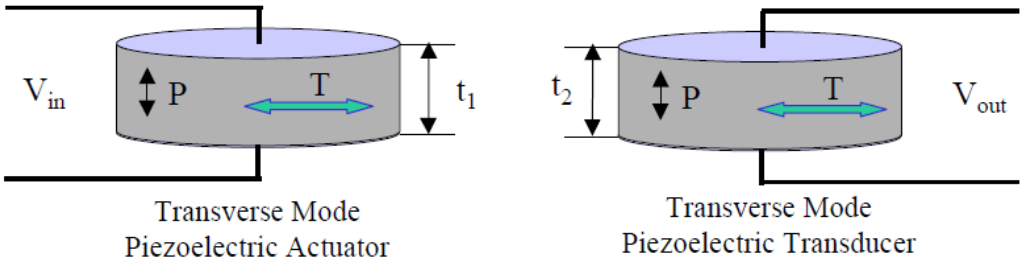

Fig. 2.6. Structure of a radial mode PT with directions of polarizations on the input side actuator (left) and output side transducer (right) [7].

An electrical voltage is applied across the electrodes, which produces an electric field in the direction of polarization. The strongest mechanical waves are produced in the radial direction. The mechanical stress is then coupled to the secondary side which produces an electric potential across the secondary electrodes. The equations (1) and (2) describe the operation inside the PT [28].

$$S = s^E T + dE \tag{1}$$

$$D = dT + \varepsilon^T E \tag{2}$$

where S = Mechanical strain inside the PT

T = Mechanical stress inside the PT

D = Electric field density

E = Electric field

s^E = elastic compliance at constant electric field

ε^T = permittivity at constant mechanical stress

d = piezoelectric constant

The constants, s, ε and d, are tensors and hence would be dependent on the mode of operation of PTs [28]. For a radial mode PT, the vibrations inside the piezoelectric actuator and transducer occurs in the radial direction. A detailed derivation of the equations and the physics based model for a radial mode PT is discussed in [7]. The results obtained from the derivation are summarize in the equations (3)-(8) and Table 2.1 for a multi-layer structure.

$$N = \frac{n_i}{n_o} \tag{3}$$

$$C_{d1} = \frac{n_i \cdot \pi \cdot r^2 \cdot {\varepsilon_{33}}^2 \cdot \left[1 - \frac{{d_{31}}^2}{{\varepsilon_{33}}^t \cdot {S_{11}}^E \cdot (1-\sigma)}\right]}{t_1} \tag{4}$$

$$C_{d2} = \frac{n_o \cdot \pi \cdot r^2 \cdot {\varepsilon_{33}}^2 \cdot \left[1 - \frac{{d_{31}}^2}{{\varepsilon_{33}}^t \cdot {S_{11}}^E \cdot (1-\sigma)}\right]}{t_2} \tag{5}$$

$$R = \frac{\sqrt{2 \cdot \rho \cdot \left({S_{11}}^E\right)^3 \cdot (1-\sigma)^3}}{32 \cdot Q_m \cdot {d_{31}}^2} \cdot \frac{(n_1 \cdot t_1 + n_2 \cdot t_2)}{{n_1}^2 \cdot r} \tag{6}$$

$$L = \frac{\rho \cdot \left({S_{11}}^E\right)^2 \cdot (1-\sigma)^2}{16 \cdot \pi \cdot {d_{31}}^2} \cdot \frac{(n_i \cdot t_1 + n_o \cdot t_2)}{{n_i}^2} \tag{7}$$

$$C = \frac{32 \cdot r^2 \cdot \left(d_{31} \cdot n_i\right)^2}{\pi \cdot {S_{11}}^E \cdot (n_i \cdot t_1 + n_o \cdot t_2) \cdot (1-\sigma)} \tag{8}$$

TABLE 2.1. MATERIAL SYMBOLS AND DEFINITION

ρ	Density
ε_{33}^T	Permittivity
tan δ	Dissipation Factor
Q_m	Mechanical Quality Factor
d_{31}	Piezoelectric Co-efficient
S^E_{11}	Elastic Compliance
N_R	Radial Mode Frequency Constant
t_1	Primary Layer Thickness
t_2	Secondary Layer Thickness

n_i	Number of input layers
n_o	Number of output layers
r	Radius of the layers

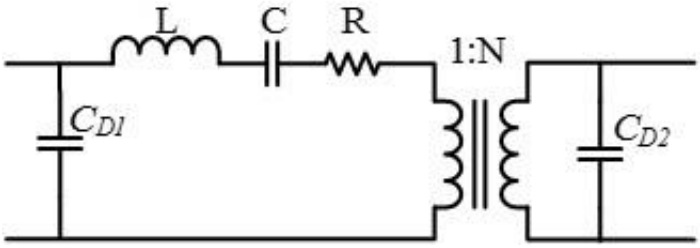

Fig. 2.7. Electrical equivalent circuit of a radial mode piezoelectric transformer.

Fig. 2.7 shows the corresponding electrical equivalent circuit. The equations (3) – (8) depict the dependence of electrical parameters of the 'lumped' electrical equivalent circuit on the physical parameters for PT design. This helps a PT designer manufacture the PT for a specific application. It is important to note that this equivalent circuit is a 1D PT model and neglects any spurious mode of vibration inside the PT. A more accurate modelling procedure for PTs which can capture higher order resonant modes of the PT has also been suggested [7],[22]. Extra L-C resonant branches in electrical equivalent circuit are used to depict the operation of the PT for a large frequency range.

Although the physical design equations (3)-(8) are based on some assumptions and might not be very accurate, a qualitative assessment of the effect of the physical structure on the electrical circuit can be made. For example, increasing the number of layers in the primary side would increase the turns ratio N and hence higher can give higher step-up gain. The primary and secondary capacitance, C_{d1} and C_{d2}, would also increase by increasing the number of layers or by reducing the thickness of each layer [15]. Such insights would be helpful when the electrical equivalent circuit is analyzed and an electrical circuit designer can then work within the physical design limitations of a PT.

2.5 Electrical Equivalent Circuit Analysis

The electrical equivalent circuit of a piezoelectric transformer represents a LCC tank circuit with an input capacitor, C_{d1}. The simplified electrical equivalent circuit is shown in Fig. 2.8.

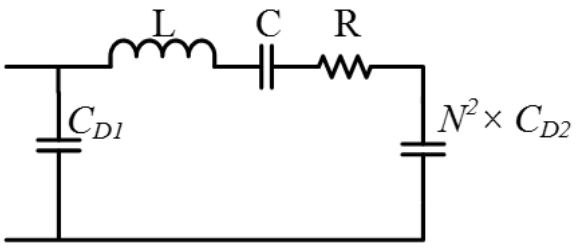

Fig. 2.8. Simplified electrical equivalent circuit of a radial mode PT. The output capacitor is reflected on to the primary side to analyze the circuit as LCC tank circuit.

The simplified circuit shown in Fig. 2.8 ignores the dielectric losses in the piezoelectric transformers. However, it can be shown that when operated near the fundamental resonant frequency of the transformer, these losses have negligible effect on the electrical equivalent circuit [41].

The typical input impedance characteristics of a piezoelectric transformer is shown in Fig. 2.9. The characteristics show two peaks, resonant and anti-resonant points. The piezoelectric transformer has capacitive impedance characteristics for most of the frequency range, however, it shows an inductive behavior between the resonant and anti-resonant frequency. When operated in this region, a PT can be used as resonant tank circuit in resonant power converters [42].

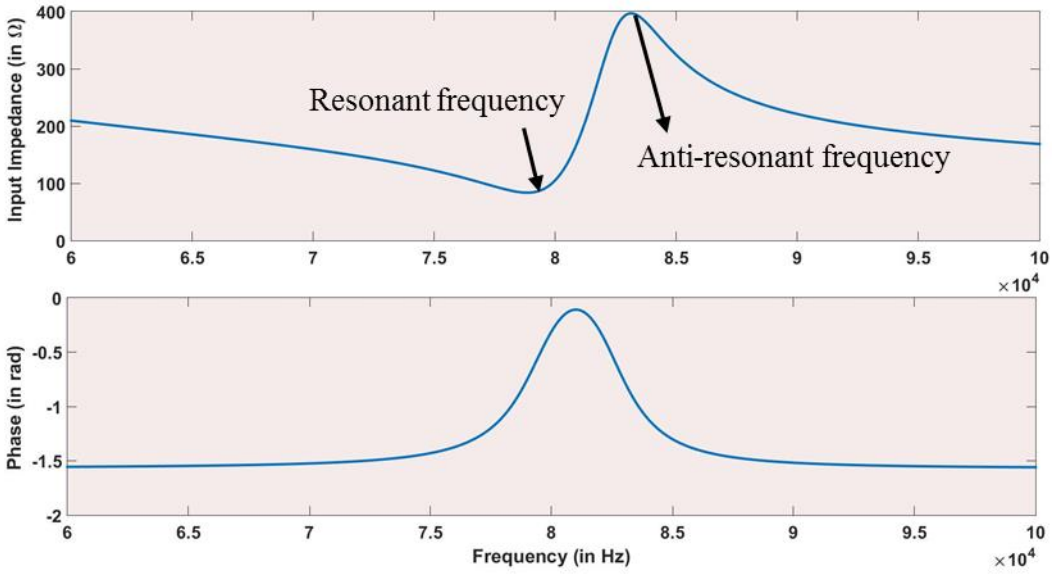

Fig. 2.9. Input impedance characteristics of a standard PT obtained using MATLAB mathematical model of a PT.

For a load resistance, R_{ac}, connected across the output terminals of the PT, equivalent circuit can be analyzed by neglecting the input capacitance, C_{d1}, as it does not interfere with the resonant frequency of the tank. Fig. 2.10 (a), shows the load resistance and output capacitance reflected to the primary side and Fig. 2.10 (b) shows the circuit after transforming the parallel load resistor and capacitor into equivalent series resistance and capacitance.

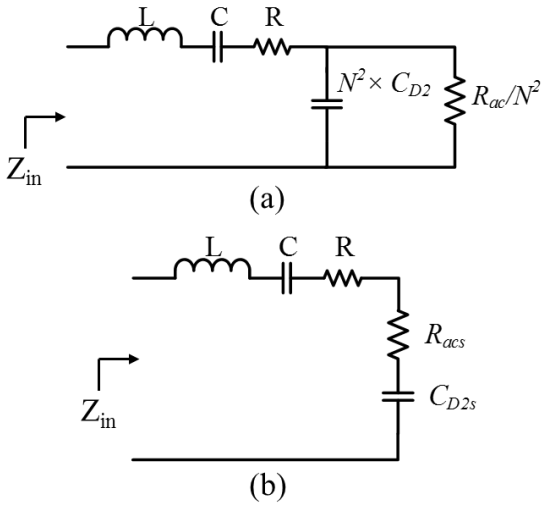

Fig. 2.10. Simplified electrical equivalent circuit of a PT with load resistance. (a) the load resistance and the output capacitance are reflected to the primary side. (b) the parallel network of output capacitor and load resistor are converted into equivalent series combination to simplify analysis.

Equations (9) – (11) describe R_{acs} and C_{d2s}.

$$C_{d2s} = N^2 \cdot C_{d2} \cdot \frac{(1+q^2)}{q^2} \tag{9}$$

$$R_{acs} = \frac{R_{ac}}{(1+q^2)\cdot N^2} \tag{10}$$

where

$$q = \omega_s \cdot C_{d2} \cdot R_{ac} \tag{11}$$

From Fig. 2.10 and equations (9)-(11), some intuitive understanding of the tank circuit can be developed.

For short circuit conditions, $R_{acs} = 0$ and $C_{d2s} = \infty$. Hence, the resonant frequency at this condition would be given by the series resonant frequency of L and C.

$$\omega_s = \frac{1}{\sqrt{L \cdot C}} \tag{12}$$

For open load conditions, $R_{acs} = 0$ and $C_{d2s} = C_{d2}*N^2$. The resonant frequency in this condition is given by the series combination of L and C and Cd_{2s}.

$$\omega_p = \frac{1}{\sqrt{L \cdot \frac{C \cdot (C_{d2} \cdot N^2)}{C + (C_{d2} \cdot N^2)}}} \tag{13}$$

Hence, the resonant frequency point of the tank circuit moves from ω_s to ω_p as the load decreases. For a nominal load, the resonant frequency would be located in between ω_s and ω_p.

The optimum load for a standard Piezoelectric Transformer has been derived in [43] which gives the maximum efficiency of the PT. Although, the analysis relies on simplified 1-D models of PT, it gives us an idea about the maximum efficiency operating point of the PTs. The maximum efficiency of the PT will occur when R_{acs} is the maximum and is given by equation (14).

$$R_{acs\_\max} = R_{ac\_opt} = \frac{1}{\omega_s \cdot C_{d2}} \tag{14}$$

The maximum power transferred to the load will occur when the value of R_{acs} is equal to R. Since R_{acs} has a convex shape, there are two points at which R_{acs} will be equal to R and hence two peaks in the graph of power transferred [44]. However, the efficiency in this condition would be 50 % and hence the PT is generally operated at the point of maximum efficiency i.e. at optimum load.

Fig. 2.11 shows the variation of power transferred and the efficiency of the PT as the quality factor of the circuit is changed.

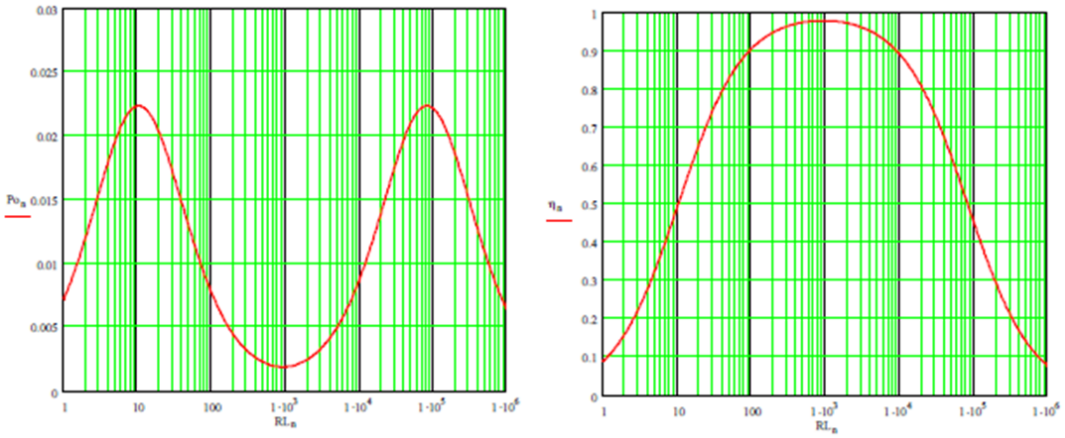

Fig. 2.11. Plot of normalized output power (left) and the efficiency of the PT vs load at resonance [14].

With the given termination, high efficiency operation of PT will be achieved. Other combinations of reactive and passive elements can be used to increase the efficiency of the PT, however, to keep the output matching networks simple, a simple resistive load given by equation (14) is chosen for design [22].

The voltage gain characteristics of a PT at different loads is shown in Fig. 2.12. As the load decreases, the gain of the tank circuit and the resonant frequency increases. As discussed previously, the resonant frequency moves towards the parallel resonant point, ω_p, from its nominal value.

To regulate the output voltage, the frequency of operation can be increased and this is the popular method to control the PT based resonant converters [19].

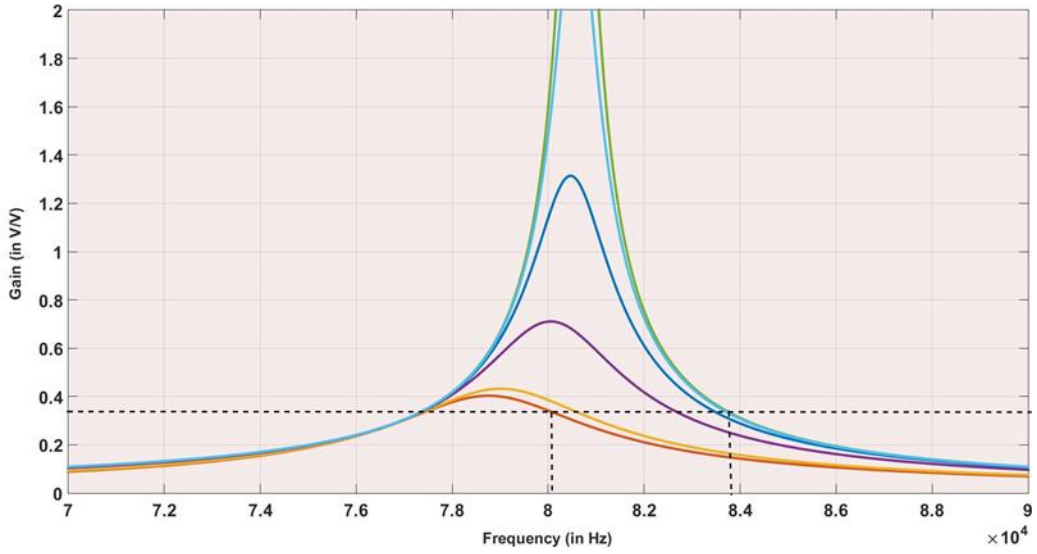

Fig. 2.12. Voltage gain characteristics of a standard PT at various load conditions obtained using SIMPLIS simulations. The voltage gain of a PT is dependent on load and frequency.

2.6 Control Schemes

The voltage gain characteristics of the piezoelectric transformers, discussed previously, show the load and frequency dependent characteristics of the piezoelectric transformers. Just like LCC resonant tank circuits, the resonant frequency and the gain of piezoelectric transformers increases as the load decreases. A common way to control the output voltage in such a situation is to use frequency control methods, namely pulse frequency modulation (PFM) [19]. In this scheme, the output voltage is regulated by changing the frequency of inverter switches and the block diagram for one of such schemes is shown in Fig. 2.13. However, the PT efficiency is maximum when it is operated around its fundamental mode of resonance [45]. Hence, a large variation in the frequency required for large load variations might lead to lower converter and PT efficiencies. Further, the range of frequency in which it is possible to obtain ZVS in the inverter switches is also limited for a piezoelectric transformer. The input impedance characteristics, discussed previously (Fig. 2.9), can be used to obtain the range of

frequencies for ZVS operation for a given PT. This window can be increased by adding inductive components at the input of the PT [46],[47]. However, for inductor-less designs, this window is narrow and hence PFM gives limited control to the PT.

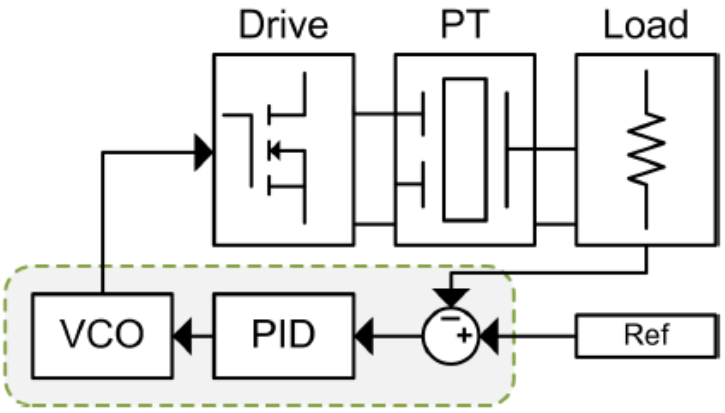

Fig. 2.13. Frequency control scheme for PT based converters [21].

For inductor-less designs, phase locked loop based control schemes have also been proposed [48]. In such schemes, the switching frequency is controlled by sensing the phase between the input and output voltage [49], or the phase between input voltage and current [50]. Fig. 2.14 shows the control block diagram for one of such schemes.

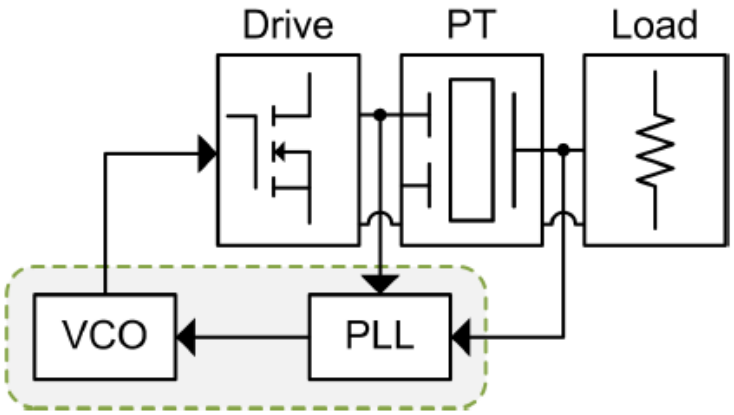

Fig. 2.14. PLL based control scheme to control the phase between input voltage and PT input current [21].

PFM techniques are not suitable for handling input voltage changes. To overcome this issue, PWM control techniques have been proposed [45]. A combination of PWM and PFM techniques have also been proposed to enable both input voltage regulation and load regulation [51]. Since the PTs are most efficient near their fundamental resonant frequency point, it is desirable to operate them at a constant frequency. Based on this idea, quantum-mode control technique has been proposed [52],[53]. In such a control, the inverter switches are turned ON and OFF at a much lower frequency when the voltage crosses a certain band of tolerance. The drawback of such a control is the presence of low frequency ripple in the output voltage which requires a large output capacitor to filter.

With the help of tunable piezoelectric transformers, most of these issues can be tackled in a very simple PWM control. This is discussed further in Chapter 4.

Chapter 3

Tunable Piezoelectric Transformers

3.1 Introduction

The design of a Tunable Piezoelectric Transformer (TPT) is based on a multilayer Transoner® PT developed by Face electronics in 1996. The input and the output section is made of radial ceramic discs as in a Transoner® PT. In addition, some extra layers (number based on a specific design), of a specific thickness, are added to the structure which forms the control section of the transformer. This makes the tunable PT a three-terminal device. Input and output sections are electrically isolated from each other using an isolation layer. The position of these layers, number of layers, the thickness and the material, all effect the impact this section has on the gain characteristics of the PT.

The control layers provide an extra terminal to the transformer which can be used to control the voltage gain characteristics of the PT. The concept of tunable PTs and their application in DC-DC converters was introduced in [54]. To help understand the concept of tunable PTs and 'Tunability', an in-depth analysis of the electrical equivalent circuit of the tunable PT will be presented in this chapter. The analysis assumes that the electrical equivalent circuit presented here is an accurate depiction of the tunable PT operation. Since the scope of this thesis is not to derive electrical model of tunable PT and design it for a specific application, those details would not be presented. However, with the electrical equivalent circuit analysis presented, some basic idea on the operation and design of TPT can be developed.

3.2 Electrical Equivalent Circuit Analysis

Fig. 3.1(c) and Fig. 3.1(d) shows the structure and electrical equivalent circuit of a Tunable PT and compares it to the structure and electrical equivalent circuit of a standard

PT in Fig. 3.1(a) and Fig. 3.1(b) respectively. The addition of a control section and the change corresponding to it is evident from the equivalent circuit diagram of the TPT. In this design, the control section is in between the output layers and the input layers are two outermost layers. Other positions of the control layers, output layers and input layers are also possible based on the design specification. It is important to note that the additional control section is represented as a separate ideal transformer with a turns ratio of $1:N_2$ between input and control. The coupling between the input and output sections is represented by an ideal transformer with a turns-ratio of $1:N_1$. These two transformers are connected in series such that the capacitor at the output (C_{d2}) and control terminal (C_{d3}) are also connected in series.

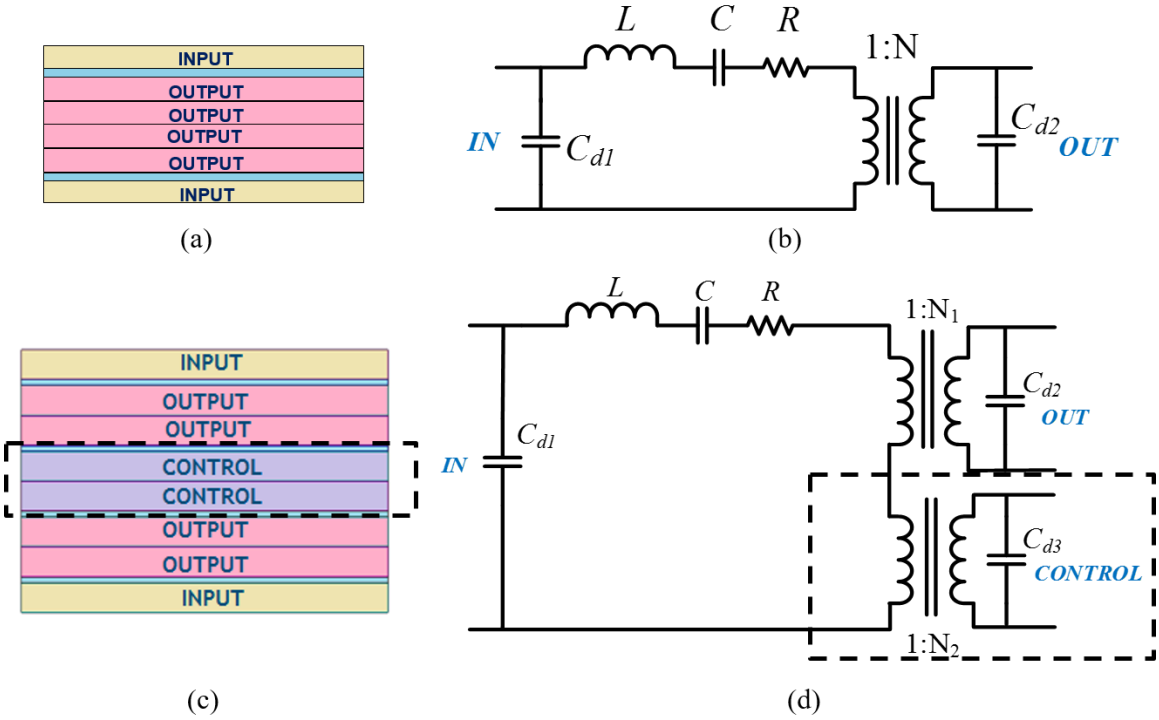

Fig. 3.1. (a) Structure of layers in a standard PT and it's Electrical equivalent circuit (b). (c) and (d) show the structure of a tunable PT with control layer sandwiched in between input and output layers and the corresponding electrical equivalent circuit.

The equations, which relate the physical properties of a PT to the parameters of the electrical equivalent circuit, were presented in Chapter 2. Additional control section embodies an equivalent capacitance, C_{d2}, at its terminals, like the output and input sections. This capacitance is dependent on the thickness of the layers, number of layers

and the type of material used [15]. The transformation ratio between the input/control is dependent on the number of input and control layers, the relative position of each layer etc.

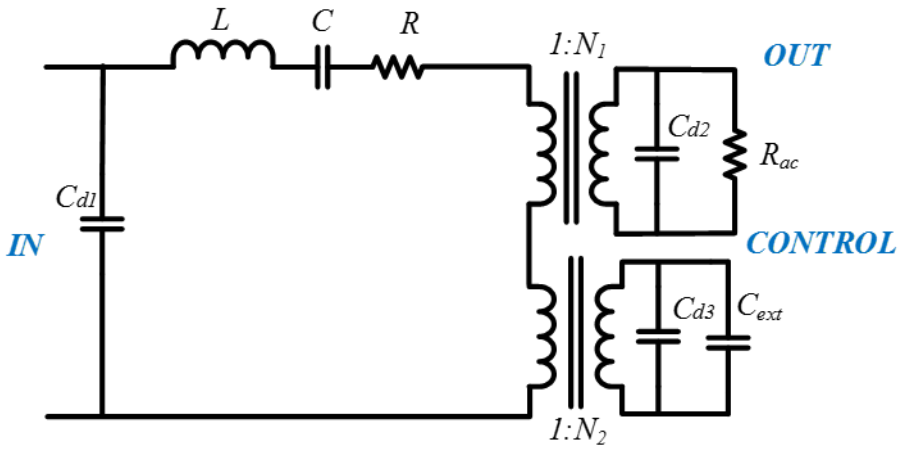

Fig. 3.2. Electrical equivalent circuit of a tunable piezoelectric transformer without the dielectric losses.

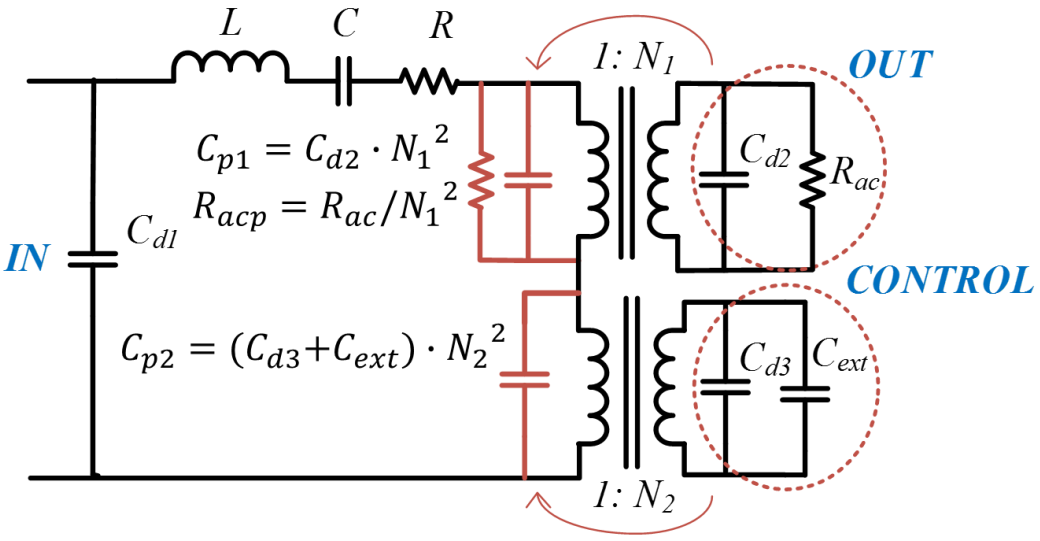

Fig. 3.3. Electrical equivalent circuit of the tunable piezoelectric transformer after reflecting the control and output components to the primary.

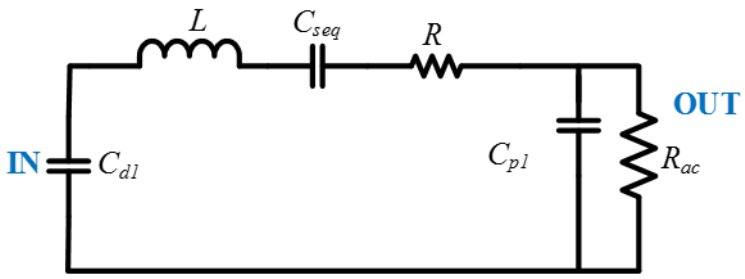

Fig. 3.4. Simplified electrical equivalent circuit of the tunable PT after simplification. The circuit resembles to that of a standard PT.

Fig. 3.2 shows a simplified equivalent circuit of the TPT without the dielectric loss resistors R_{cd1}, R_{cd2} and R_{cd3} to simplify the analysis. The capacitors and the resistors at the control and output terminals can now be reflected to the primary side as shown in Fig. 3.3. It must be noted that the reflected control capacitance, C_{p2} and a parallel combination of R_{acp} and C_{p1} are in series and not in parallel. This makes the series capacitance of the LCC tank circuit (C_{seq}) in Fig. 3.4 a series combination of C_{p2} and C. To verify the series connection of C_{p2} and C experimentally, the resonant frequency of the transformer was measured under increasing values of C_{ext} (1 nF to 2.2 µF), and the resonant frequency for each case was recorded. The resonant frequency did not decrease continuously which would have been the case if the capacitors were in parallel. Fig. 3.5 shows the experimental results of this test performed on one of the TPTs.

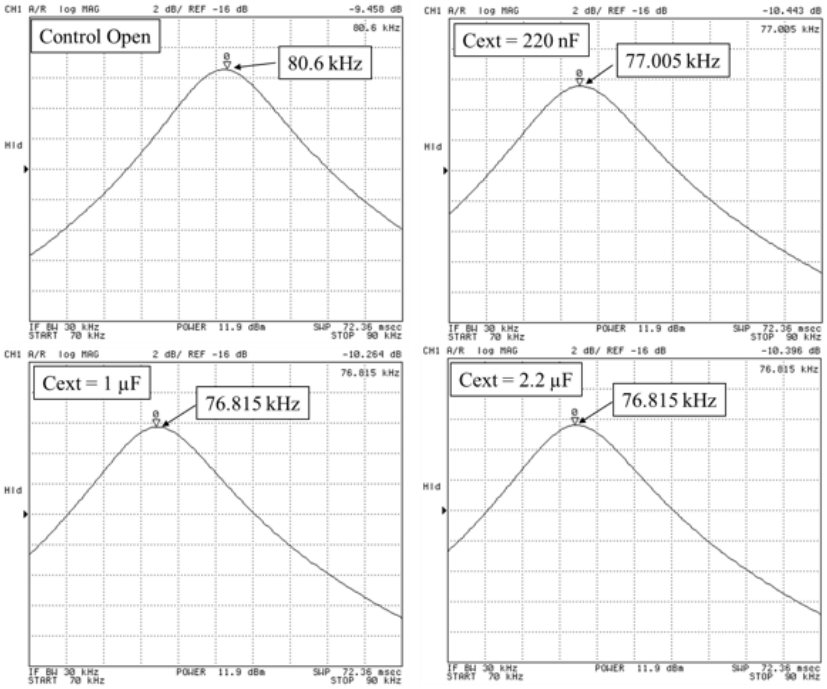

Fig. 3.5. Voltage gain characteristics of a tunable PT sample at fixed load and varying values of external control capacitor obtained from a network analyzer. The resonant frequency of the tunable PT doesn't decrease further after a certain value of external control capacitor (2.2 µF) depicting series connection of reflected control capacitance (C_{p2}) and series capacitance (C).

To understand this better, the design equations of the PT, which relate the physical parameters to the electrical circuit values, can be studied. The control layers in the TPT structure can be considered as extra output layers intended for control. The capacitance embodied by the control layer is dependent on the number of control layers and their thickness as shown in equation (15) below (apart from being dependent on other parameters). The transformation ratio from input to control is a ratio of number of input layers to the number of control layers, shown in equation (16).

$$C_{d3} \propto \frac{N_c}{t_c} \tag{15}$$

$$N_2 \propto \frac{N_p}{N_c} \tag{16}$$

$$C_{d3p} = C_{d3} \cdot N_2^{\,2} \tag{17}$$

where C_{d3} = Control terminal internal capacitance

N_c = number of control layers

N_p = number of primary layers

1: N_2 = transformation ratio between input and control

t_c = thickness of each control layer

C_{d3p} = control capacitance reflected on the input side

Let number of primary layers (N_p) and their thickness be constant. If the number of control layers increase by a ratio β, the control capacitance (C_{d3}) would increase by β (assuming other physical conditions to be constant). However, N_2 decreases by the same ratio which in turn causes C_{d3p} to decrease by β. Hence, the addition of layers in the control section decreases the equivalent primary side reflected capacitance of the control (C_{p2}). The same analysis would also be true for the output section. If the capacitance of these layers were in parallel, an increase in the number of layers in the control section would increase equivalent capacitance of these two sections. This shows that the output and control layer capacitors, when reflected to the input side appear to be in series.

From the above circuit analysis, it is seen that the series capacitance of the LCC tank circuit (C_{seq}), in case of the tunable PT, is dependent on the control capacitance. Thus, a change in the capacitance at the control terminal would change the resonant frequency of the tank circuit. Fig. 3.6 shows the voltage gain curves of a tunable PT at a given load and two different values of an external fixed capacitor connected across the control terminal.

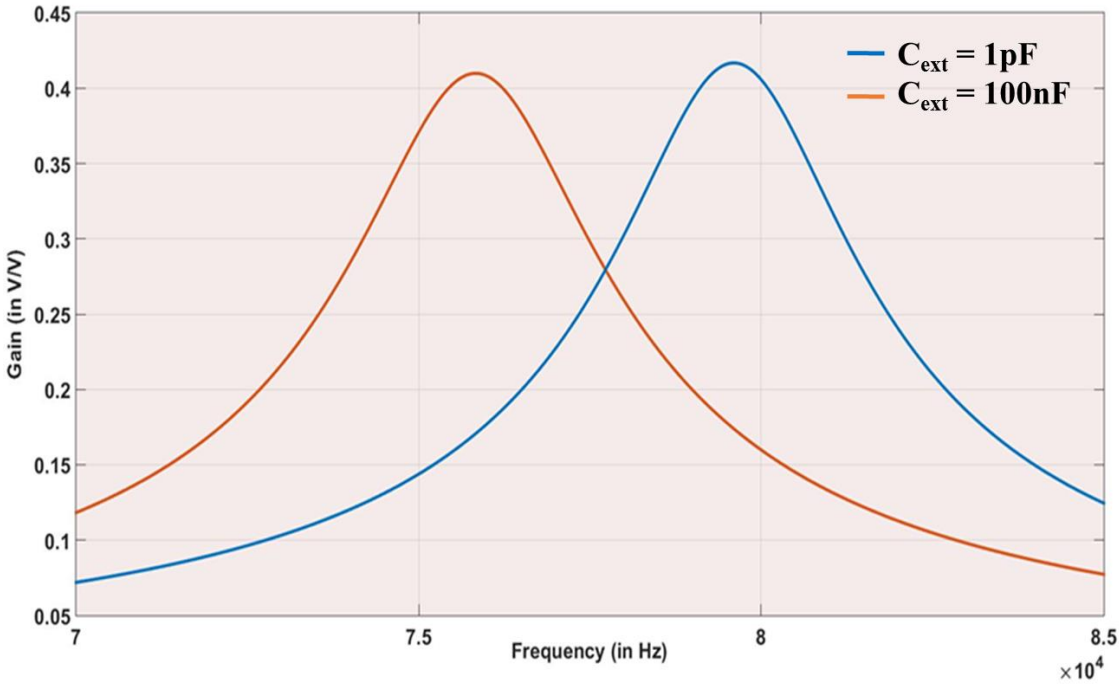

Fig. 3.6. Voltage gain characteristics of a tunable PT at a fixed load and different external capacitor values obtained using SIMPLIS simulations.

An increase in the external capacitor across the control terminal (C_{ext}) increases the series capacitance, C_{seq}, of the LCC tank circuit and hence the resonant frequency of the tunable PT decreases. Since the equivalent series capacitance (C_{seq}) is a series combination of C_{p2} and C, the maximum value of C_{seq} is limited to the value of C. This happens when the external capacitance, C_{p2}, becomes much larger than C and hence has no effect on the resonant frequency of the tunable PT. This is when the transformer 'saturates' and no it is no longer controllable by varying the control capacitance. The ability of the tunable PT to change its resonant frequency by changing the loading conditions at the control terminal, is hereby referred to as the 'Tunability' of the TPT. A quantitative definition of Tunability will be presented later in section 3.5.

It is also interesting to note that the control terminal can also be loaded by other passive elements such as resistors and inductors. Addition of any resistor would also bring a change to the resonant characteristics of the tunable PT, however, extra losses incurred in the resistor would deteriorate the system efficiency. Addition of an inductor would increase the order of the system and can make the analysis more complicated. An extra capacitor, on the other hand, helps the tunable PT retain characteristics similar to a

LCC tank circuit which makes it easier to design. The voltage gain characteristics of the tunable PT also take on a familiar shape for various load conditions and this will be discussed in the further sections. Having said that, it would be interesting to explore a combination of other active/passive elements at the control terminal in the future.

This thesis explores the effect of capacitor loading at the control terminal and the ways to use it for the design of a DC-DC converter. If the capacitance at the control terminal can be varied under different operating conditions, then the voltage gain characteristics of the tunable PT can be adjusted such that the output voltage is regulated.

3.3 Optimum load

The optimum load for a standard Piezoelectric Transformer was discussed in Chapter 1. For a tunable PT, the determination of optimum load is very similar. From the equivalent circuit analysis, we can reduce a tunable PT to an electrical equivalent circuit similar to a standard PT. This enables us to apply same analytical techniques developed for a standard PT. Since the series capacitance of a tunable PT changes with load, the optimum load would also change. Hence, when determining the optimum load for a TPT, the value of C_{ext} corresponding to the nominal load must be considered. To achieve maximum tunability, this is the lowest value of C_{ext} possible. Fig. 3.7 shows the optimum load of a TPT for a minimum C_{ext} value, derived using circuit analysis, and it can be seen that the nominal load can still be represented by the equation (18) as that for a standard PT.

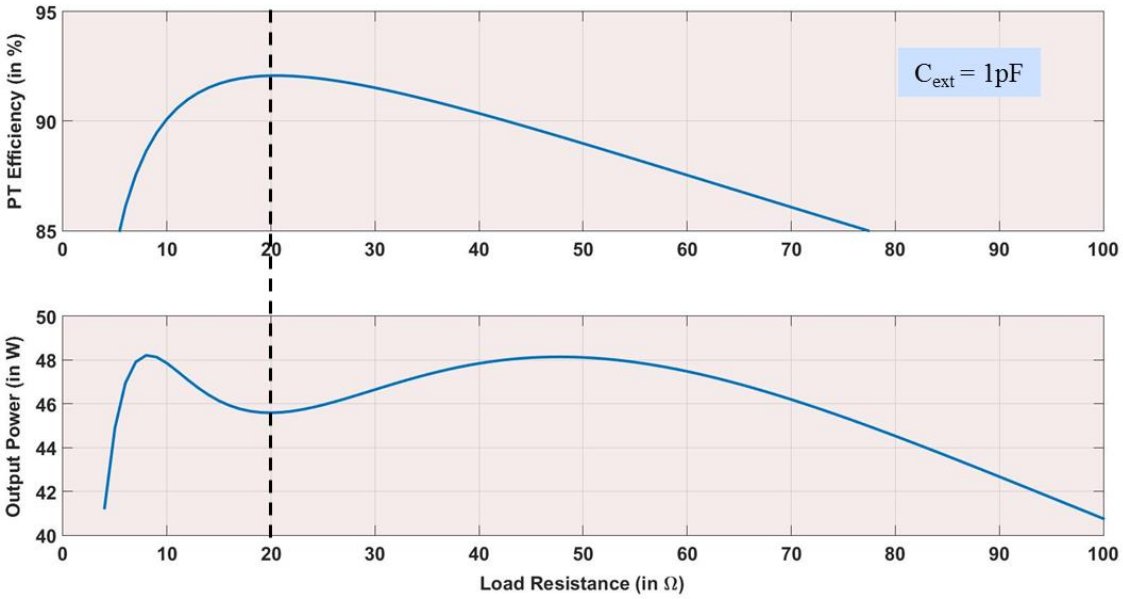

Fig. 3.7. Efficiency of a tunable PT and output power vs. load resistance at the resonant frequency obtained using mathematical circuit analysis in MATLAB.

$$R_L = \frac{1}{\omega * C_{d2}} \tag{18}$$

3.4 Voltage Gain Characteristics

The voltage gain characteristics of a tunable PT at a given load and with the control circuit open is shown in Fig. 3.8. The electrical equivalent circuit of the tunable PT being similar to a LCC tank circuit, the gain of the TPT is dependent on the load conditions.

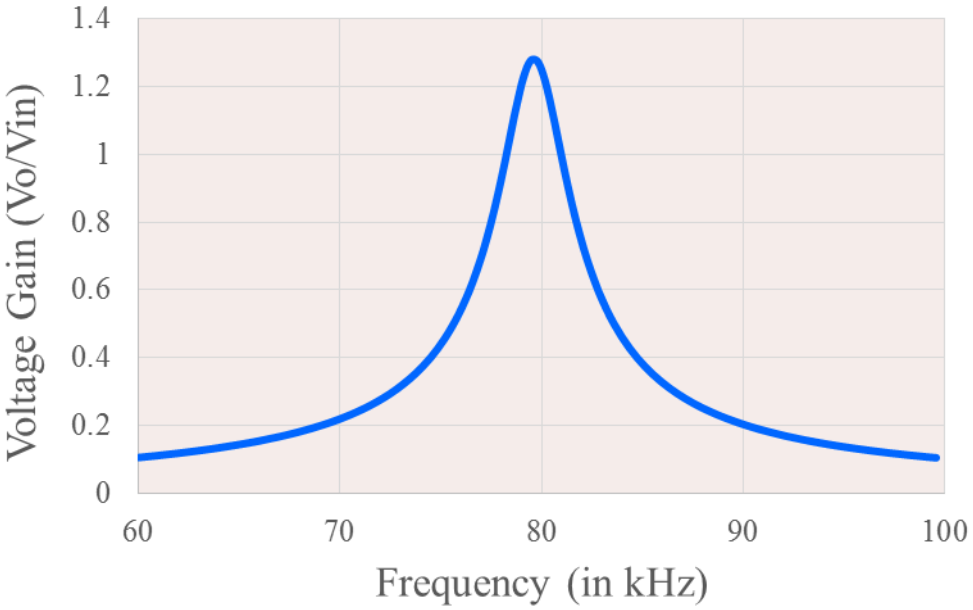

Fig. 3.8. Voltage gain characteristics of a tunable PT at optimum load and no external control capacitor obtained using SIMPLIS.

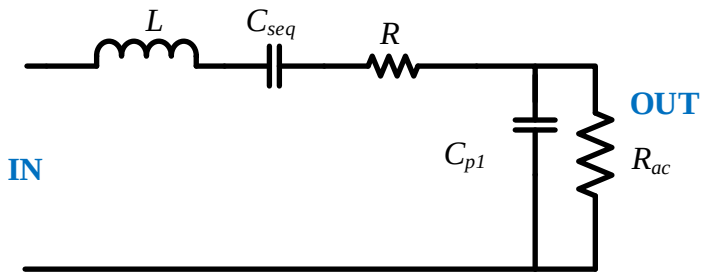

Fig. 3.9. The electrical equivalent circuit for a tunable PT at optimum load. The input capacitor can be neglected in calculation of voltage gain near resonant frequency.

A simplified LCC tank circuit is shown in Fig. 3.9. The input capacitor does not affect the voltage gain of the voltage gain of the tunable PT near its resonance frequency and can be ignored in the analysis. It is also assumed that the tunable PT is lossless and hence R = 0.

Under these assumptions, there are two frequencies at which the gain of the tunable PT is equal to one. One of the frequencies is the series resonant frequency of the circuit i.e. the resonant frequency of C_{seq} – L given by equation (19) and can be seen intuitively from the circuit.

$$\omega_s = \frac{1}{\sqrt{L * C_{seq}}} \tag{19}$$

The other frequency point is rather intriguing and can be found out by solving the electrical equations for the tank circuit. The voltage gain of the LCC tank circuit is given by equation (20) [55]. Solving this equation for a frequency with a unity gain, we get one of the solutions as (19) and another equation, shown in (22). This shows that other frequency would be a function of the load at the tunable PT output terminals, along with other circuit parameters.

$$\frac{V_o}{V_{in}} = \frac{1}{1 + \frac{X_{Cseq}}{X_{Cp1}} - \frac{X_L}{X_{Cp1}} + j\left[\frac{X_L}{R_{ac}} - \frac{X_{Cseq}}{R_{ac}}\right]} \tag{20}$$

$$\left|1 + \frac{X_{Cseq}}{X_{Cp1}} - \frac{X_L}{X_{Cp1}} + j\left[\frac{X_L}{R_{ac}} - \frac{X_{Cseq}}{R_{ac}}\right]\right| = 1 \tag{21}$$

$$\frac{1}{X_{Cp1}^{\ 2}} - \frac{2}{X_{Cp1}(X_{Cseq} - X_L)} + \frac{1}{R_{ac}^{\ 2}} = 0 \tag{22}$$

If $R_{ac} = X_{Cp1}$, which would be the optimum load of the tunable PT, the other frequency can be calculated by substituting this value in equation (22) and is calculated to be the parallel resonant frequency of the LCC tank circuit given by equation (23). It is important to note that the C_{seq} in equation (23) corresponds to the value of series capacitance of the equivalent LCC tank circuit at optimum load conditions for a given TPT.

$$\omega_p = \frac{1}{\sqrt{L * \frac{(C_{seq} * C_{p1})}{(C_{seq} + C_{p1})}}} \tag{23}$$

Now, if the load across the tunable PT decreases, the resonant frequency and the gain of the tunable PT increases as shown in Fig. 3.10. The load dependent frequency for

which gain is unity also changes and is no more the parallel resonant frequency of the tank. Equations (24)-(25) shows the new frequency at which the gain of the tank circuit will be unity at a given light load condition.

For a given light load condition, if

$$R_{ac} = \beta * X_{Cp1} \tag{24}$$

Substituting equation (24) in equation (22), and solving for frequency, we get

$$\omega' = \frac{1}{\sqrt{L * \frac{(C_{seq} * C_{p1} * (1+1/\beta^2))}{(2 * C_{seq} + (1+1/\beta^2) * C_{p1})}}} \tag{25}$$

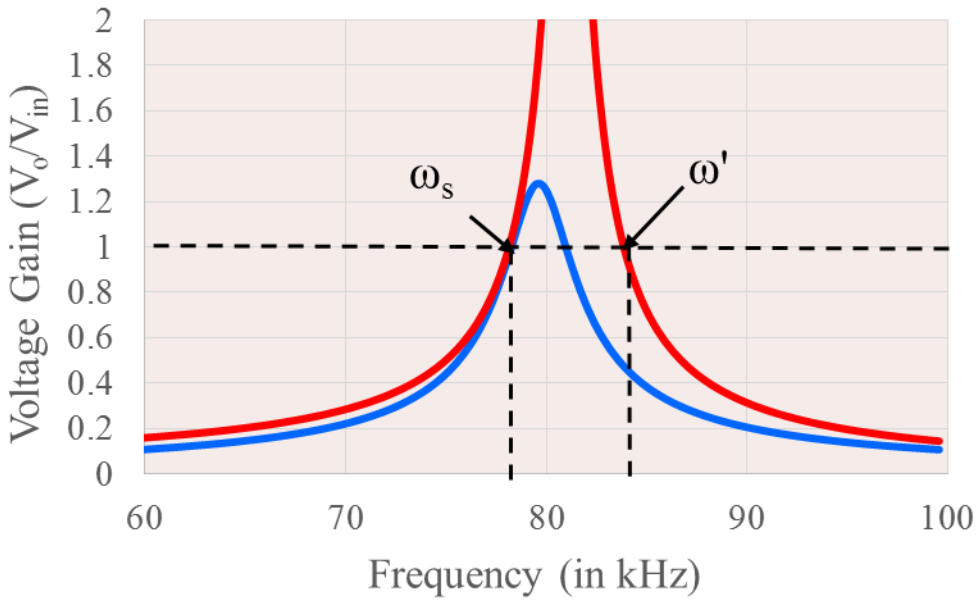

Fig. 3.10. Voltage gain characteristics of the tunable PT at nominal and light load conditions with no extenal capacitor at the control terminal obtained using SIMPLIS.

To regulate the output voltage, the control capacitance can be increased (by increasing the external capacitor (C_{ext}), which decreases the resonant frequency of the tank circuit. At a certain value of the external capacitance (C_{ext_new}), the voltage gain of the tank circuit will be equal to one at the parallel resonant frequency of the tank, ω_p, as

shown in Fig. 3.11. The frequency obtained in equation (25) is the frequency at which the gain of the tank is unity at light load. The external capacitor is now increased to C_{ext_new}, such that for the corresponding value of series capacitance, C_{seq_new}, ω' becomes equal to parallel resonant frequency, ω_p. This unique value, C_{seq_new}, can be calculated by solving equation (26) and is shown in equation (27).

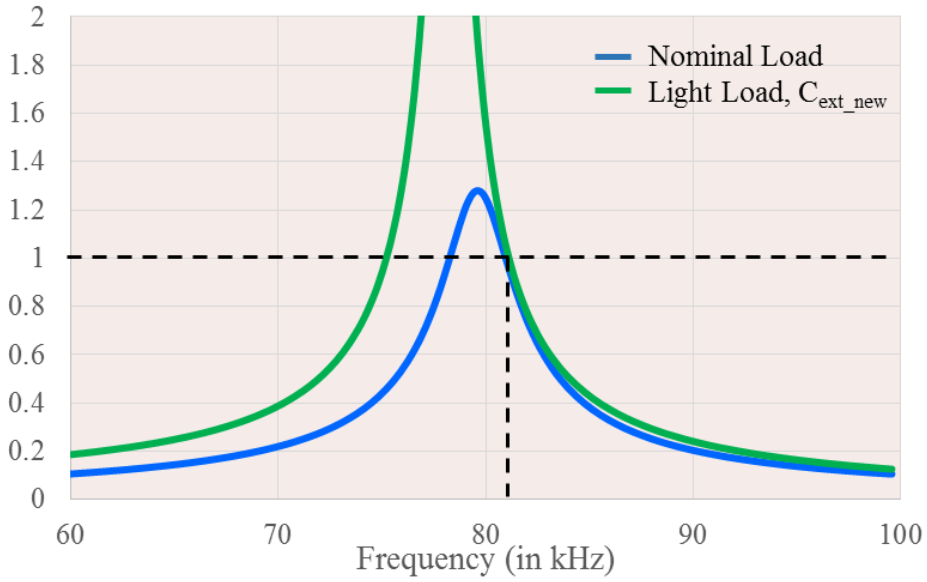

Fig. 3.11. Voltage gain characteristics of the tunable PT at nominal load and no external capacitor obtained using SIMPLIS. The voltage gain at light load and the corresponding value of external control capacitor at which gain of the tunable PT is 1 at ω_p.

$$\frac{1}{\sqrt{L*\frac{(C_{seq}*C_{p1})}{(C_{seq}+C_{p1})}}}=\frac{1}{\sqrt{L*\frac{(C_{seq\_new}*C_{p1}*(1+1/\beta^2))}{(2*C_{seq\_new}+(1+1/\beta^2)*C_{p1})}}} \tag{26}$$

$$C_{seq\_new}=\frac{(1+1/\beta^2)*C_{seq}*C_{p1}}{(C_{seq}+C_{p1})*(1+1/\beta^2)-2*C_{seq}} \tag{27}$$

Hence, if it is physically possible for a given TPT design to achieve this new value of C_{seq}, it would be able to regulate the output voltage by changing the external capacitor at the control terminal, for any given light load condition. The voltage gain characteristics of a given tunable PT for various load conditions and the corresponding C_{ext} value are shown in Fig. 3.12.

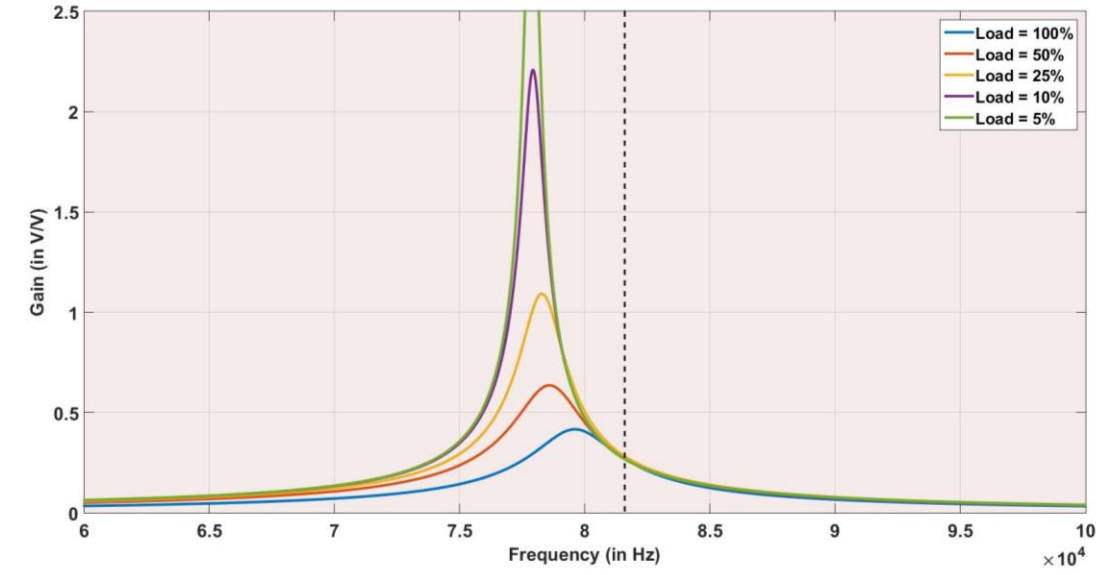

Fig. 3.12. The voltage gain characteristics of the tunable PT at various load conditions and the corresponding value of C_{ext_new} obtained using SIMPLIS. All the load curves have a constant gain at ω_p.

The voltage characteristics in Fig. 3.12 give a unique characteristic to a tunable PT, as such, it resembles closely to that of a LLC converter. With such characteristics, it becomes possible to operate the converter at a fixed frequency and regulate the output voltage for load variations. A way to implement a variable capacitor and the corresponding control scheme to achieve such a regulation is proposed in Chapter 4.

3.5 Tunability

The ability of the tunable PT to regulate the output voltage under varying load conditions by only changing the control terminal capacitance/other loading conditions at a fixed frequency and nominal input voltage is referred to as the 'Tunability' here. Equation (28) and (29) quantifies Tunability as used in this document.

$$Tunability = \left(1 - \frac{1}{\beta}\right) * 100 \tag{28}$$

where

$$\beta = \frac{R_{ac\_\max}}{R_{ac\_opt}} \tag{29}$$

(at a constant output and input voltage)

It is important to note that Tunability is 100% if $\beta = \infty$, which means that the tunable PT is able to regulate the output voltage even at open load conditions. A TPT can also have more than 100% Tunability. In this scenario, the TPT would have more shift in the resonant frequency than required for 100% load regulation. This would be discussed in detail later in this section.

The two main design parameters, from the electrical equivalent circuit, which affect tunability are:

- Ratio of C to C_{p2} (C/C_{p2})
- Ratio of C_{seq} to C_{p1} (C_{seq}/C_{p1})

Ratio of C to C_{p2}

The total change in the equivalent series capacitance of the LCC tank circuit that can be achieved by changing the control capacitance (C_{ext}) depends on the ratio C/Cp2. The ratio is calculated without any external capacitor across the control terminal. Hence, the ratio is purely a function of the tunable PT design. Since C and C_{p2} are in series, the closer the ratio C/C_{p2} to 1, the more is the tunability. Fig. 3.13 shows the total shift in the resonant frequency for two different C/C_{p2} ratios in a hypothetical TPT design. In both the cases C_{ext} is varied from a very low value (such as 1 pF) to a relatively high value such that the maximum shift in each case is recorded.

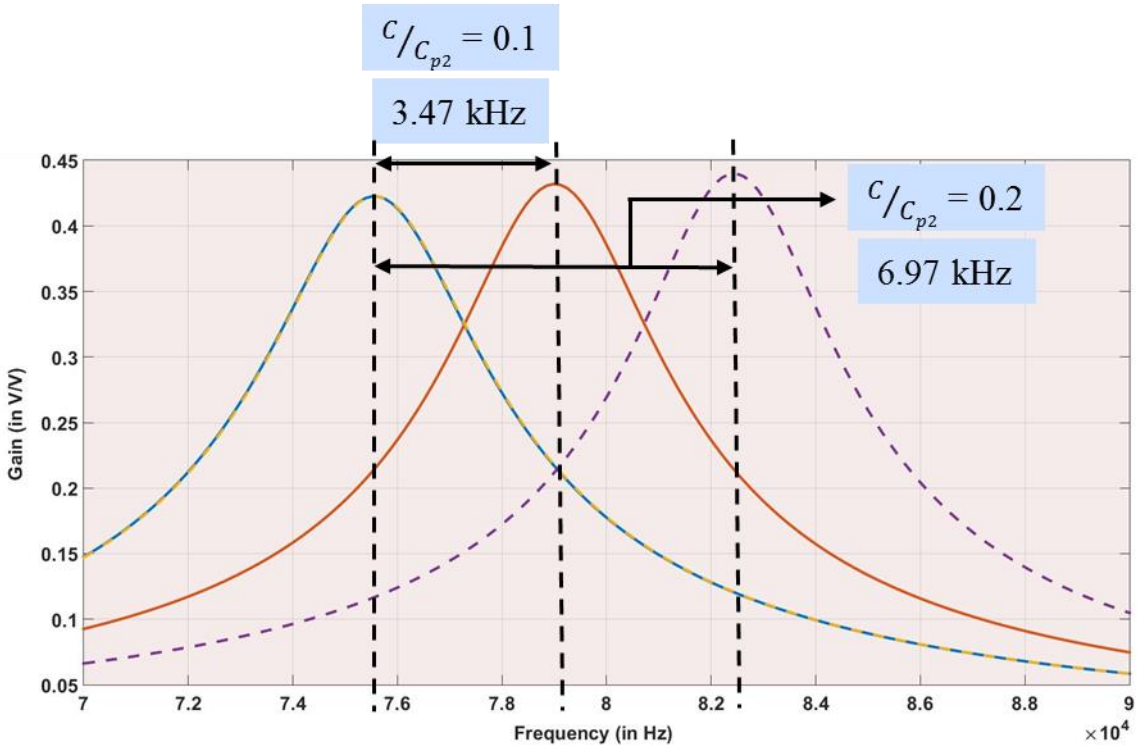

Fig. 3.13. Shift in the resonant frequency of tunable PT by changing the capacitance at the control terminal for two different design examples obtained using SIMPLIS.

Ratio of C_{seq} to C_{p1}

The effect of the ratio C_{p2}/C on tunability is more intuitive and easier to understand. However, the ratio of C_{seq}/C_{p1} is also an important design criteria to consider while designing tunable PT. The impact of this design parameter can be understood by analyzing the electrical equivalent circuit of the TPT shown in Fig. 3.9. Just like a LCC tank circuit, the series and parallel resonance of the TPT is given by equations (30) and (31) respectively.

$$\omega_s = \frac{1}{\sqrt{L * C_{seq}}} \tag{30}$$

$$\omega_p = \frac{1}{\sqrt{L * \frac{C_{seq} * C_{p1}}{C_{seq} + C_{p1}}}} \tag{31}$$

For a short circuit across the tunable PT terminals, the resonant frequency of the tunable PT would be at the series resonant point and for an open circuit, it would be at the parallel resonant point. Hence, when the load across the TPT is reduced, the resonant frequency shifts from nominal resonant frequency (in between series and parallel resonant point) to parallel resonant frequency. At the same time, the gain of the TPT also increases. Hence, the tunable PT must be able to change its resonant frequency to make up for this change. Larger the difference between the series resonant point and the parallel resonant point, more change in series capacitance of the LCC tank would be required.

Fig. 3.14 shows the variation of the resonant frequency of a LCC tank circuit vs C_{seq} for a fixed value of C_{p1}. The change in the resonant frequency per unit change in C_{seq} is much larger for small values of C_{seq}. This means that for small C_{seq}/C_{p1} ratios, less change in C_{seq} is required for a same amount of change in the resonant frequency as compared to a larger C_{seq}/C_{p1} ratio. Hence, 'Tunability' is higher for small C_{seq}/C_{p1} ratios.

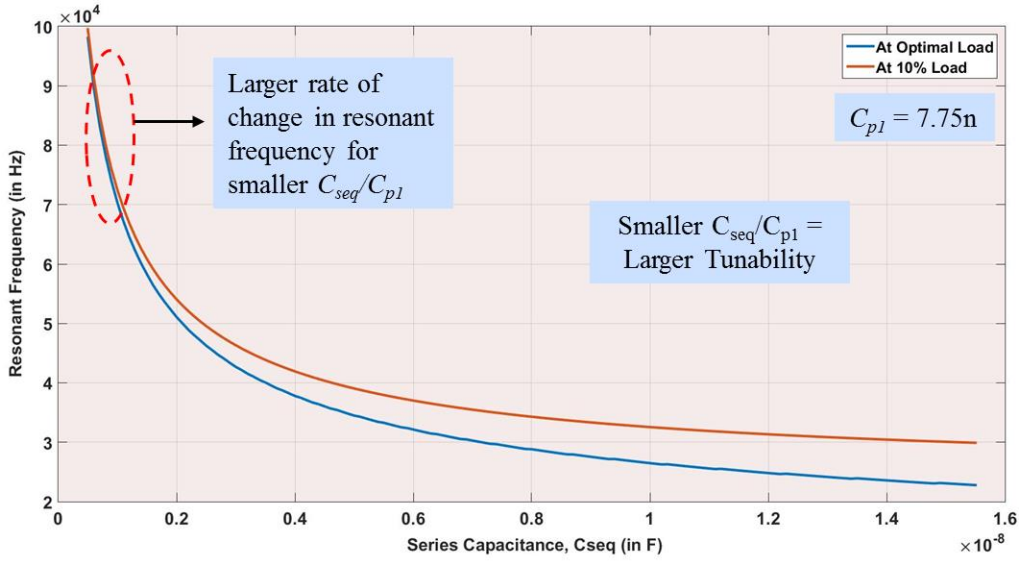

Fig. 3.14. Resonant frequency of a tunable PT vs. series capacitance for a fixed value of C_{p1} obtained using mathematical analysis of electrical equivalent circuit in MATLAB. The plot shows that the rate of change of resonant frequency is faster for a smaller C_{seq}/C_{p1} ratio.

This can also be understood by calculating the series and parallel resonant frequencies for the two cases with different C_{seq}/C_{p1} ratios, shown in Fig. 3.15 and Fig. 3.16. For a higher C_{seq}/C_{p1} ratio, the series and parallel resonant frequencies are farther apart and hence more change in series resonant capacitance (C_{seq}) is needed for the same amount of load variation as compared to a smaller C_{seq}/C_{p1} ratio design. The design in Fig. 3.15 has a higher C_{seq}/C_{p1} ratio and hence the difference between the full load to light load resonant frequency is 2.04 kHz. Fig. 3.16, on the other hand, shows another design with a smaller C_{seq}/C_{p1} ratio and the difference between the full load and the light load resonant frequency is 1.58 kHz.

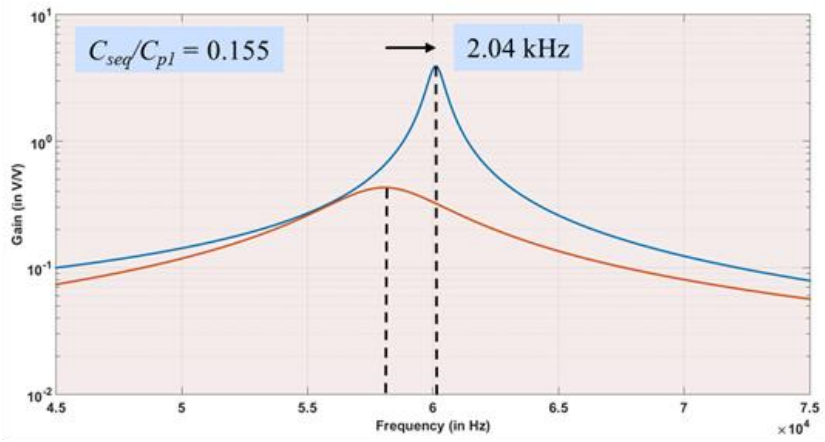

Fig. 3.15. Shift in resonant frequency from nominal load to 10% load condition for the given tunable PT design with C_{seq}/C_{p1} ratio equal to 0.155. This was obtained using SIMPLIS.

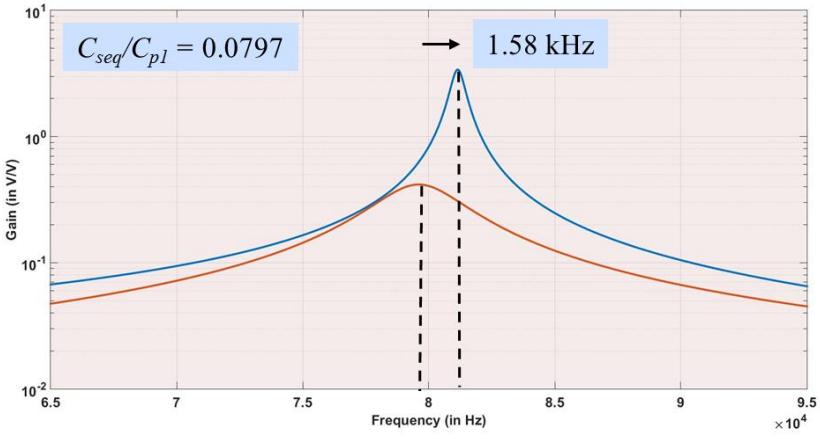

Fig. 3.16. Shift in resonant frequency from nominal load to 10% load condition for the given tunable PT design with C_{seq}/C_{p1} ratio equal to 0.0797. This was obtained using SIMPLIS.

Condition for 100 % Tunability

Based on the discussions above, electrical equivalent circuit of the tunable PT can be analyzed to come up with a design criteria for 100% tunability in a TPT design. Equation (27) was derived in the previous sections to calculate the new value of series capacitance (C_{seq_new}) required for regulating the output voltage at a given light load condition. With this result, the corresponding value of external control capacitor (C_{ext}) can be derived. For 100 % Tunability ($\beta = \infty$) a similar condition can be derived as well. Before proceeding with these calculations, the following assumptions are made:

- $\beta_{max} = \frac{R_{ac\_max}}{R_{ac\_opt}}$; where R_{ac_max} is the load resistance across the PT corresponding to minimum load.
- The design is done such that PT sees optimum load resistance at full load.
- It is feasible to have large capacitor value range in external control capacitor. This means $C_{ext\_min} << C_{d3}$ and $C_{seq\_max} = C$.

For any given β_{max}, the maximum value of C_{seq} would be required at light load and minimum value of C_{seq} at full load. If $C_{seq\_max} = C$, then the corresponding minimum value of C_{seq} (C_{seq_min}) can be calculated by rearranging the terms of the equation (27) and is shown in equation (32).

$$C_{seq\_min} = \frac{\left(1+1/\beta_{max}^{\ 2}\right)\cdot C\cdot C_{p1}}{C_{p1}\cdot\left(1+1/\beta_{max}^{\ 2}\right)+C\cdot\left(1-1/\beta_{max}^{\ 2}\right)} \tag{32}$$

For 100 % Tunability, $\beta = \infty$. Substituting this value of β in equation (32)

$$C_{seq\_min} = \frac{C\cdot C_{p1}}{C_{p1}+C} \tag{33}$$

The value of C_{seq_min} obtained from equation (33) is the minimum value of C_{seq} required to achieve 100 % Tunability. We also know from the equivalent circuit that C_{seq} is a parallel combination of C and C_{p2}, given by equation (34). Hence, using equations (34)

and (35) the limiting value of reflected control capacitance required for 100% tunability can be derived. This is shown in equation (35).

$$C_{seq} = \frac{C \cdot C_{p2}}{C_{p2} + C} \tag{34}$$

$$N_2^{\ 2} \cdot C_{d3} \leq N_1^{\ 2} \cdot C_{d2} \tag{35}$$

Range of external capacitor values

The total change in the series capacitance of the LCC tank circuit that can be achieved in a specific design is dependent on the ratio of the series capacitance (C) and the reflected control capacitance (C_{p2}). For a given TPT design, series capacitance (C), is generally fixed and defined by other design parameters. Hence, we can only change the control capacitance by varying the external control capacitance. Since C_{p2} and C are in series, the value of C_{ext} is chosen such that increasing C_{ext} beyond that value would not change the effective series capacitance (C_{seq}) any further. This sets the upper limit of the effective control capacitance. The lower limit is generally set by the inherent control terminal capacitance of the PT (C_{d3}). This value is determined by the design of the control layers in TPT and must be designed keeping in mind the tunability needed. As discussed, if the reflected value of C_{d3} is closer to the value of C, C_{ext} will have more effect on the equivalent series capacitance (C_{seq}). Hence, the lower limit of C_{ext}, for a specific design, should be reasonably smaller than C_{d3} so that, at its minimum value, it does not change the effective control capacitance and maximum tunability can be achieved from the TPT design.

3.6 Input Voltage Regulation

Regulating the output voltage for a range of input values is a requirement for most of the converters. PWM techniques using active clamp have been proposed for PT based converters to achieve load and line regulation [45]. In case of tunable PTs, line regulation can also be achieved by changing the capacitance at the control terminal.

Fig. 3.17 shows the voltage gain characteristics of a TPT at nominal load but minimum and maximum external control capacitor conditions. At the frequency of

operation, the total reduction in the gain which this tunable PT can achieve is 2.37 times of the nominal gain. Hence, a maximum of 2.37x increment from the nominal input voltage range can be regulated by the tunable PT. However, if the load changes along with the input voltage, the range of line regulation reduces as part of the external capacitor range is used for regulating the load changes. This can be seen from Fig. 3.18 where at 50 % load the line input voltage regulation range reduced to 1.54 times the nominal input voltage.

It is of course possible to regulate for both an increase and decrease in the input voltage by choosing a nominal gain in between the extreme values. Based on this analysis, if both line and load regulation is desired, the TPT must be designed for more than 100 % tunability.

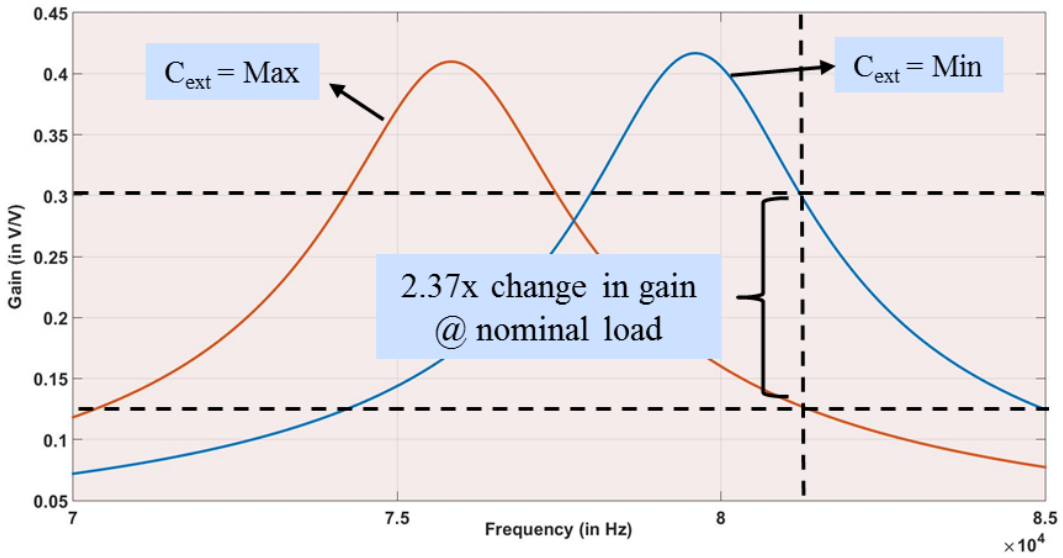

Fig. 3.17. Voltage gain characteristics of a tunable PT at minimum and maximum values of external capacitor for nominal load obtained using SIMPLIS. The change in voltage gain at operating frequency gives the input voltage regulation range.

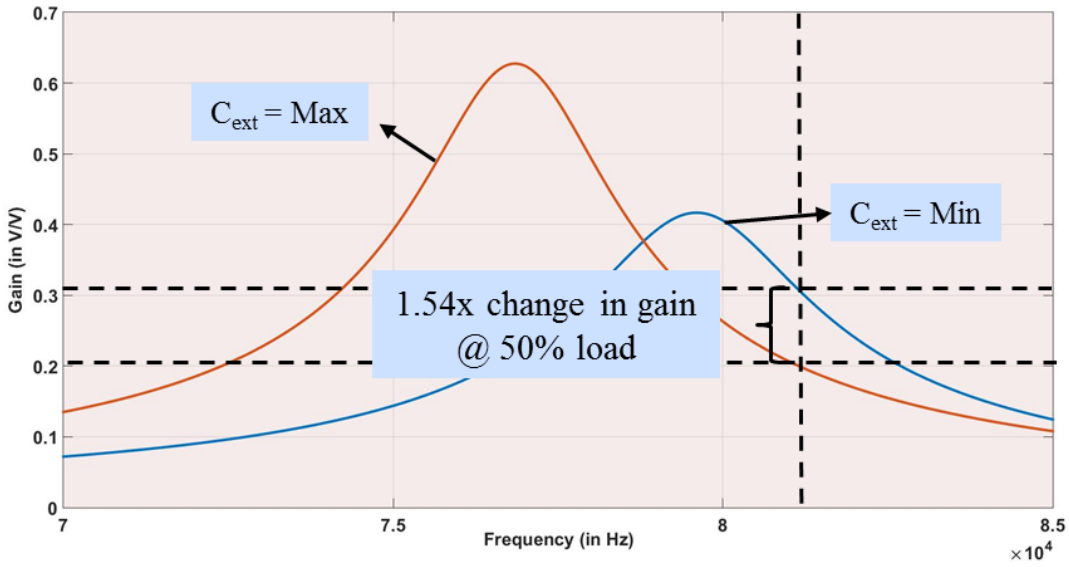

Fig. 3.18. Voltage gain characteristics of a tunable PT at minimum and maximum values of external capacitor for 50% load obtained using SIMPLIS. The change in voltage gain at operating frequency gives the input voltage regulation range.

Chapter 4

Design of DC-DC Converters using Tunable PTs

4.1 Introduction

Due to the band pass nature of the PTs and a high Q, they have been widely used in resonant converter topologies. Resonant power converters offer the potential to be high efficiency, high power density converter as it becomes possible to achieve ZVS in the switches and eliminate significant losses. Hence, achieving ZVS with the PT based resonant converters also becomes a major design criteria. A lot of research has been done with a focus on enabling ZVS in the inverter switches of a PT based resonant converter. Adding extra passive elements, such as inductors [56],[57] and inductor-less solutions reducing the footprint of the converter [58],[10],[11] have been proposed.

For a tunable PT, the design concept is the same. The input side consists of an inverter which converts the DC input voltage into a fixed frequency AC signal. This is fed to the Tunable which, being a band pass filter, passes only the frequencies near its resonance with a certain gain. This AC signal is then rectified by an output rectifier and then given to a load. However, due to different control scheme, design for ZVS conditions for tunable PT differs slightly. Since the operating frequency of the inverter is fixed, verifying the design for ZVS becomes easier. An input series inductor is used to help achieve ZVS and is discussed in detail in section 4.2 [59], [60].

The input driving topology is chosen to be a simple half-bridge and a full bridge rectifier with current load is chosen to rectify the AC output voltage from tunable PT. A design methodology for each these is discussed in this chapter. Since, the focus of this research is to demonstrate the use of tunable PTs in DC-DC converters, detailed analysis and comparison of topologies is not in the scope of work. Previous researches done on

topology analysis and comparison provide a good background to select the topologies for tunable PT.

4.2 Design of Input Inductor

The input impedance characteristics of a PT consists of both capacitive and inductive regions. The inductive property of the PTs is used when they are employed in DC-DC converters. Addition of an additional input inductor in series with the PT helps achieve several purposes [47].

It prevents the higher order harmonics generated by the inverter from entering the PT. This puts less stress on the PT and avoids the excitation of any spurious modes of vibration that might exist in the PT design. Hence, the PT efficiency is improved.

It helps in achieving ZVS in the inverter switches. The input capacitor, C_{d1}, in the PT makes input impedance of PT capacitive in nature over a certain range. Addition of input inductor of appropriate value can offset this nature in the frequency range of interest.

It also helps in suppressing any high frequency common mode noise that might exist in the PT due to its low pass nature [61].

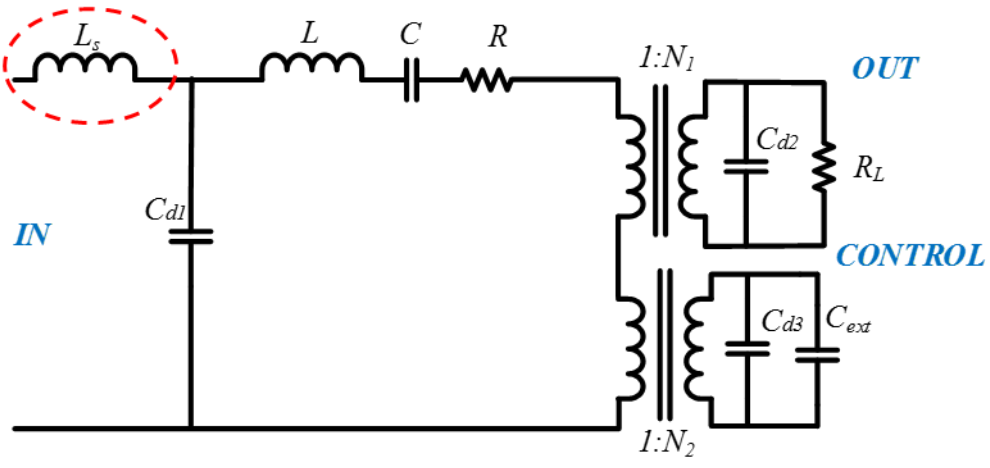

Fig. 4.1. Electrical equivalent circuit of a tunable PT with input inductor.

Fig. 4.1 shows the electrical equivalent circuit of a tunable PT along with the series input inductor L_s. The design of L_s must be done keeping in mind the ZVS condition, suppression of higher order harmonics, maximum input voltage rating of the tunable PT and the voltage gain required [47].

Fig. 4.2 shows the voltage gain characteristics of a tunable PT with different values of L_s. The input series inductor, L_s and C_{d1} form a second order low pass filter which suppresses the higher order harmonics from entering the PT. Hence, a larger L_s value would favor the suppression of higher order harmonics. This can be seen from Fig. 4.2. However, a large input inductor would also interfere with the gain of the tunable PT at the frequency of interest (close to the resonant frequency of the PT). If the frequency of operation is moved far away from the optimum frequency of the tunable PT to get the required gain, then it may affect the efficiency of the tunable PT.

It is also important to note that the L_s-C_{d1} resonant frequency must not be close to the 3rd harmonic frequency of the operation. This may cause short-circuit like conditions for the 3rd harmonic component and would cause large currents to flow through the switches and might cause them to fail. The other important criteria to select the series inductor is ZVS in the inverter switched and will be discussed in the next section.

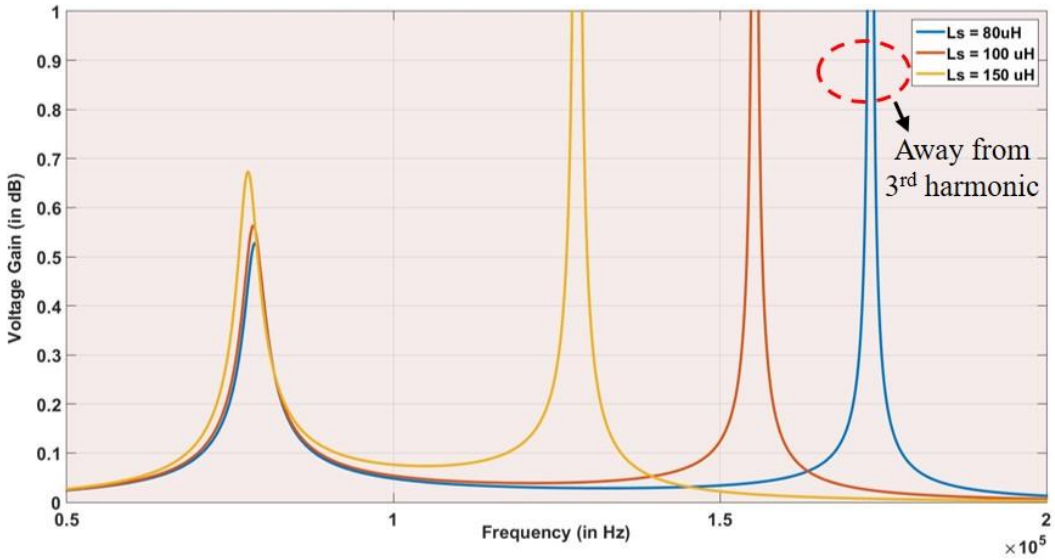

Fig. 4.2. Voltage gain characteristics of the tunable PT with input inductor obtained using SIMPLIS simulations. A second resonance is caused by L_s-C_{d1}.

4.3 ZVS in the inverter switches

For achieving ZVS in the inverter switches, it is important to have the input current to the PT lagging the input voltage. Hence, it is important that the phase of the input impedance is positive in the region of operation. Although, a positive phase of input impedance does not always ensure ZVS in the inverter switches, it is a safe approximation. For certain PT designs, the input capacitance can be high enough such that this region is very limited and does not cover the entire range of frequencies for regulation. An input inductor helps increase the inductive region and makes ZVS easier to achieve in the inverter switches. Although, with an optimized PT design, it is possible to achieve ZVS without having any inductor in the input [62].

For tunable PTs, a similar criterion is required. However, with the proposed method of control (by changing the effective capacitance at control terminal), the frequency of operation remains fixed various loads. Hence, the phase of the input impedance needs to be positive only for that frequency. Even though the frequency of operation is fixed, the input impedance changes with a change in load conditions as the value of effective control capacitance is also changed. Fig. 4.3 shows the imaginary part of the input impedance at various load conditions and L_s = 100 μH for a given TPT design. It can be seen that at the frequency of operation and with L_s = 100 μH, the imaginary part of the input impedance is positive for all the load conditions. This ensures that ZVS is achieved in the inverter switches for all the load conditions.

Note that if the input voltage is also regulated by changing the control capacitance, then input impedance plots must be constructed for all the extreme cases to ensure ZVS operation throughout the input voltage and load range.

Thus, a large inductor also favors the ZVS conditions for the inverter. However, with a large inductor, the converter gets bulkier, the gain of the PT is altered and the input voltage across the PT would increase. Hence, a careful consideration of all the design criteria must be made for selecting an inductor.

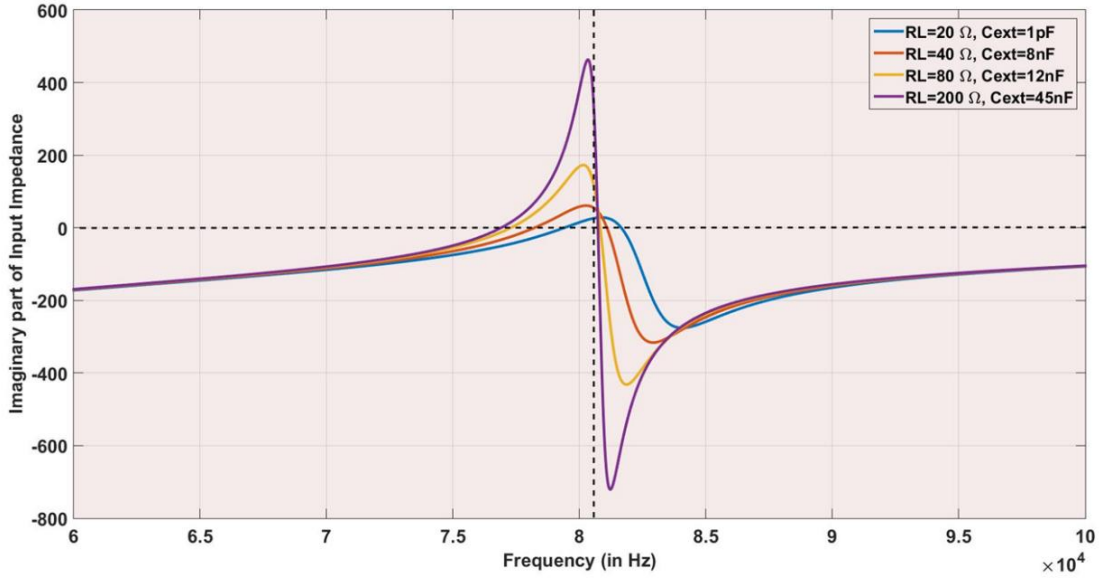

Fig. 4.3. Imaginary part of the input impedance for the tunable PT obtained using mathematical analysis of electrical circuit of the TPT in MATLAB. The imaginary part of the input impedance is positive for all load conditions at the frequency of operation.

4.4 Driving Topology

The function of the inverter topology is to convert the input DC voltage into AC waveform of the required frequency to drive the tunable PT. The efficiency of the PT is improved with a pure sinusoidal input driving the PT [2]. However, producing a pure sine wave requires more components and can increase the size of the converter. Various inverter topologies such as half bridge, single-ended multi-resonant (SE-MR), single-ended quasi-resonant (SE-QR), push-pull inverter and class E inverters can be used to drive the PT. For step down applications, half bridge, SE-MR, class E and push pull topologies are suitable. Half-bridge topology, in comparison with the SE-MR topology gives a higher efficiency and generates less noise compared to the SE-MR and class E topologies. Thus, it is preferred for higher power applications [22],[63].

Considering these arguments, a half bridge inverter is the desired topology for the design of DC-DC converter using tunable PTs. A series inductor is connected between the half bridge and the tunable PT terminals to achieve ZVS in the inverter switches. Fig. 4.4 shows the schematic diagram using a half bridge inverter to drive the TPT. The

switching frequency of the inverter is selected to be the parallel resonant frequency of the LCC tank circuit as given by equation (23).

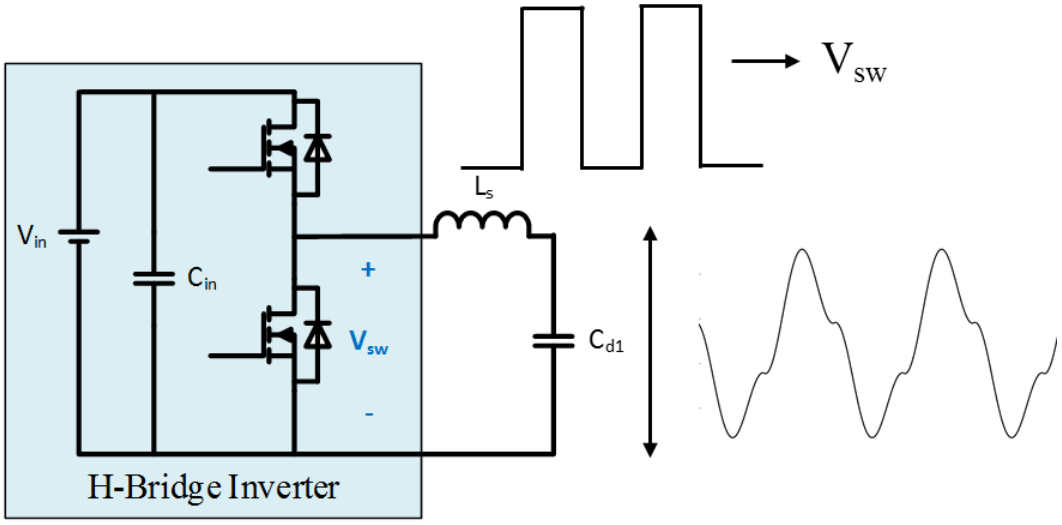

Fig. 4.4. Schematic diagram of a half bridge inverter with a series input inductor. The voltage waveforms at the switch node and across the capacitor C_{d1} are shown as well.

The fundamental frequency component of output voltage from the half-bridge inverter is given by equation (36)

$$V_{sw(1)} = V_{in} * \frac{2}{\pi} * \sin(\omega t) \tag{36}$$

Based on the design of L_s and the input impedance characteristics of the tunable PT, certain level of high frequency might enter which would cause the input voltage at the PT to be not a pure sinusoid, as shown in Fig. 4.4. A fixed amount of dead time is added to the circuit which helps prevent any short circuit across the input power supply and ensures there is enough time for the output capacitors of the MOSFET to be discharged by the input inductor current. The half-bridge circuit is driven with a fixed frequency and a fixed duty cycle.

4.5 Comparison of Rectifier Topologies

The voltage seen at the output terminals of the tunable PT is sinusoidal due to its high Q band pass characteristic. This voltage can be rectified using various rectifier topologies. The selection of a rectifier topology would depend on the application and the gain required. Each rectifier topology along with a filter, loads the output terminals of the tunable PT with an equivalent AC resistance. This AC resistance can be used as the load resistance across the tunable PT to derive the gain equations. Fig. 4.5 shows some of the rectifier circuits with the output filters and their equivalent AC resistance [22]. These are derived under the assumptions that the input voltage to the rectifier is purely sinusoidal and the output current is a constant DC value.

Rectifier circuits also affect the efficiency of the overall converter. The diodes in the rectifier circuits are a major source of losses in the converter and can deteriorate the efficiency of the converter significantly. Full-bridge rectifiers, consisting of twice the number of diodes compared to the current doubler and half way rectifier, can cause more losses compared to the other rectifiers. The equivalent AC load seen by the tunable PT is also different for each topology of the rectifier. Current-doubler rectifier requires a smaller load resistance across the rectifier compared to the full bridge rectifiers for the same AC load resistance seen by the tunable PT. This means that higher power can be achieved in current-doubler at lower output voltages. Hence, this circuit is suitable for low voltage, high current applications [64]. However, the design of current doubler must be done considering both the overlapping modes and non-overlapping modes [65]. A current-doubler rectifier also requires two output filter inductors. Depending on the converter, these can be big and hence would increase the weight and size of the converter.

Full bridge rectifier with current load also amplifies the load resistance across its terminals whereas a tunable PT with full bridge rectifier with voltage load sees a smaller equivalent AC resistance for the same load resistance. Hence, for the same output power, full bridge rectifier with current load will have lower output voltage. For higher powers, a more efficient rectifier design with MOSFETs and a center-tapped output must be considered in the future.

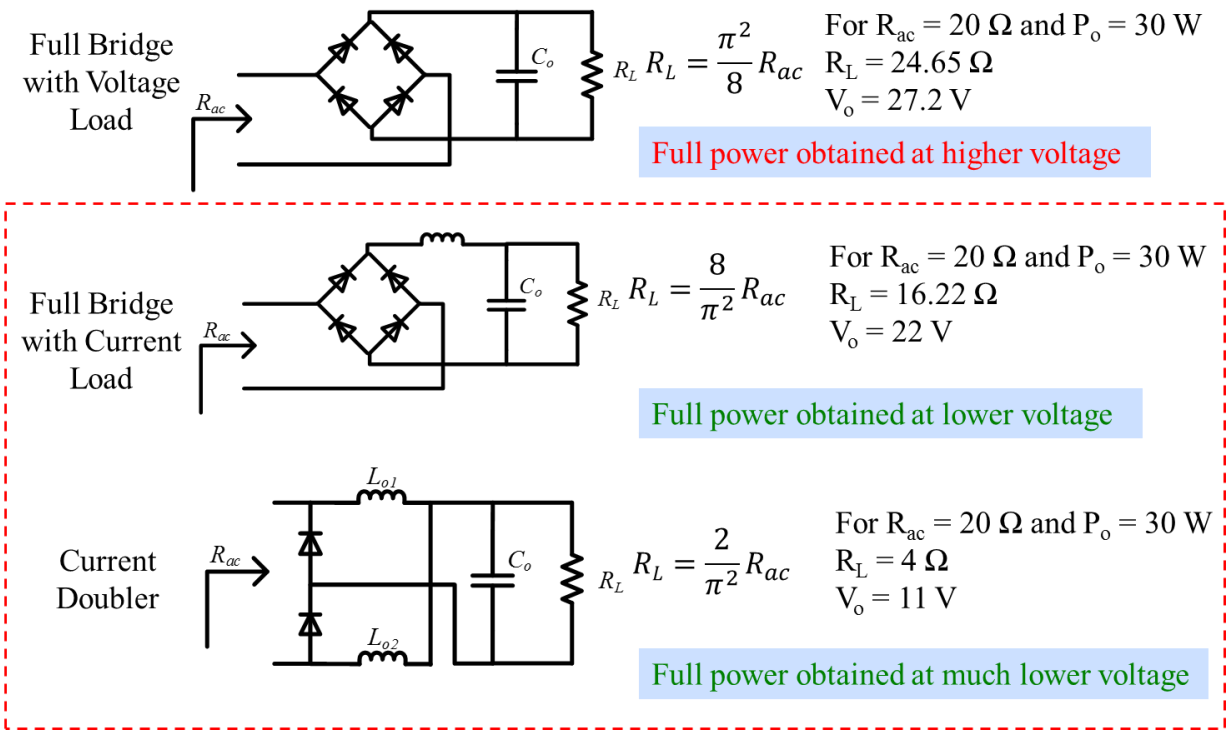

Fig. 4.5. A comparison of output rectifier topologies. The effective load resistance seen by PT for each rectifier topology has been shown and an example for a given power has been presented.

4.6 Implementation of a variable capacitor: Switched Capacitor PWM Control

To enable smooth regulation of output voltage over a range of load, it is envisioned to have a 'variable' capacitor at the control terminal. With a fine control over this external capacitor, smooth regulation of output voltage can be achieved. To implement such a capacitor, a switched capacitor circuit with a duty cycle control is used at the control terminal [66]. Similar ideas have been used in the past to implement a fixed frequency control of LLC converter by varying the capacitor of the tank circuit [67],[68].

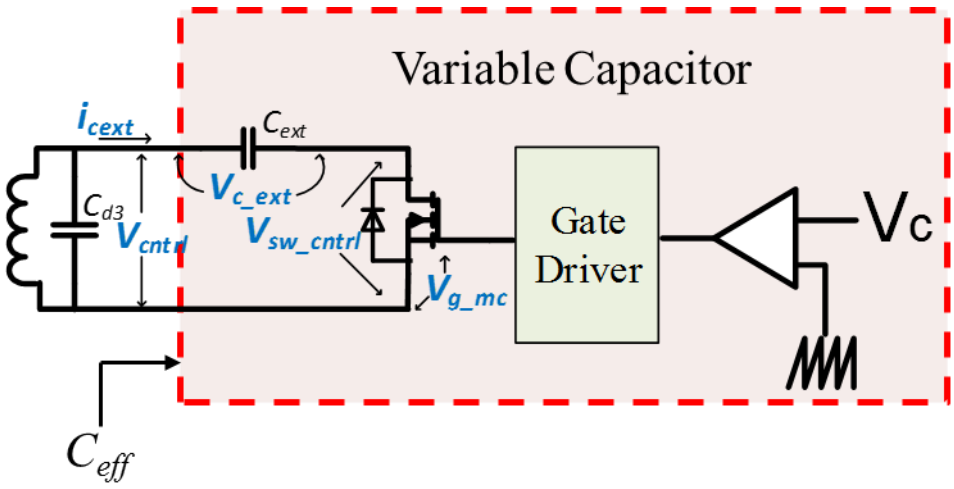

Fig. 4.6. Electrical schematic for implementation of a variable capacitor. A fixed capacitor (C_{ext}) is connected in series with a switch which can be used to control the effective value of the fixed external capacitor.

The schematics of the control terminal along with the proposed scheme is shown in Fig. 4.6. The control terminal consists of a fixed capacitor in series with a switch. The value of the capacitor can now be controlled by controlling the switching instant and the duty cycle of this control switch. Due to the band-pass filter characteristic of the TPT, the voltage waveform seen at the control terminal is sinusoidal in nature. The turn-on of the MOSFET (M_c) is synchronized to the zero crossing of the current in the control terminal. The waveforms shown in Fig. 4.7 are after steady state has been reached. The detailed operation of the control circuit with the waveforms is explained below [66].

Mode $t_0 – t_1$: At t_0, the control MOSFET (M_c) is switched ON and the current at the control terminal starts charging the external capacitor. During this time interval, the external capacitor is connected to the control terminal and contributes to the effective value of the control capacitance.

Mode t_1-t_2: At t_1, the switch is turned OFF. At this instant, the external capacitor is disconnected from the control terminal and its voltage is maintained constant at V_{cext}. On the other hand, the voltage across the internal control capacitor (C_{d3}) follows the input voltage and continues to rise.

Mode $t_2 – t_3$: At t_2, the control voltage (V_{cntrl}) falls below V_{c_ext} and the external cap can now discharge with the anti-parallel diode of the MOSFET. The negative

current flowing through the diode of the control MOSFET enables zero voltage switching (ZVS) at the control switch. At t_3, the next switching cycle begins.

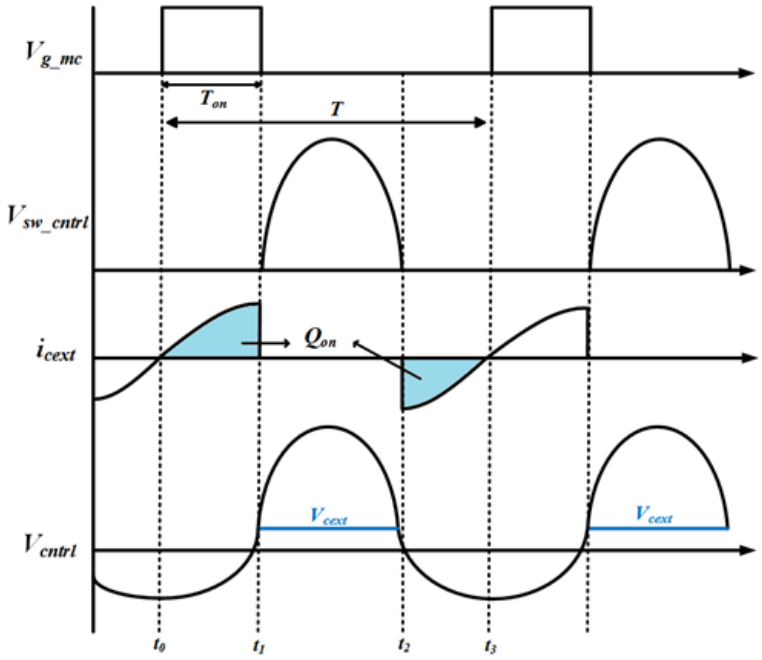

Fig. 4.7. Waveforms of the various electrical parameters of the control circuit.

Based on the charging and discharging time of the external capacitor, the effective value of the capacitor can be determined. The effective value of the capacitance can be derived by assuming the sinusoidal nature of the current. The equation (37) shows the value of effective external capacitance.

$$C_{eff} = \frac{\Delta Q_{on}}{Q_{tot}} \cdot C_{ext} = \frac{1-\cos(2\pi D_{Mc})}{2} \cdot C_{ext} \tag{37}$$

Based on the equation (37), we can vary the duty cycle of the control MOSFET, $D_{Mc}=T_{on}/T$, from 0–0.5 to achieve full range of capacitor values. It is important to note that the sinusoidal current assumption does not hold true for very small duty cycles as the current through the external capacitor becomes triangular and so, the effective capacitance is no longer a cosine function.

4.7 Closed Loop Design: Voltage mode control

Traditionally, the regulation of output voltage in the resonant topologies has been done using frequency control. Since PTs have been widely used in resonant topologies, such control methods have been proposed for PT too. For achieving both load and line regulation, PWM control and a combination of PWM and PFM control has also been suggested [51]. For the inductor-less PT designs, dead time becomes an important design parameter to achieve ZVS. It is also important that the phase of the current is always lagging the voltage throughout the load conditions. Control schemes have also been proposed which monitor the phase angle of the input current to ensure ZVS [53] and which optimize the dead time between the inverter switches to ensure ZVS and high efficiency [69].

For a PT, moving the frequency away from the optimum point can deteriorate the efficiency of the PT. Hence, it desirable to operate the PT at a fixed frequency. Some control strategies have been suggested which allow fixed frequency operation of the PT, however, the quantum resonant control suggested makes the output voltage a combination of low frequency and high frequency component. This makes filtering difficult [59].

The design of tunable PT based DC-DC converter along with the variable capacitor at the control terminal helps solve this problem. The output voltage regulation for a tunable PT can be done by changing the capacitance at the control terminal. Using the variable capacitor implementation discussed in section 4.6, a simple PWM control can be used to regulate the output voltage. Fig. 4.8 shows the complete electrical schematic of the tunable PT with voltage mode control. The voltage is sensed using a resistor divider sensing network and compared with a reference voltage using a compensator. The error from the compensator produces a duty cycle at PWM controller which regulates the output voltage. Hence, regulation of the output voltage can be achieved by traditional PWM control which is easy to implement. The control scheme also does not require any isolation in the feedback circuit as there is no control in the primary side. This reduces the number of components needed in the feedback circuit.

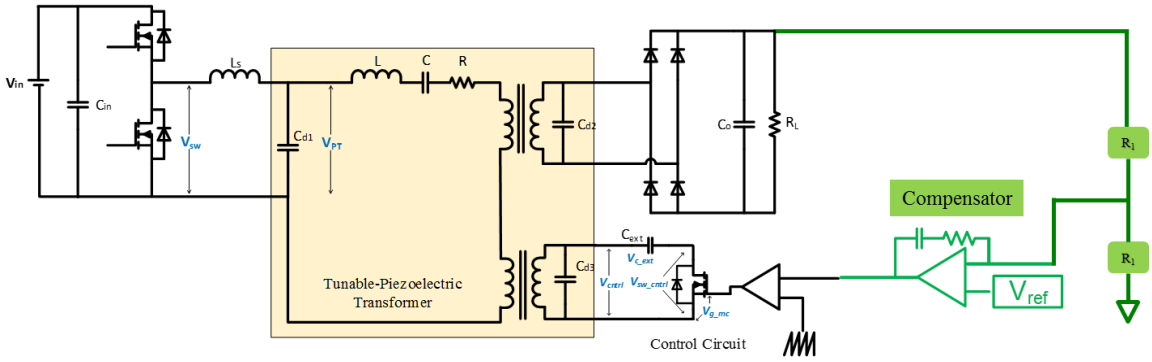

Fig. 4.8. Complete electrical schematic of a tunable PT based DC-DC converter.

4.8 Design of Compensator

The design of the compensator can be done by studying the open loop control to output transfer function of the plant. For the proposed control scheme, an AC signal is injected in the DC reference of the PWM circuit and the output voltage is recorded for a range of frequencies. This can be implemented in a software like SIMPLIS to derive the control to output plant characteristics. Fig. 4.9 shows the control to output characteristics of a tunable PT. The plant has a low frequency pole and a double pole due to which the phase drops sharply around that frequency. For such characteristics, a type II compensator can be used to close the loop and achieve the required close loop characteristics.

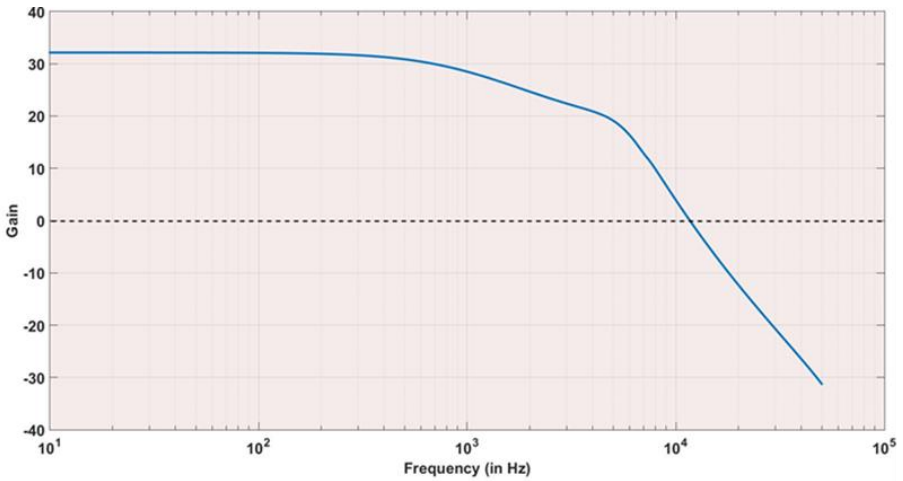

(a)

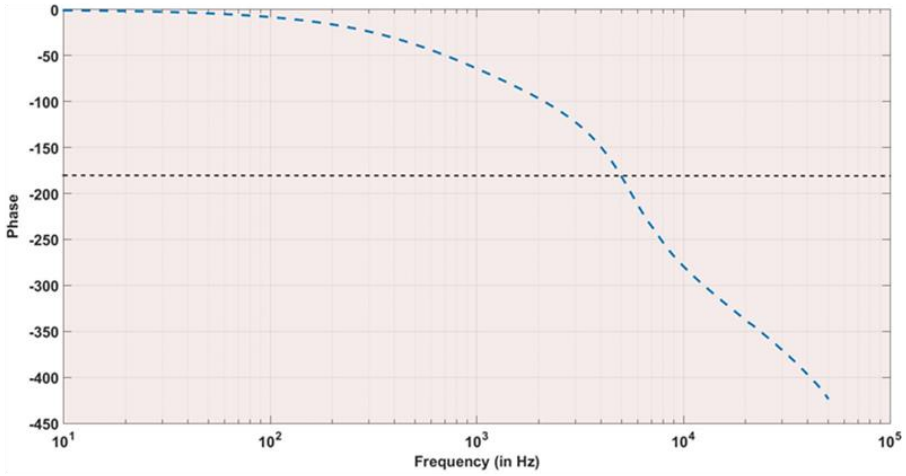

(b)

Fig. 4.9. Open loop control to output small signal characteristics of a tunable PT with switched capacitor PWM control as obtained from simulations using SIMPLIS.

Fig. 4.10 shows an implementation of a type II compensator using operational trans-conductance amplifier. A pole is placed at low frequency to achieve low steady state error and high DC gain. A zero is placed near the plant pole frequency to provide the necessary phase boost. A high frequency pole is placed at frequencies above the desired bandwidth to attenuate the high frequency noise.

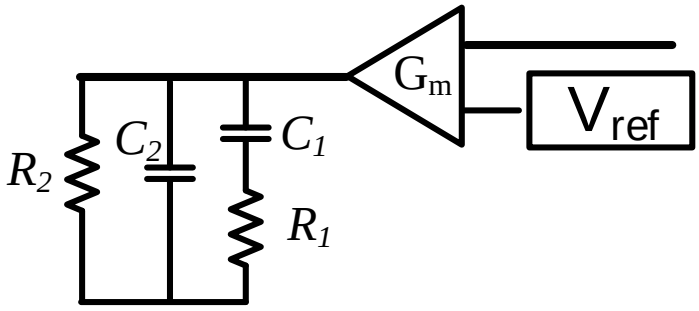

Fig. 4.10. Implementation of a type II compensator using operational trans-conductance amplifier.

The loop gain characteristics of the closed loop converter is shown in Fig. 4.11. For the given design, the following specifications were achieved:

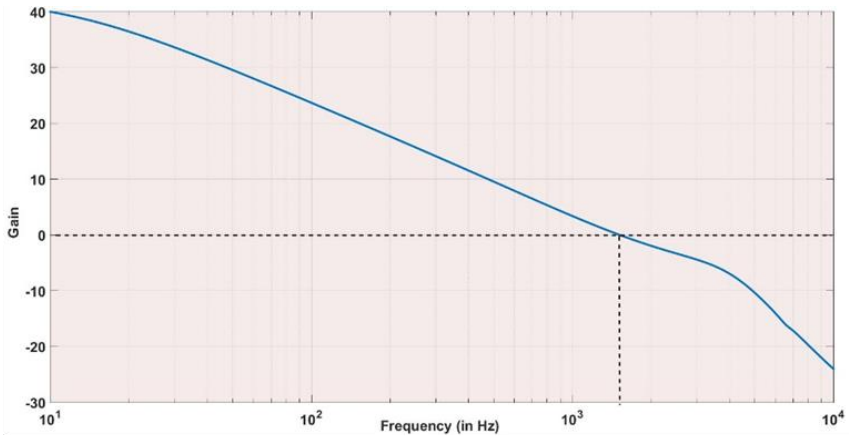

(a)

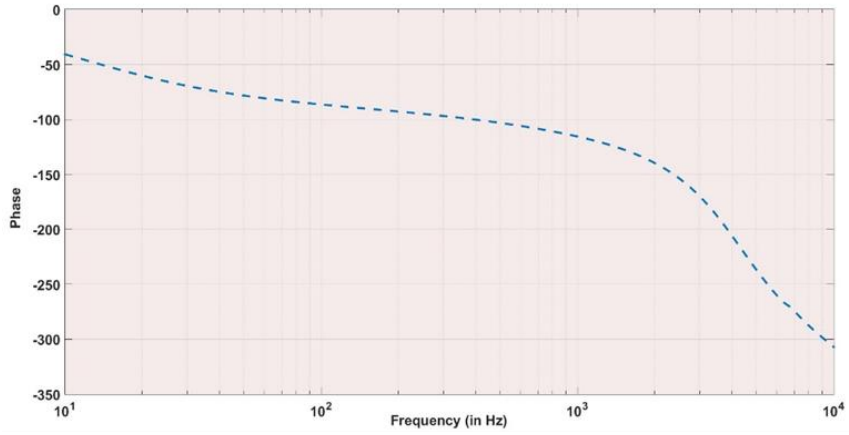

(b)

Fig. 4.11. Closed loop gain of tunable PT with voltage mode control using switched capacitor PWM control obtained using SIMPLIS simulations. Good bandwidth and phase margins can be achieved using the proposed design.

Chapter 5

Hardware Design and Results

5.1 Introduction

With the analysis and design of the tunable PTs presented before, a hardware prototype was developed to verify the results. Two tunable PTs were tested, namely, Gen 2 and Gen 3 TPT. The concept of tunability was introduced in chapter 3 and the two important ratios, namely C/C_{p2} and C_{seq}/C_{p1}, were discussed which affect the tunability. Two different physical designs of the tunable PT with different tunability will be discussed here. Both the tunable PTs have the same power and hence use the same diameter discs. However, a difference in the number and thickness of the layers changes the equivalent circuit of the tunable PT. The differences between the electrical equivalent circuit, their effect on the performance of the tunable PT and the difference in the structure, which causes that, is discussed. The experimental results from the hardware prototype developed using the two tunable PTs are also presented.

The complete physical design details of the tunable PT design are out of scope for this research. However, with the comparative analysis of two different TPT designs, a qualitative assessment of the physical TPT design on the performance can be done. This can help a designer to design tunable PT to meet a certain circuit performance criteria.

5.2 Electrical Equivalent Circuit and Structure

The structural differences between a tunable PT and a standard PT were presented in Chapter 3. The addition of a control layer makes the tunable PT a three-terminal device with an additional control section which has been used, in this case, to control the resonant frequency of the PT and hence regulate the output voltage. The design goals of the control section were discussed in section 3.5 which would help achieve the desired

tunability in the tunable PT. Expanding on those designs and with the two ratios, C/C_{p2} and C_{seq}/C_{p1}, reference designs of two tunable PTs are discussed.

Error! Reference source not found. compares the physical structure of the Gen 2 and Gen 3 tunable PT. The number of control layers, output layers and the thickness of each layer is shown in the figure as well. For the given design, the corresponding electrical equivalent circuits are shown in Fig. 5.2.

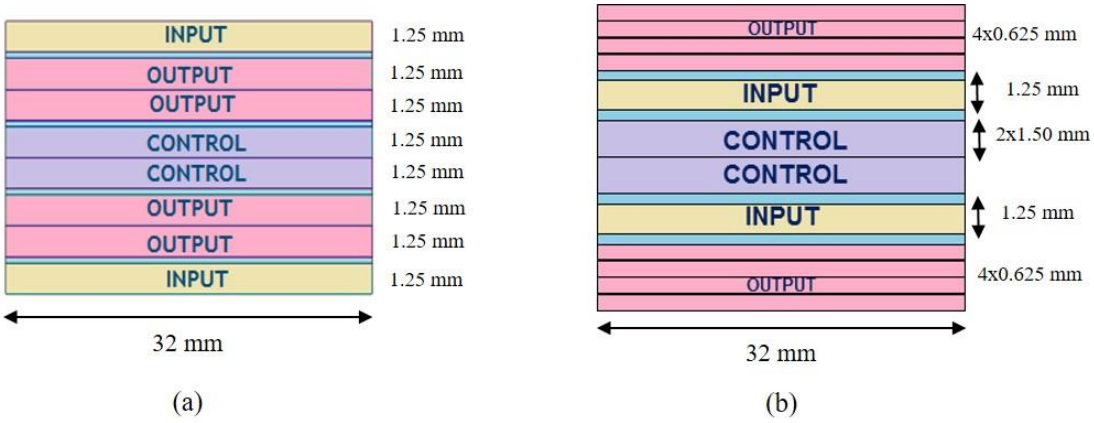

Fig. 5.1. (a) Physical structure of the Gen 2 TPT and (b) physical structure of the Gen 3 TPT.

Gen 2 tunable PT has output layers sandwiched between the two input layers. This design provides a symmetrical structure to the PT and helps in the suppression of spurious bending modes [3]. All the ceramic layers are made of thickness polarized hard Navy type III piezoelectric material with a diameter of 32mm and a thickness of 1.25mm. An insulation layer is added between the input, output and control sections to provide a galvanic isolation between all the terminals. The electrical connections are made on the surface of each layer using metallic electrodes. The given design has a power handling capacity of 30 W.

Gen 3 tunable PT structure uses the same material discs with the same diameter. Hence, the power level is also the same as Gen 2 tunable PT, i.e. 30 W. However, in this case, the number of output layers have increased. This structure uses 8 output layers of 0.625mm thickness each. The output section is split into two halves of 4 layers each and it sandwiches the input and control sections in between. Even though the layout of the

layers is different, the symmetry of the structure has been retained. The control layers are thicker for this design.

The qualitative impact of the physical designs on the electrical equivalent circuit can now be discussed. Fig. 5.2 compares the electrical equivalent circuit of the Gen 2 and Gen 3 tunable PT.

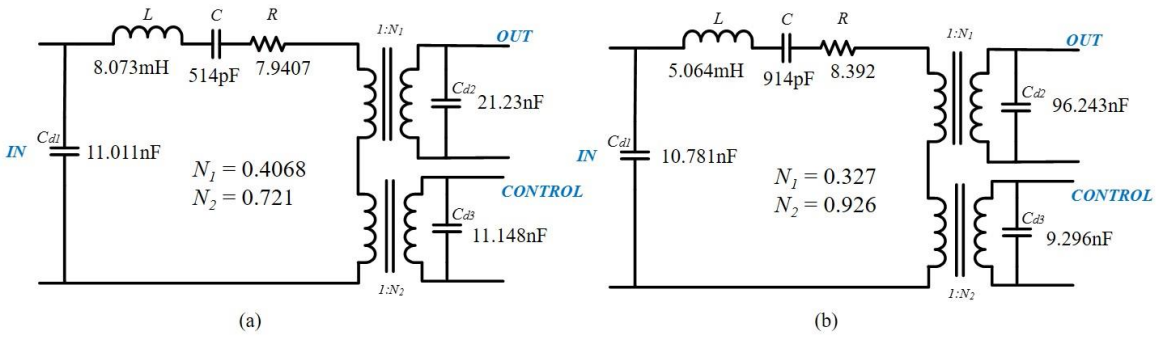

Fig. 5.2. (a) Electrical equivalent circuit of the Gen 2 TPT and (b) electrical equivalent circuit of Gen 3 TPT.

Thinner and larger number of output layers provide a higher output capacitance and smaller step down ratio (N_1) to the Gen 3 tunable PT. The optimum load for each tunable PT can be calculated using (38). Due to this, the optimum load resistance for Gen 3 tunable PT is lower than that of Gen 2 tunable PT. Table 5.1 compares the optimum load for Gen 2 and Gen 3 tunable PT.

$$R_{Lopt} = \frac{1}{\omega * C_{d2}} \tag{38}$$

TABLE 5.1 COMPARISON OF OPTIMUM LOADS OF GEN 2 AND GEN 3 TPT

Electrical Parameter	Gen 2 TPT	Gen 3 TPT
Optimum Load	85 Ω	20 Ω

Because of the lower optimum load resistance, the Gen 3 tunable PT can operate at lower voltages for the same amount of power. Hence, Gen 3 physical design gives higher step down ratios compared to Gen 2. Thicker control layers reduce the control capacitance, and it can be seen from the electrical equivalent circuit.

5.3 Tunability

The simplified equivalent circuits of Gen 2 and Gen 3 tunable PTs are shown in Fig. 5.3

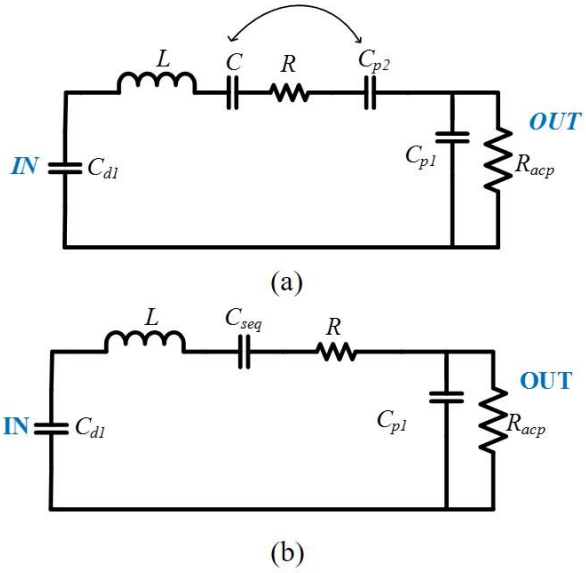

Gen 2 TPT	Gen 3 TPT
L = 8.073 mH	L = 5.064 mH
C = 514 pF	C = 0.914 nF
R = 7.9407 Ω	R = 8.392 Ω
C_{p2} = 5.8 nF	C_{p2} = 7.97 nF
C_{p1} = 3.51 nF	C_{p1} = 10.291 nF
C_{seq} = 0.472 nF	C_{seq} = 0.82 nF

Fig. 5.3. The simplified electrical equivalent circuits of a tunable PT. The corresponding electrical circuit parameter values for Gen 2 and Gen 3 TPT are given for comparison.

Tunability of a tunable PT design was discussed in section 3.5 and the effect of two ratios on tunability was elaborated. The ratios for the Gen 2 and Gen 3 tunable PT are compared in Table 5.2.

TABLE 5.2 COMPARISON OF TUNABILITY RATIOS OF GEN 2 AND GEN 3 TPT

Electrical Parameter	Gen 2 TPT	Gen 3 TPT
C/C_{p2}	0.0887	0.1147
C_{seq}/C_{p1}	0.1344	0.0797

A larger C/C_{p2} ratio in Gen 3 tunable PT provides more shift in the resonant frequency when the external control capacitor is increased from a minimum to a maximum value. Fig. 5.4 compares the shift in the resonant frequency for Gen 2 and Gen 3 tunable PTs for the same minimum and maximum values of C_{ext} (10 pF and 100 nF) and at optimum load.

In addition, a smaller C_{seq}/C_{p1} for Gen 3 tunable PT corresponds to a smaller difference in the series resonant and parallel resonant frequency. Fig. 5.5 shows the shift the resonant frequency of the tunable PTs when the load is decreased from its nominal value to 10% of nominal load. Since the shift in Gen 3 tunable PT is smaller, it would require smaller change in the C_{seq} to regulate the output voltage through that range. It is important to note that the reduction in resonant frequency required to regulate through the load range is larger than the shift in resonant frequency from light load to full load.

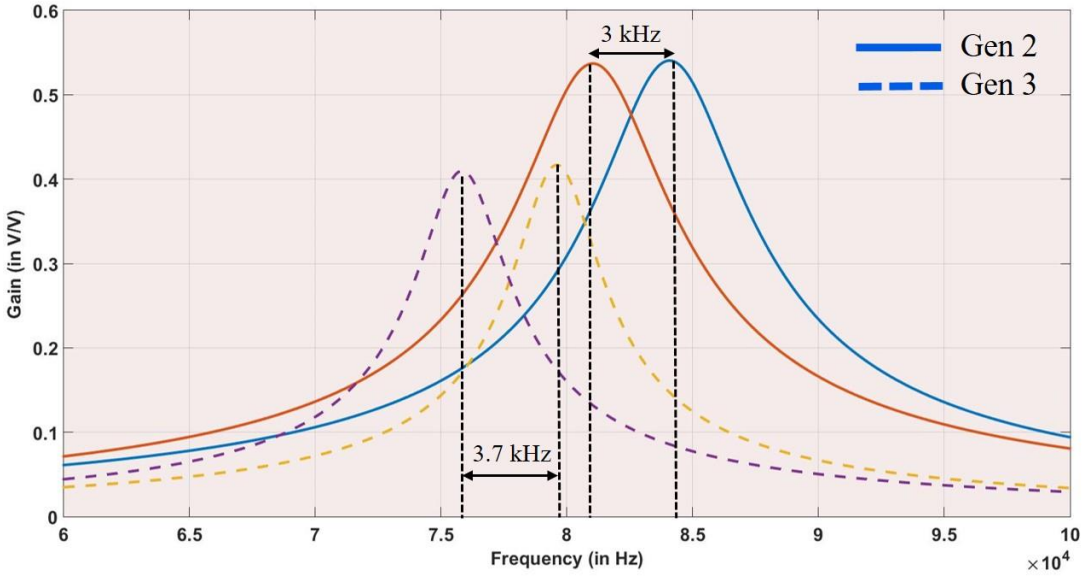

Fig. 5.4. Shift in resonant frequency of the Gen 2 and Gen 3 TPT designs for minimum and maximum value of C_{ext} at optimum load obtained using SIMPLIS. This is dependent on the ratio C/C_{p2}.

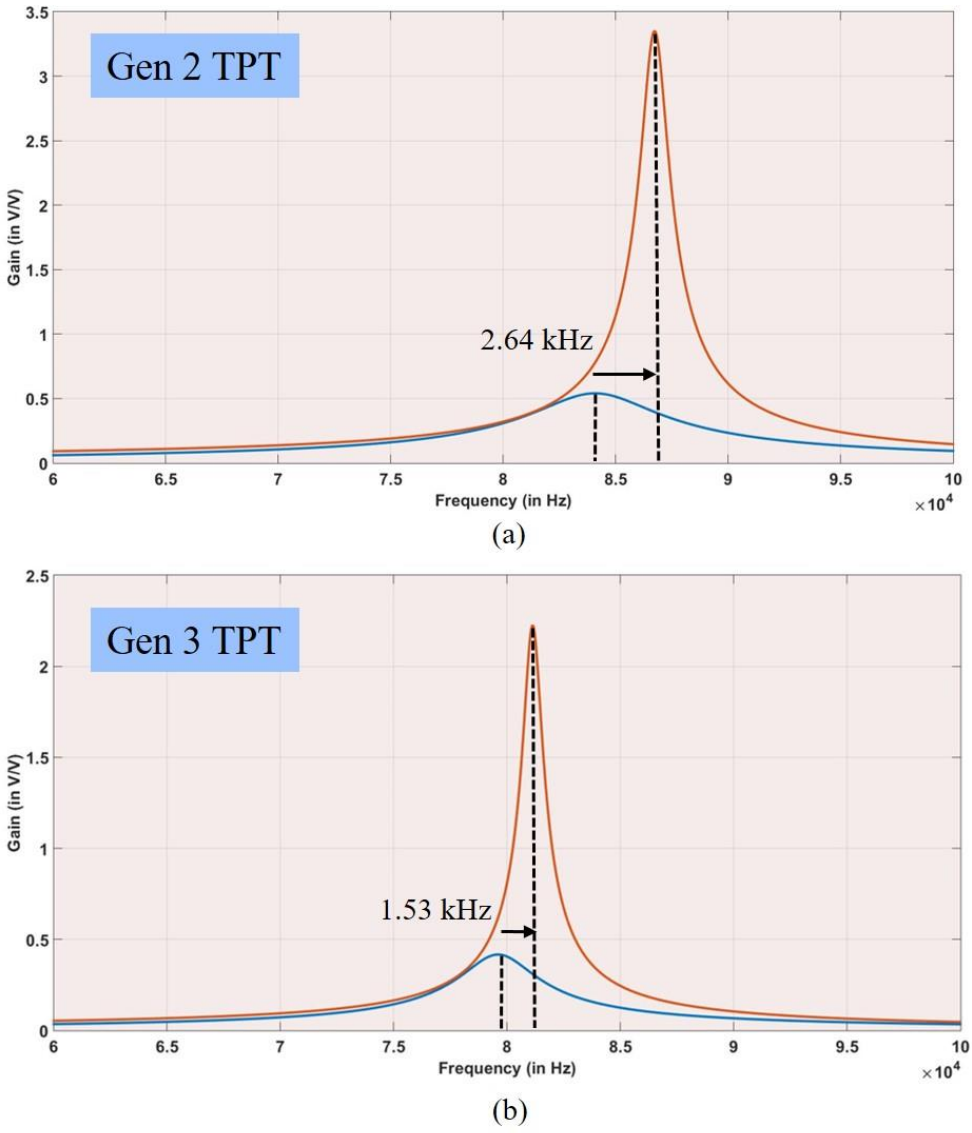

Fig. 5.5. Shift in the resonant frequency for (a) Gen 2 TPT and (b) Gen 3 TPT from nominal load to 10% load obtained using SIMPLIS. This is dependent on the ration C_{seq}/C_{p1}.

The condition for tunability established earlier can be used to check for tunability in the given designs. The Table 5.3 below summarizes the results from the test.

TABLE 5.3 COMPARISON OF TUNABILITY CONDITION FOR GEN 2 AND GEN 3 TPT

TPT	$N_1^2*C_{d2}$	$N_2^2*C_{d3}$	100% Tunable?
Gen 2	3.51 nF	5.79 nF	No
Gen 3	10.291 nF	7.97 nF	Yes

The calculations in Table 5.3 show that Gen 3 TPT has 100 % tunability while Gen 2 TPT doesn't. In both scenarios, further design information is needed for design. In this analysis, one of the assumptions was that large range of C_{ext} is possible. This may not be practically implementable. Hence, for Gen 3 TPT, since the tunability is 100%, the minimum value of C_{ext} required to achieve tunability can be calculated using equations (39) - (41). This is found to be C_{ext_FT} = 32.136 nF. Hence, the maximum shift possible with the chosen C_{ext} values (10 pF and 100 nF) is more than what is required for 100 % tunability. The designer can choose to go with a smaller value of C_{ext}, as that would give a finer control to the effective value of the capacitor. In this case, C_{ext} = 100nF is chosen as the 'extra' control can help in input voltage regulation.

For Gen 2 TPT, the value of C_{ext} is chosen such that the transformer control 'saturates' beyond that value as discussed in the previous sections.

$$C_{seq\_FT} = \frac{C_{p1} * C_{seq\_\min}}{C_{p1} - C_{seq\_\min}} \tag{39}$$

$$C_{p2\_FT} = \frac{C * C_{seq\_FT}}{C - C_{seq\_FT}} \tag{40}$$

$$C_{ext\_FT} = \frac{C_{p2\_FT}}{N_2^{\,2}} - C_{d3} \tag{41}$$

A suitable value of the external control capacitor (C_{ext}), for this design, was found to be 100 nF. With the proposed duty cycle control this can give a wide range of capacitor values. If the design is such that the optimum load is the maximum load for a converter, then the lowest value of β will be 1. At the same time, the maximum value of β would correspond to the light load condition beyond which converter is unable to regulate the output voltage by changing the control capacitance. Hence, the theoretical value of β_{max} and tunability and be calculated by the equations (42) and (43) respectively. It is important to note that equations (42) and (43) are only valid for designs with tunability ≤ 100%.

$$\beta_{\max} = \frac{1}{\sqrt{\left[\frac{2(C_{seq\_\min} * C_{seq\_\max})}{(C_{seq\_\min} + C_{p1})(C_{seq\_\max} - C_{seq\_\min} * C_{p1})}\right]} - 1} \tag{42}$$

$$\text{Tunability} = \left(1 - \frac{1}{\beta_{\max}}\right) * 100 \tag{43}$$

Table 5.4 compares the theoretical tunability of the PTs calculated using the equations.

TABLE 5.4 COMPARISON OF CALCULATED TUNABILITY OF GEN 2 AND GEN 3 TPT.

Electrical Parameter	Gen 2 TPT	Gen 3 TPT
Tunability	45.72 %	100 %

5.4 Voltage Gain Characteristics

The voltage gain characteristics for Gen 2 and Gen 3 tunable PT, obtained by simulating the lumped electrical equivalent circuit, are shown in Fig. 5.6. As expected from the calculations, the voltage gain can be maintained constant at a specific frequency for 45 % load variation in Gen 2 TPT and for 100 % load variation in Gen 3 TPT. The operating frequency, voltage gain of tunable PT, and the value of external control capacitance needed for a given load can be calculated using the mathematical equations presented in the previous chapters. Table 5.5 summarizes the results for Gen 2 and Gen 3 tunable PT.

TABLE 5.5 COMPARISON OF CALCULATED OPERATING FREQUENCY AND GAIN FOR GEN 2 AND GEN 3 TPT

Electrical Parameter	Gen 2 TPT	Gen 3 TPT
Operating Frequency	86.77 kHz	81.15 kHz
Gain	0.4	0.3132

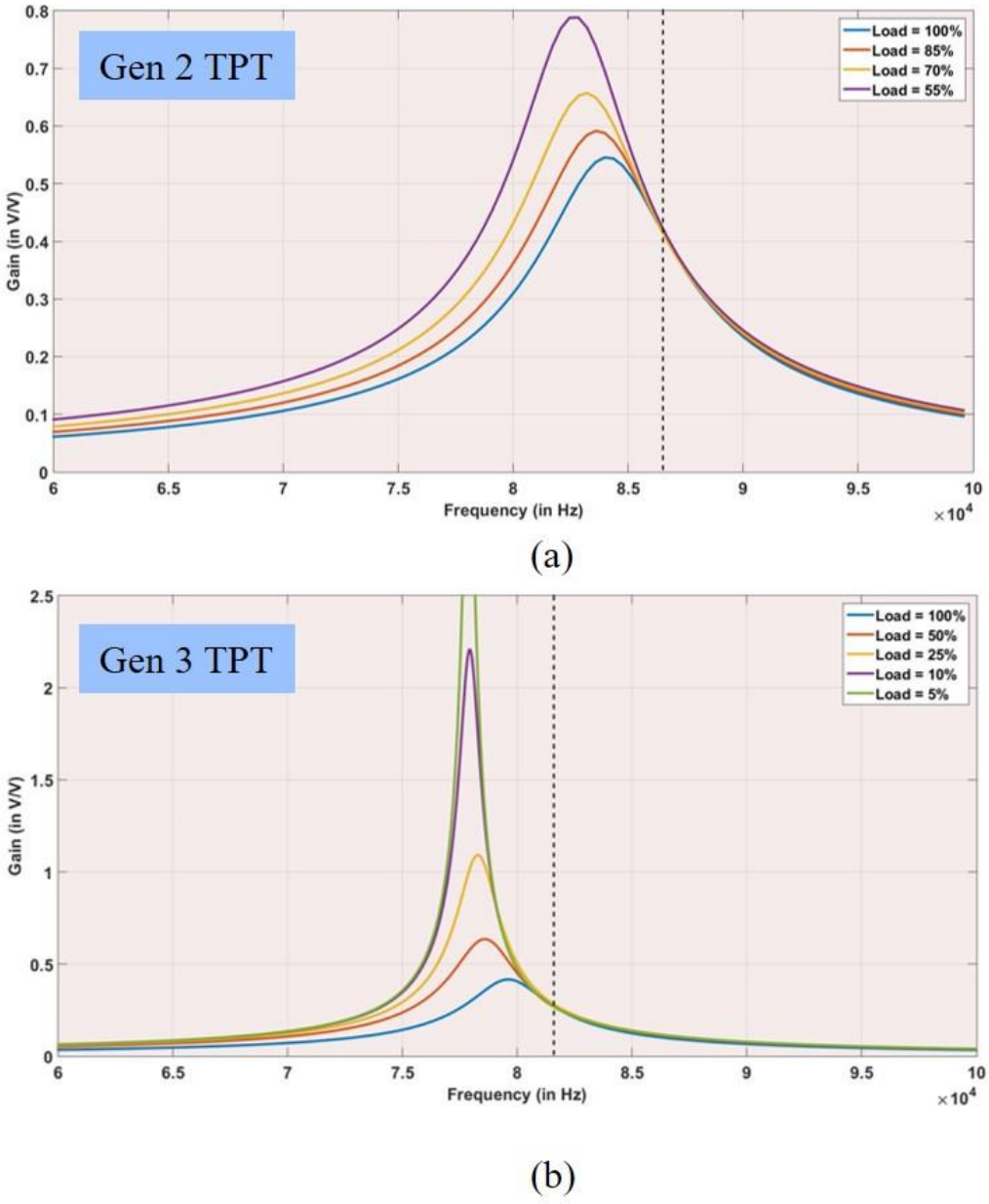

Fig. 5.6. Voltage gain characteristics for (a) Gen 2 TPT and (b) Gen 3 TPT at various load conditions and the corresponding value of C_{ext_new} obtained using SIMPLIS.

5.5 Design of DC- DC Converter

The design of the DC-DC converter for both Gen 2 and Gen 3 tunable PT was done as per the steps discussed in chapter 4. An input inductor of 100 µH was used for both Gen 2 and Gen 3 tunable PTs. The rectifier topology for Gen 2 was chosen to be a full bridge rectifier with voltage load due to higher output voltage and lower output currents.

The design of the voltage mode control was done using the type II compensator. The rectifier for Gen 3 was chosen to be a full bridge rectifier with current load. Fig. 5.7 and Fig. 5.8 shows the complete electrical schematic of the two DC-DC converters.

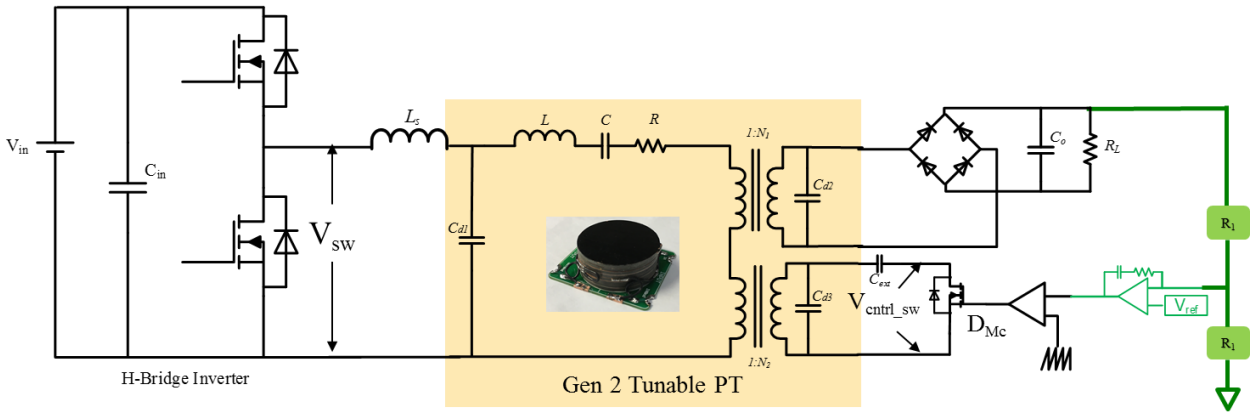

Fig. 5.7. Complete electrical schematic for Gen 2 TPT based DC-DC converter.

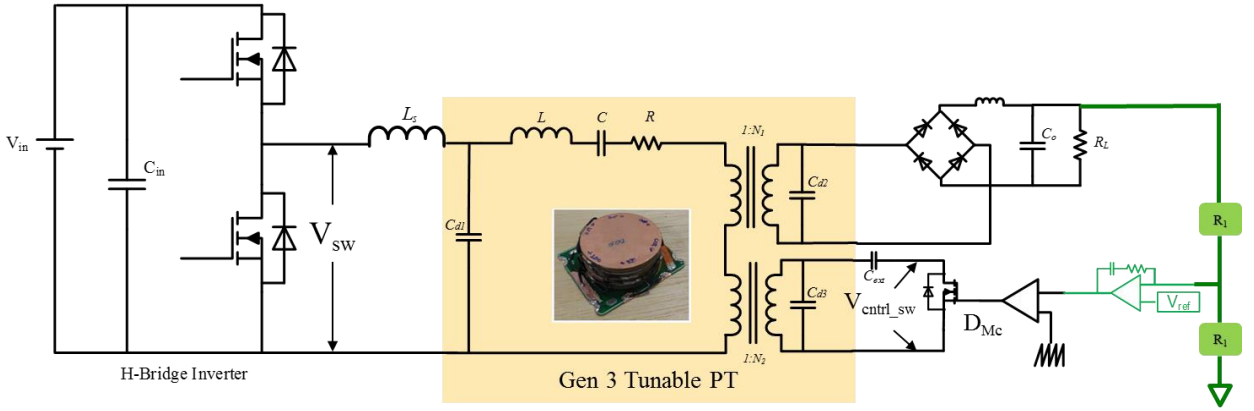

Fig. 5.8. Complete electrical schematic for Gen 3 TPT based DC-DC converter.

To test the tunable PTs at full power and ensure the highest efficiencies at nominal operating conditions, the input voltage is determined by the total power delivered by the tunable PT at optimum load conditions. The Table 5.6 and Table 5.7 summarizes the final specifications of the converter developed using Gen 2 and Gen 3 tunable PTs respectively.

TABLE 5.6 SPECIFICATIONS OF THE DC-DC CONVERTER WITH GEN 2 TPT.

Electrical Parameter	Value
V_{in}	220 V
V_o	55 V
Power	30 W – 16 W
R_L	85 Ω
F_{sw}	82.5 kHz

TABLE 5.7 SPECIFICATIONS OF THE DC-DC CONVERTER USING GEN 3 TPT.

Electrical Parameter	Value
V_{in}	173 V
V_o	24 V
Power	30 W – 1 W
R_L	20 Ω
F_{sw}	81.2 kHz

The switching frequency used in the experiments for Gen 2 tunable PT is different from that obtained using the calculations. This is due to an error in the electrical equivalent circuit. A more accurate method for extracting the electrical equivalent circuit was used in case of Gen 3 tunable PT.

5.6 PCB Layout and design

A common board design for both tunable PTs was used. The Fig. 5.9 shows the layout of the power components and the placement of the radial mode tunable PT. The tunable PT was mounted on the main converter PCB board to minimize the footprint.

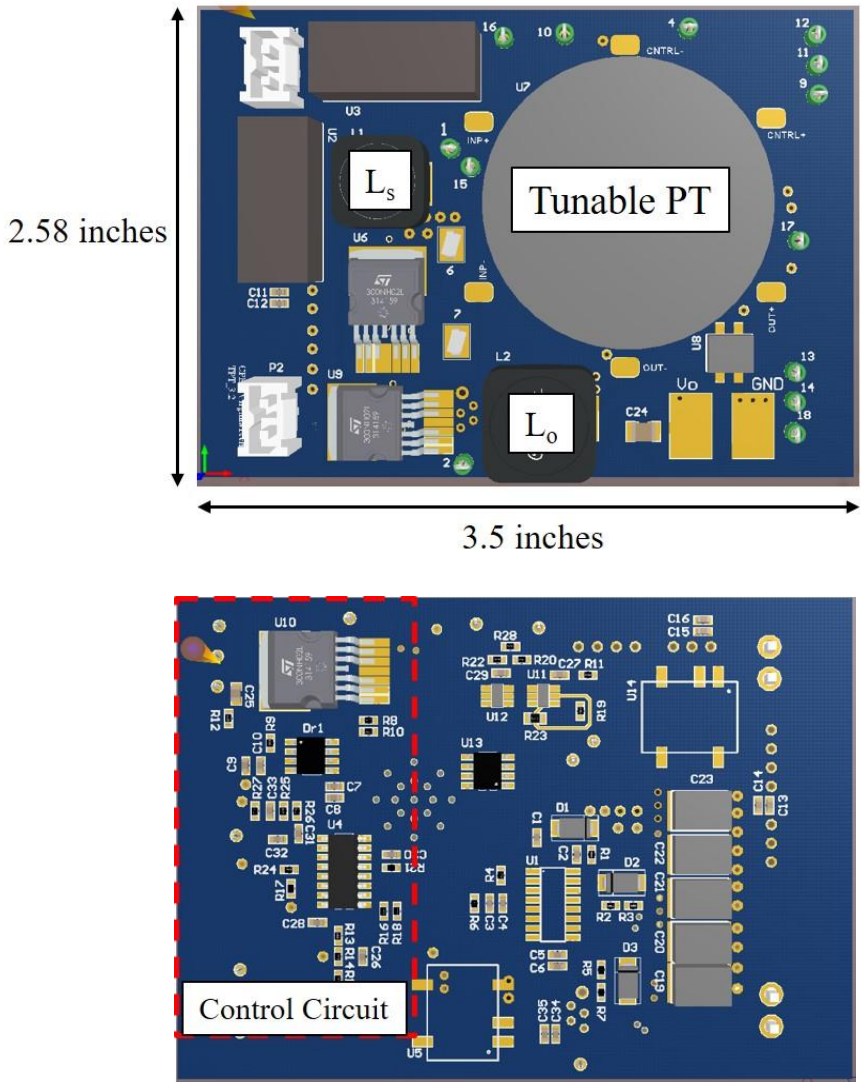

Fig. 5.9. PCB layout for DC-DC converters using Gen 2 and Gen 3 TPT. A common layout for both TPT based converters was used.

A fixed frequency oscillator with a constant dead time is used to drive the H-bridge inverter switches. The control circuit consists of a MoSFET along with a fixed 100nF external capacitor. LM3524D PWM controller from Texas Instruments is used to implement the closed loop voltage mode control. Fig. 5.10 shows the board after assembling all the components and the tunable PT.

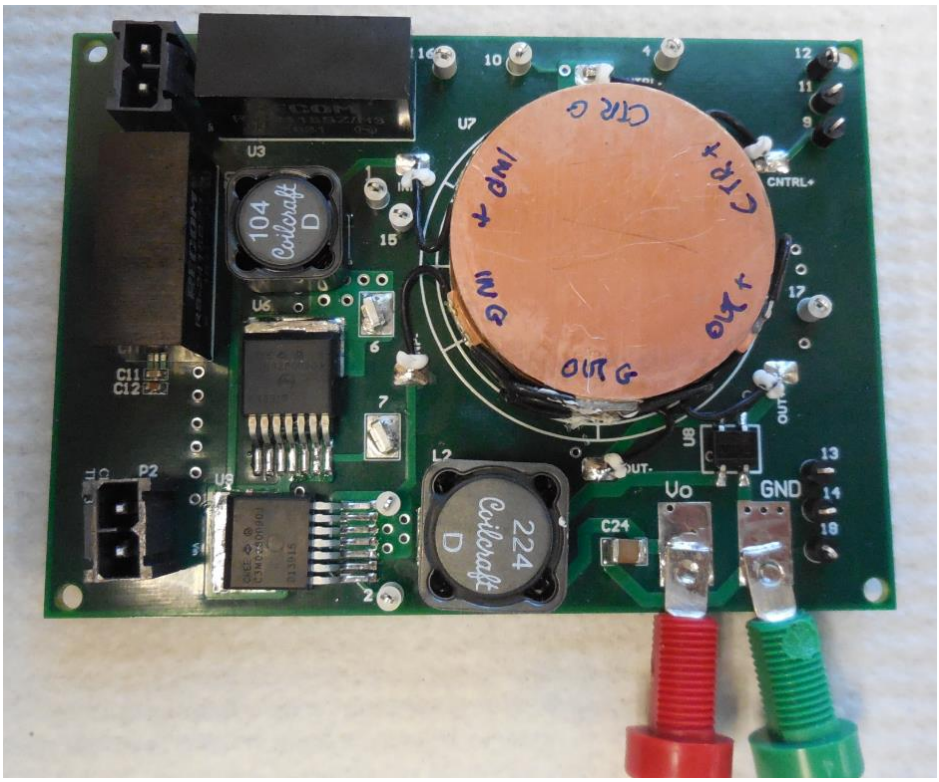

Fig. 5.10. Picture of the Gen 3 TPT based DC-DC converter.

5.7 Experimental results

Fig. 5.11 shows the experimental waveforms obtained from the Gen2 tunable PT based converter. The duty cycle of the control switch (D_{Mc}) is shown in green and it is evident that as the load decreases the duty cycle increases to regulate the output voltage. The maximum value of effective control capacitance will occur at 50% duty cycle and for Gen 2 TPT, this occurs at 47% of the nominal load condition. Thus, the tunability of the TPT is verified to be 53% which is close to the value calculated.

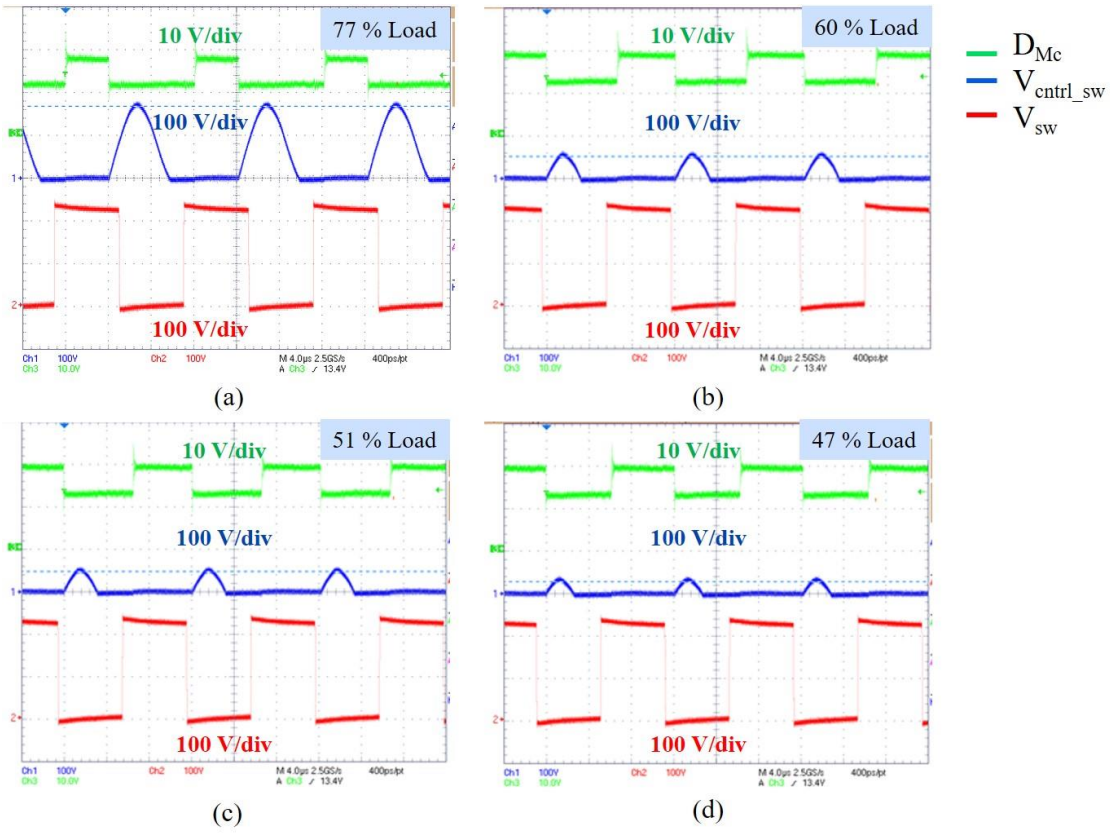

Fig. 5.11. Experimental results obtained from the Gen 2 TPT based DC-DC converter. The fixed frequency operation and the variation of control duty cycle with load can be seen from the figure.

The complete variation of duty cycle with a change in load and the efficiency of the converter at each operating point, as obtained from the experimental results is plotted in Fig. 5.12.

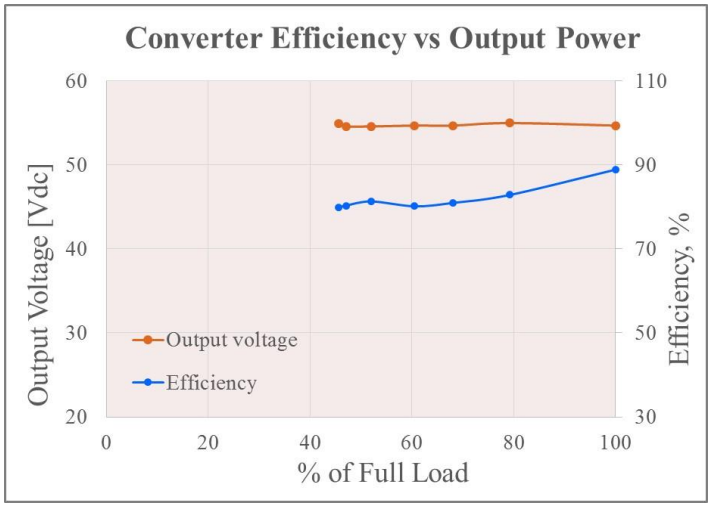

Fig. 5.12. Variation of output voltage and efficiency vs load for Gen 2 TPT as obtained from the experiments.

The experimental results obtained for Gen 3 TPT are shown in Fig. 5.13. The control switch duty cycle (D_{Mc}) is shown in dark blue and the voltage across the switch in light blue. The results are in good agreement with the predicted waveforms. For Gen 3 TPT, as predicted, the range of load regulation is much higher. Load regulation results for up to 10 % load condition are shown in Fig. 5.13. The complete results of the duty cycle vs. load and the efficiency at the corresponding points are shown in Fig. 5.14. The poor efficiency for Gen 3 TPT is partly due to the large current flowing through the diode bridge. Efficiency can be improved with a MoSFET rectification at the output.

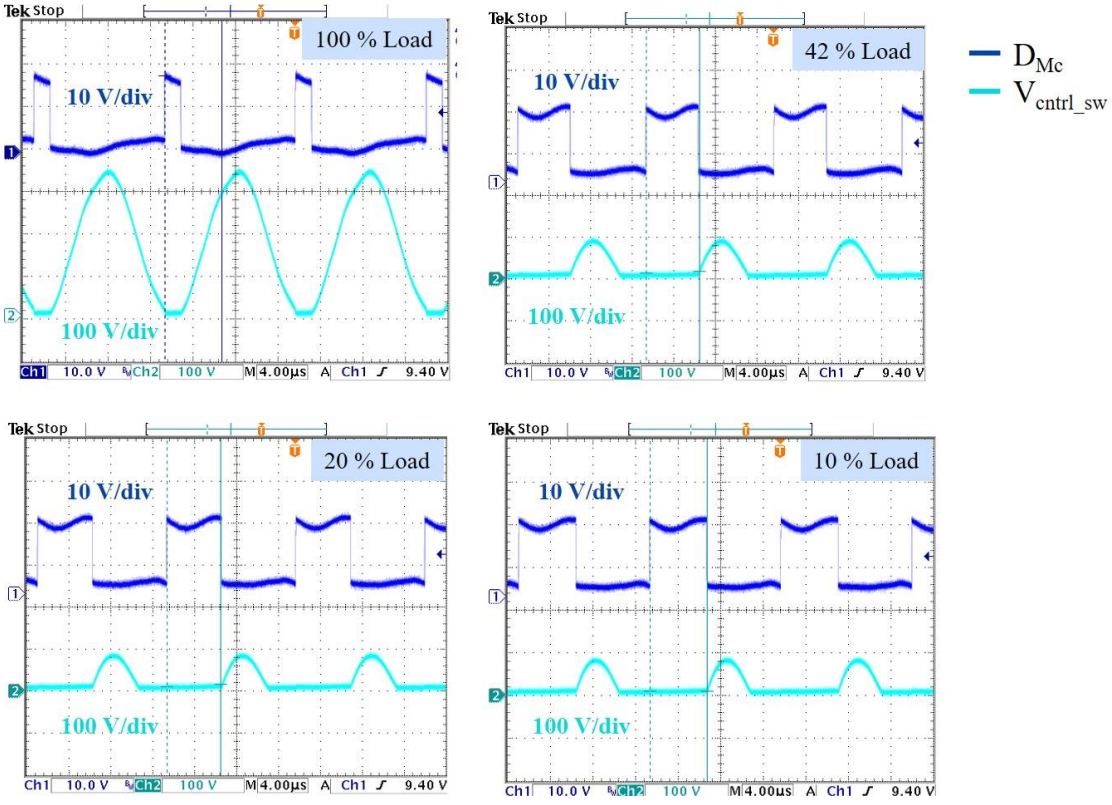

Fig. 5.13. Experimental results obtained from the Gen 3 TPT based DC-DC converter. The fixed frequency operation and the variation of control duty cycle with load can be seen from the figure.

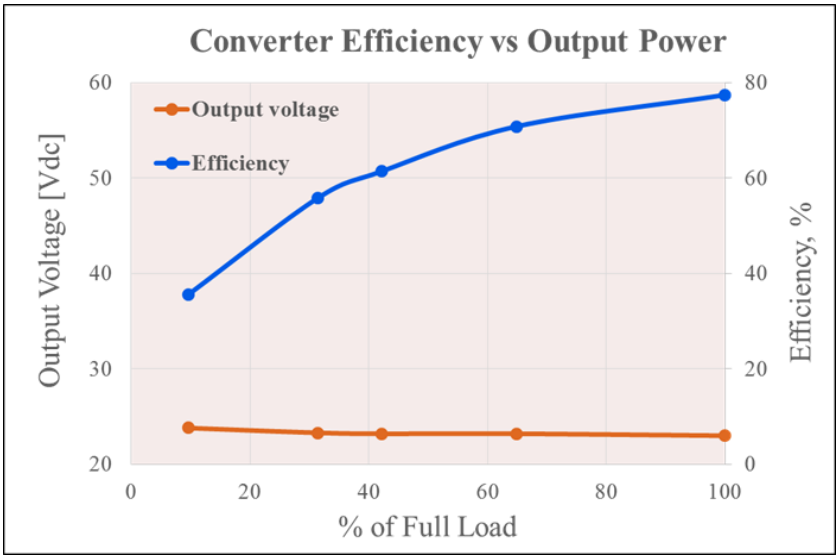

Fig. 5.14. Variation of output voltage and efficiency vs load for Gen 3 TPT as obtained from the experiments.

Chapter 6

Conclusion and Future Work

6.1 Conclusion

Piezoelectric transformers can be a potential replacement for magnetic transformers in certain applications. The use of PTs in resonant circuit topologies for DC-DC converters has been demonstrated extensively in the academic field. With challenges such as high power density and high efficiency and efficient driving circuits, more research is needed on the PTs to make a compelling case for commercial applications.

This thesis introduces a new structure of piezoelectric transformers, namely, tunable piezoelectric transformers. The proposed structure follows a radial mode PT design and has an additional section, called 'control', which makes the tunable piezoelectric transformers a three-terminal device. The thesis has successfully demonstrated the use of this control terminal to 'tune' the resonant frequency of the PT itself.

A change in the loading conditions at the control terminal causes a change in the resonant frequency of the tunable piezoelectric transformer. This thesis proposed to use a variable capacitor at the control terminal causing the series capacitance of the LCC tank circuit to change. By having a fine control over a large range of control capacitance the output voltage can be regulated for load and line variations.

The thesis gives a detailed circuit analysis of the proposed control method. The voltage gain characteristics of the TPT with a variable capacitor obtained were similar to a LLC tank circuit. This enabled a constant frequency of operation of the TPT based converter. Mathematical analysis on the electrical equivalent circuit of the TPT has been done to prove that such voltage characteristics can be achieved using appropriate design methods.

The concept of 'Tunability' for a tunable piezoelectric transformer has been quantitatively defined. The circuit design parameters which effect the tunability have

been discussed in detail and the condition for achieving a tunability target for a specific TPT design has been derived. This gives a TPT designer a clear design guideline to achieve the required performance specification from the TPT.

Based on the electrical circuit analysis of a TPT, a design methodology for a TPT based converter has been discussed. The effect of input inductor on TPT based converter design has and the criteria to enable ZVS on the inverter switches for the entire range of load variations has been discussed. This thesis also successfully implemented a variable capacitor which is based on a switched capacitor concept. With the proposed scheme the effective value of a fixed external control capacitor can be easily controlled by simple duty cycle control. This enables the designer to implement a closed loop control of the TPT by using PWM modulation technique. The key advantages of this scheme are listed below

- Since the control is entirely on the secondary side, there is no cross-talk between the primary and secondary in the feedback loop. Hence, there is no requirement for any isolation in the feedback loop.
- The TPT is operated a fixed switching frequency. This allows for the TPT be operated near its optimum switching frequency and high efficiency of TPTs can be achieved throughout the operating range of the converter.
- The control scheme is simple and can be implemented by PWM control. This can potentially eliminate the need for expensive control ICs required for frequency control.

In the end, two different TPT designs and a comparison of their circuit performance have been presented. This gives the reader a good understanding of the physical design of the TPT and its impact on circuit performance. The experimental results and findings from each design have been presented to validate the claims.

6.2 Recommended Future Work

Based on the learnings from this thesis, the following are some of the recommendations for future work in tunable piezoelectric transformers.

Inductor-less design for tunable piezoelectric transformers

The series input inductor in the proposed TPT based converter designs has been used to mainly to enable ZVS in the inverter switches. With a design optimization of TPT, the internal ZVS capabilities of the TPT can be utilized to eliminate the series input indictor. Such a design has not be proposed for TPTs yet and hence more work would need to be done enable ZVS for the entire range of load and line variation.

Integration of AC/DC rectifier stage with PFC correction

Addition of AC/DC rectifier stage would enable a TPT based AC/DC converter which can be used for adapter applications. Radial mode PTs have been proposed in the past to be used in universal AC/DC adapter applications. With higher power (100W) capabilities, new TPT based AC/DC adapters can be a promising research topic. Power factor correction methods have been proposed for the electronic lamp ballast applications using radial mode PTs in the past. Research in this direction for tunable PTs can also be explored to enable an AC/DC adapter with PFC correction.

Improvised control strategy

The control scheme proposed in this work is easy to implement for load regulation. Even though line regulation can also be tackled using the same scheme, it might not be the most optimal way. In addition, a design of TPT which can handle large input voltage range along with large load variation might not be practically feasible. Hence, further work on this direction is required to explore other control options or propose intelligent modifications to the existing control to handle a large range of input and output load variations.

Modeling and design of TPT for a specific application

The concept of tunability and the conditions required to achieve the desired tunability from a TPT were introduced in this thesis. The approach in this thesis was to derive these conditions using the electrical equivalent circuit of the TPT. Using this thesis as the groundwork, research can be done in the direction of modeling and design of tunable piezoelectric transformers for a specific application. Various modeling techniques have been proposed in the past to design standard PTs for a specific application such as physics based modeling, finite element analysis based approach, etc. With the help of such techniques and the results obtained from this research, application specific design of TPTs can be done.

References

[1] C. Rosen, "Electromechanical transducer," Patent US Patent 2,830,274., 1958.

[2] A. V. Carazo, "50 years of piezoelectric transformers. Trends in the technology," in *MRS Proceedings*, 2003, vol. 785, p. D1. 7: Cambridge Univ Press.

[3] A. V. Carazo, "Piezoelectric converters for DC/DC and AC/DC applications," in *Portable Power Developers Conference*, San Jose, CA, USA, 18–20 April 2005.

[4] T. Andersen, "Piezoelectric Transformer Based Power Supply for Dielectric Electro Active Polymers," Ph.D. Thesis, Department of Electrical Engineering, Technical University of Denmark, Lyngby, Denmark, 2012.

[5] M. Day and B. S. Lee, "Understanding piezoelectric transformers in CCFL backlight applications."

[6] E. L. Horsley, M. P. Foster, and D. A. Stone, "State-of-the-art Piezoelectric Transformer technology," in *2007 European Conference on Power Electronics and Applications*, 2007, pp. 1-10.

[7] R.-L. Lin, "Piezoelectric transformer characterization and application of electronic ballast," PhD Dissertation, Electrical Engineering, Virginia polytechnic institute and state University, Blacksburg, 2001.

[8] E. L. Horsley, A. V. Carazo, N. Nguyen-Quang, M. P. Foster, and D. A. Stone, "Analysis of Inductorless Zero-Voltage-Switching Piezoelectric Transformer-Based Converters," *IEEE Transactions on Power Electronics*, vol. 27, no. 5, pp. 2471-2483, 2012.

[9] S. Bronstein, "Piezoelectric transformers in power electronics," Ph.D, Ben-Gurion University of the Negev, 2005.

[10] K. S. Meyer, M. A. E. Andersen, and F. Jensen, "Parameterized analysis of Zero Voltage Switching in resonant converters for optimal electrode layout of Piezoelectric Transformers," in *2008 IEEE Power Electronics Specialists Conference*, 2008, pp. 2543-2548.

[11] M. P. Foster, J. N. Davidson, E. L. Horsley, and D. A. Stone, "Critical Design Criterion for Achieving Zero Voltage Switching in Inductorless Half-Bridge-Driven Piezoelectric-Transformer-Based Power Supplies," *IEEE Transactions on Power Electronics*, vol. 31, no. 7, pp. 5057-5066, 2016.

[12] R. P. Bishop, "Multi-layer piezoelectric transformer " US Patent US5834882 A, 1998.

[13] A. V. Carazo, "Multilayer piezoelectric transformer," USA Patent US6614144 B2, Sept. 2, 2003.

[14] W. Huang, "Design of a radial mode piezoelectric transformer for a charge pump electronic ballast with high power factor and zero voltage switching," M.S Thesis, Electrical Engineering, Virginia Polytechnic Institute and State University, Blacksburg, 2003.

[15] E. M. Baker, W. Huang, D. Y. Chen, and F. C. Lee, "Radial mode piezoelectric transformer design for fluorescent lamp ballast applications," in *2002 IEEE 33rd Annual IEEE Power Electronics Specialists Conference. Proceedings (Cat. No.02CH37289)*, 2002, vol. 3, pp. 1289-1294 vol.3.

[16] T. Zaitsu, Y. Fuda, Y. Okabe, T. Ninomiya, S. Hamamura, and M. Katsuno, "New piezoelectric transformer converter for AC-adapter," in *Proceedings of APEC 97 - Applied Power Electronics Conference*, 1997, vol. 2, pp. 568-572 vol.2.

[17] J. Navas, T. Bove, J. A. Cobos, F. Nuno, and K. Brebol, "Miniaturised battery charger using piezoelectric transformers," in *APEC 2001. Sixteenth Annual IEEE Applied Power Electronics Conference and Exposition (Cat. No.01CH37181)*, 2001, vol. 1, pp. 492-496 vol.1.

[18] S. Nittayarumphong, F. Bisogno, M. Radecker, A. V. Carazo, A. Riedlhammer, and H. Guldner, "High efficiency control methods for class-E resonant converter for step-down applications using Piezoelectric Transformers (PT)," in *2007 European Conference on Power Electronics and Applications*, 2007, pp. 1-10.

[19] T. Zaitsu, T. Shigehisa, T. Inoue, M. Shoyama, and T. Ninomiya, "Piezoelectric transformer converter with frequency control," in *Proceedings of INTELEC 95. 17th International Telecommunications Energy Conference*, 1995, pp. 175-180.

[20] R. Myounghwan, C. Sungjin, L. Sangmin, and B. H. Cho, "A new piezoelectric transformer driving topology for universal input AC/DC adapter using a constant frequency PWM control," in *Twenty-First Annual IEEE Applied Power Electronics Conference and Exposition, 2006. APEC '06.*, 2006, p. 4 pp.

[21] M. S. Rødgaard, M. A. E. Andersen, and E. Bruun, "Piezoelectric transformer based power converters; design and control," PhD Thesis, Electrical Engineering, Technical University of Denmark,, 2012.

[22] C. Lin, "Design and analysis of piezoelectric transformer converters," Ph.D. Dissertation, Electrical Engineering, Virginia Polytechnic Institute and State University, Blacksburg, VA, 1997.

[23] W. P. Mason, *Electromagnetic Transducers and Wave filters*, 2nd ed. NY: D. Van Nostrand Company Inc., 1948, pp. 399-404.

[24] H. W. Katz, *Solid State Magnetic and Dielectric Devices*. NY: Wiely, 1959, pp. 94-126.

[25] E. L. Horsley, A. V. Carazo, M. P. Foster, and D. A. Stone, "A Lumped Equivalent Circuit Model for the Radial Mode Piezoelectric Transformer," in *2009 Twenty-Fourth Annual IEEE Applied Power Electronics Conference and Exposition*, 2009, pp. 1747-1753.

[26] S. Bronshtein, A. Abramovitz, A. Bronshtein, and I. Katz, "A Method for Parameter Extraction of Piezoelectric Transformers," *IEEE Transactions on Power Electronics*, vol. 26, no. 11, pp. 3395-3401, 2011.

[27] T. Tsuchiya, Y. Kagawa, N. Wakatsuki, and H. Okamura, "Finite element simulation of piezoelectric transformers," *IEEE Transactions on Ultrasonics, Ferroelectrics, and Frequency Control*, vol. 48, no. 4, pp. 872-878, 2001.

[28] T. Ikeda, *Fundamentals of Piezoelectricity*. Oxford University Press, 1990.

[29] S. T. Ho, "Design of the Longitudinal Mode Piezoelectric Transformer," in *2007 7th International Conference on Power Electronics and Drive Systems*, 2007, pp. 1639-1644.

[30] S. Kawashima *et al.*, "Third order longitudinal mode piezoelectric ceramic transformer and its application to high-voltage power inverter," in *1994 Proceedings of IEEE Ultrasonics Symposium*, 1994, vol. 1, pp. 525-530 vol.1.

[31] J. M. Alonso, C. Ordiz, M. A. D. Costa, J. Ribas, and J. Cardesin, "High-Voltage Power Supply for Ozone Generation Based on Piezoelectric Transformer," *IEEE Transactions on Industry Applications,* vol. 45, no. 4, pp. 1513-1523, 2009.

[32] C. S. Moo, W. M. Chen, and H. K. Hsieh, "Electronic ballast with piezoelectric transformer for cold cathode fluorescent lamps," *IEE Proceedings - Electric Power Applications,* vol. 150, no. 3, pp. 278-282, 2003.

[33] E. Wells, "Comparing magnetic and piezoelectric transformer approaches in CCFL applications," *Analog Applications Journal,* no. Q1, 2002.

[34] W. Huang, D. Chen, E. M. Baker, J. Zhou, H. I. Hsieh, and F. C. Lee, "Design of a Power Piezoelectric Transformer for a PFC Electronic Ballast," *IEEE Transactions on Industrial Electronics,* vol. 54, no. 6, pp. 3197-3204, 2007.

[35] C. Sungjin, K. Taeil, L. Sangmin, and B. H. Cho, "Modeling and Characterization of Radial-mode Disk-type Piezoelectric Transformer for AC/DC Adapter," in *2005 IEEE 36th Power Electronics Specialists Conference*, 2005, pp. 624-629.

[36] A. V Carazo, "Piezoelectric Transformers: An Historical Review," in *Actuators*, 2016, vol. 5, no. 2, p. 12: Multidisciplinary Digital Publishing Institute.

[37] T. Zaitsu, T. Inoue, O. Ohnishi, and A. Iwamoto, "2 MHz power converter with piezoelectric ceramic transformer," in *Telecommunications Energy Conference, 1992. INTELEC '92., 14th International*, 1992, pp. 430-437.

[38] O. Ohnishi, H. Kishie, A. Iwamoto, Y. Sasaki, T. Zaitsu, and T. Inoue, "Piezoelectric ceramic transformer operating in thickness extensional vibration mode for power supply," in *IEEE 1992 Ultrasonics Symposium Proceedings*, 1992, pp. 483-488 vol.1.

[39] T. Bove, W. Wolny, E. Ringgaard, and K. Breboel, "New type of piezoelectric transformer with very high power density," in *ISAF 2000. Proceedings of the 2000 12th IEEE International Symposium on Applications of Ferroelectrics (IEEE Cat. No.00CH37076)*, 2000, vol. 1, pp. 321-324 vol. 1.

[40] D. Jinlong, H. Junhui, and T. King-Jet, "High-power, multioutput piezoelectric transformers operating at the thickness-shear vibration mode," *IEEE Transactions on Ultrasonics, Ferroelectrics, and Frequency Control,* vol. 51, no. 5, pp. 502-509, 2004.

[41] A. V. Mezheritsky, "Elastic, dielectric, and piezoelectric losses in piezoceramics: how it works all together," *IEEE Transactions on Ultrasonics, Ferroelectrics, and Frequency Control,* vol. 51, no. 6, pp. 695-707, 2004.

[42] T.-G. Zsurzsan, Andersen, M. A. E., Zhang, Z., & Andersen, N. A., "Advances in Piezoelectric Systems: An Application-Based Approach," PhD Department of Electrical Engineering, Technical University of Denmark, Denmark, 2016.

[43] C. Y. Lin and F. C. Lee, "Design of a piezoelectric transformer converter and its matching networks," in *Power Electronics Specialists Conference, PESC '94 Record., 25th Annual IEEE*, 1994, pp. 607-612 vol.1.

[44] G. Ivensky, I. Zafrany, and S. Ben-Yaakov, "Generic operational characteristics of piezoelectric transformers," *IEEE Transactions on Power Electronics,* vol. 17, no. 6, pp. 1049-1057, 2002.

[45] T. Zaitsu, T. Shigehisa, M. Shoyama, and T. Ninomiya, "Piezoelectric transformer converter with PWM control," in *Applied Power Electronics*

Conference and Exposition, 1996. APEC '96. Conference Proceedings 1996., Eleventh Annual, 1996, vol. 1, pp. 279-283 vol.1.

[46] T. Yamane, S. Hamamura, T. Zaitsu, T. Minomiya, M. Shoyama, and Y. Fuda, "Efficiency improvement of piezoelectric-transformer DC-DC converter," in *PESC 98 Record. 29th Annual IEEE Power Electronics Specialists Conference (Cat. No.98CH36196)*, 1998, vol. 2, pp. 1255-1261 vol.2.

[47] M. J. Prieto, J. Diaz, J. A. Martin, and F. Nuno, "A very simple DC/DC converter using piezoelectric transformer," in *2001 IEEE 32nd Annual Power Electronics Specialists Conference (IEEE Cat. No.01CH37230)*, 2001, vol. 4, pp. 1755-1760 vol. 4.

[48] S. Ben-Yaakov and S. Lineykin, "Maximum power tracking of piezoelectric transformer HV converters under load variations," *IEEE Transactions on Power Electronics*, vol. 21, no. 1, pp. 73-78, 2006.

[49] S. Nakashima, T. Ninomiya, H. Ogasawara, and H. Kakehashi, "Piezoelectric-transformer inverter with maximum-efficiency tracking and dimming control," in *APEC. Seventeenth Annual IEEE Applied Power Electronics Conference and Exposition (Cat. No.02CH37335)*, 2002, vol. 2, pp. 918-923 vol.2.

[50] J. M. Alonso, C. Ordiz, and M. A. D. Costa, "A Novel Control Method for Piezoelectric-Transformer Based Power Supplies Assuring Zero-Voltage-Switching Operation," *IEEE Transactions on Industrial Electronics*, vol. 55, no. 3, pp. 1085-1089, 2008.

[51] S. Hamamura, D. Kurose, T. Ninomiya, and M. Yamamoto, "New control method of piezoelectric transformer converter by PWM and PFM for wide range of input voltage," in *7th IEEE International Power Electronics Congress. Technical Proceedings. CIEP 2000 (Cat. No.00TH8529)*, 2000, pp. 3-8.

[52] J. A. Martin-Ramos, M. A. J. Prieto, F. N. Garcia, J. D. Gonzalez, and F. M. F. Linera, "A new full-protected control mode to drive piezoelectric transformers in DC-DC converters," *IEEE Transactions on Power Electronics*, vol. 17, no. 6, pp. 1096-1103, 2002.

[53] J. Diaz, J. A. Martin-Ramos, M. J. Prieto, and F. Nuno, "A double-closed loop DC/DC converter based on a piezoelectric transformer," in *Applied Power Electronics Conference and Exposition, 2004. APEC '04. Nineteenth Annual IEEE*, 2004, vol. 3, pp. 1423-1428 Vol.3.

[54] M. Khanna, R. Burgos, Q. Wang, K. Ngo, and A. V. Carazo, "New Tunable Piezoelectric Transformers and Their Application in DC-DC Converters," *IEEE Transactions on Power Electronics*, vol. PP, no. 99, pp. 1-1, 2017.

[55] R. L. Steigerwald, "A comparison of half-bridge resonant converter topologies," in *1987 2nd IEEE Applied Power Electronics Conference and Exposition*, 1987, pp. 135-144.

[56] M. Shoyama, K. Horikoshi, T. Ninomiya, T. Zaitsu, and Y. Sasaki, "Operation analysis of the push-pull piezoelectric inverter," in *Proceedings of APEC 97 - Applied Power Electronics Conference*, 1997, vol. 2, pp. 573-578 vol.2.

[57] T. Ninomiya, M. Shoyama, T. Zaitsu, and T. Inoue, "Zero-voltage-switching techniques and their application to high-frequency converter with piezoelectric transformer," in *Industrial Electronics, Control and Instrumentation, 1994. IECON '94., 20th International Conference on*, 1994, vol. 3, pp. 1665-1669 vol.3.

[58] R. L. Lin and H. M. Shih, "Piezoelectric Transformer Based Current-Source Charge-Pump Power-Factor-Correction Electronic Ballast," *IEEE Transactions on Power Electronics*, vol. 23, no. 3, pp. 1391-1400, 2008.

[59] J. Diaz, F. Nuno, J. M. Lopera, and J. A. Martin-Ramos, "A new control strategy for an AC/DC converter based on a piezoelectric transformer," *IEEE Transactions on Industrial Electronics*, vol. 51, no. 4, pp. 850-856, 2004.

[60] M. Sanz, P. Alou, R. Prieto, J. A. Cobos, and J. Uceda, "Comparison of different alternatives to drive piezoelectric transformers," in *APEC. Seventeenth Annual IEEE Applied Power Electronics Conference and Exposition (Cat. No.02CH37335)*, 2002, vol. 1, pp. 358-364 vol.1.

[61] S. Hamamura, T. Zaitsu, T. Ninomiya, and M. Shoyama, "Noise characteristics of piezoelectric-transformer DC-DC converter," in *PESC 98 Record. 29th Annual IEEE Power Electronics Specialists Conference (Cat. No.98CH36196)*, 1998, vol. 2, pp. 1262-1267 vol.2.

[62] A. M. Flynn and S. R. Sanders, "Fundamental limits on energy transfer and circuit considerations for piezoelectric transformers," *IEEE Transactions on Power Electronics*, vol. 17, no. 1, pp. 8-14, 2002.

[63] F. E. Bisogno *et al.*, "Comparison of resonant topologies for step-down applications using piezoelectric transformers," in *2004 IEEE 35th Annual Power Electronics Specialists Conference (IEEE Cat. No.04CH37551)*, 2004, vol. 4, pp. 2662-2667 Vol.4.

[64] G. Ivensky, S. Bronstein, and S. Ben-Yaakov, "Analysis and design of a piezoelectric transformer AC/DC converter in a low voltage application," in *2002 IEEE 33rd Annual IEEE Power Electronics Specialists Conference. Proceedings (Cat. No.02CH37289)*, 2002, vol. 2, pp. 409-414 vol.2.

[65] G. Ivensky, S. Bronstein, and S. Ben-Yaakov, "A comparison of piezoelectric transformer AC/DC converters with current doubler and voltage doubler rectifiers," *IEEE Transactions on Power Electronics*, vol. 19, no. 6, pp. 1446-1453, 2004.

[66] S. K. Chung, B. G. Kang, and M. S. Kim, "Constant frequency control of LLC resonant converter using switched capacitor," *Electronics Letters*, vol. 49, no. 24, pp. 1556-1558, 2013.

[67] Y. Hu, A. Amara, and A. Ioinovici, "LLC resonant converter operated at constant switching frequency and controlled by means of a switched-capacitor circuit," in *2013 1st International Future Energy Electronics Conference (IFEEC)*, 2013, pp. 691-696.

[68] Z. Hu, Y. Qiu, L. Wang, and Y. F. Liu, "An Interleaved LLC Resonant Converter Operating at Constant Switching Frequency," *IEEE Transactions on Power Electronics*, vol. 29, no. 6, pp. 2931-2943, 2014.

[69] M. Ekhtiari, T. Andersen, M. A. E. Andersen, and Z. Zhang, "Dynamic Optimum Dead Time in Piezoelectric Transformer-Based Switch-Mode Power Supplies," *IEEE Transactions on Power Electronics*, vol. 32, no. 1, pp. 783-793, 2017.

Appendix A

List of Softwares

TABLE A.1. LIST OF SOFTWARES USED IN THIS THESIS FOR ANALYSIS AND DESIGN.

Software	Analysis	Figure/Equation number	Location of files
SIMPLIS	Electrical circuit simulation of the TPT Steady state transient analysis of the converter Small signal AC analysis of the DC-DC converter	Fig. 2.12, Fig. 3.6, Fig. 3.8, Fig. 3.10, Fig. 3.11, Fig. 3.12, Fig. 3.13, Fig. 3.15, Fig. 3.16, Fig. 4.2, Fig. 5.4, Fig. 5.5, Fig. 5.6	\\adfs\temporary storage\Mudit\DARPA\Simplis_files
MATLAB	Mathematical modeling of the electrical equivalent circuit of the TPT Tunability calculations	Fig. 2.9, Fig. 3.7, Fig. 3.14, Fig. 4.3, Fig. 4.9, Fig. 4.11	\\adfs\temporary storage\Mudit\DARPA\ MATLAB_files
Altium	PCB design and schematic development	N/A	\\adfs\temporary storage\Mudit\DARPA\Alitum_files

Appendix B

Schematic and Bill of Materials

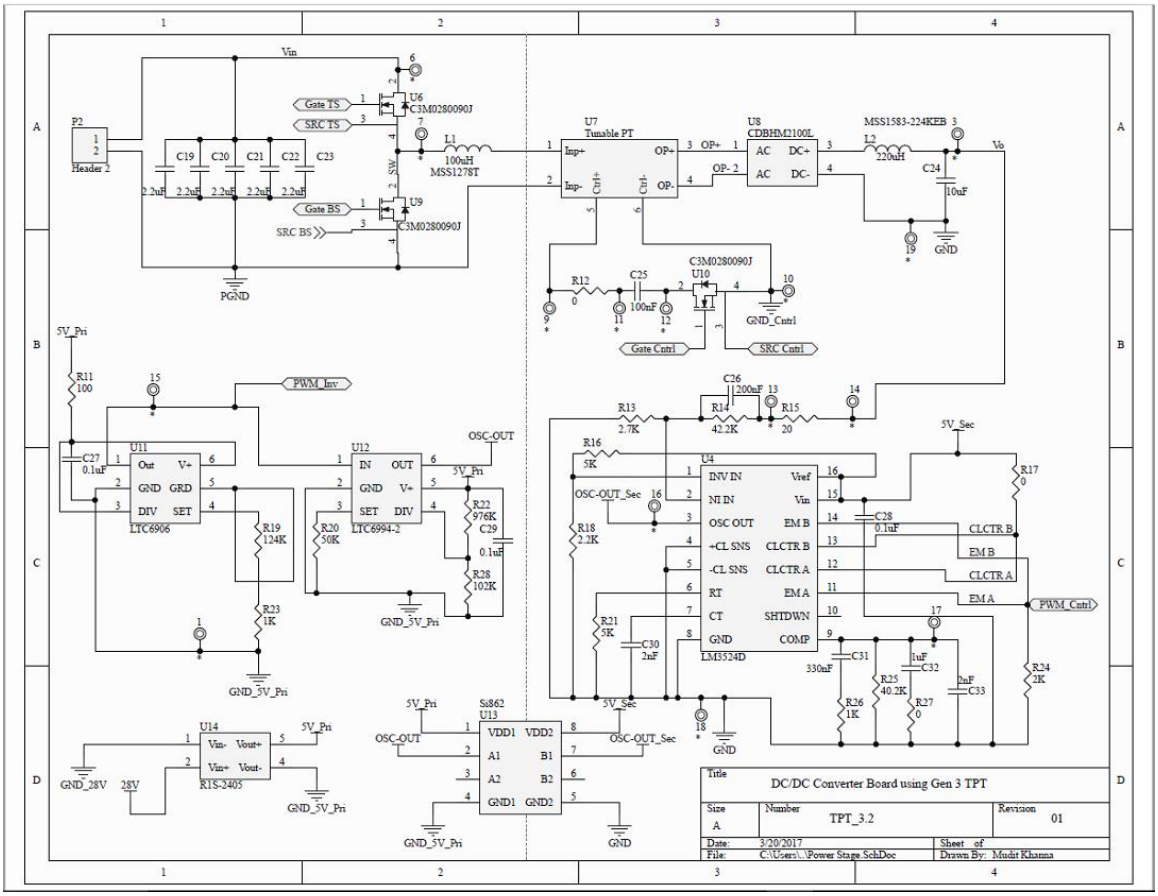

Fig. B.1. Page 1 of the schematic diagram of the DC-DC converter using tunable PT for PCB design developed using Altium.

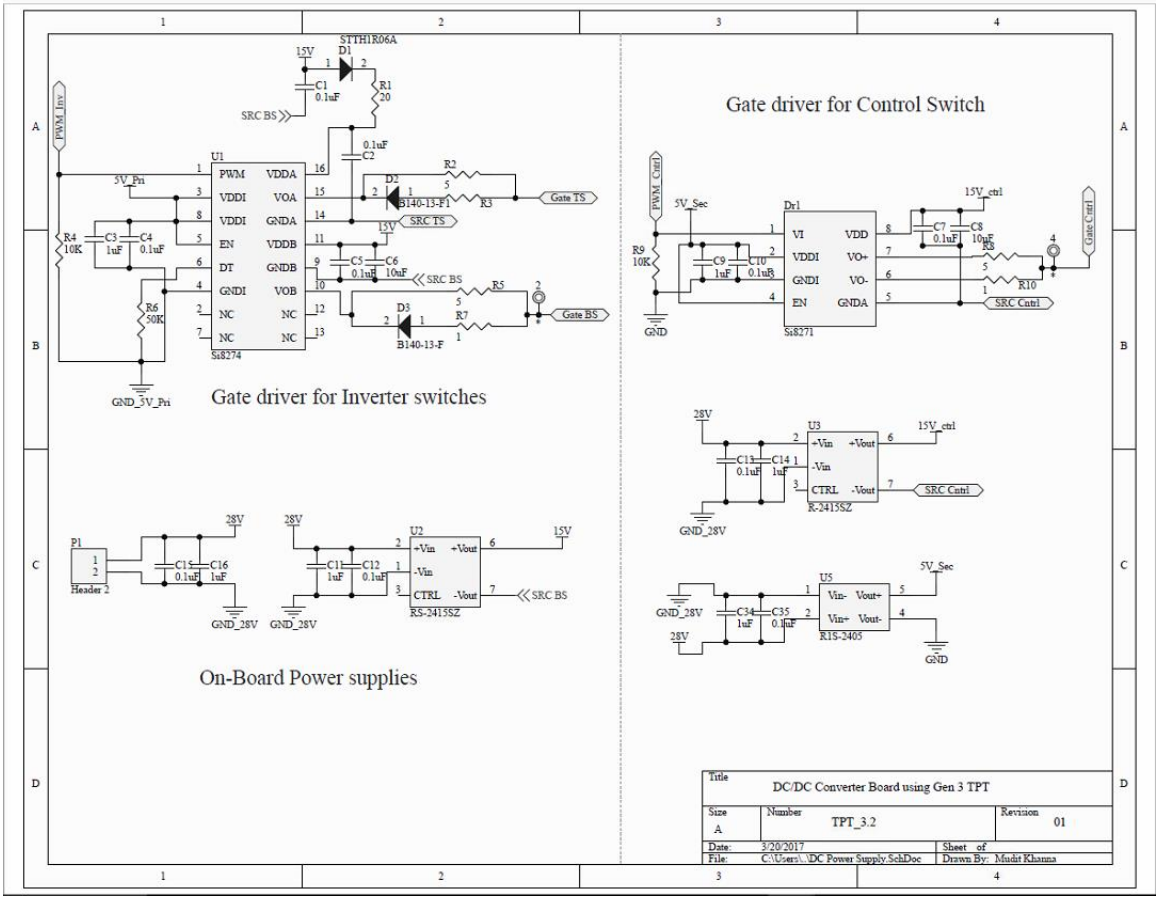

Fig. B.2. Page 2 of schematic diagram of the DC-DC converter using tunable PT for PCB design developed using Altium.

TABLE B.1. BILL OF MATERIALS FOR THE GEN 3 TPT BASED TPT CONVERTER PCB.

Part Number	Description	Designator	Qty.
Any	CAP CER 0.1UF 50V X7R 0603	C1, C2, C4, C5, C7, C10, C12, C13, C15 C27, C29, C28, C35	13
Any	CAP CER 1UF 35V X7R 0603	C3, C9, C11, C14, C16, C34	7
Any	CAP CER 10UF 35V X7R 0603	C6, C8	2
445-7749-1-ND	CAP CER 0.1UF 250V X7T 0805	C25	1
445-7108-1-ND	3.3µF 250V Ceramic Capacitor X7T	C19, C20, C21,	5

	Stacked SMD	C22, C23	
STTH1R06A	DIODE GEN PURP 600V 1A SMA	D1	1
B140-13-F	Schottky diode, 40V, 1A, Surface Mount	D2, D3	2
Si8271AB-IS	Gate Drivers 4A ISO DRIVER, 2.5kV	Dr1	1
MSS1278T	Input Inductor, 100 uH, 1 A	L1	1
MSS1583224KEB	Output Inductor, 220 uH, 2 A	L2	1
IPBT-102 H1TSGP	Header, 2-Pin	P1, P2	2
Si8274AB4DIS1	Isolated gate driver HS/LS	U1	1
RS-2415SZ/H3	Isolated Pwr Supply, Single OP, 2W	U2	1
RS2415SZ/H3	Isolated Pwr Supply, Single OP, 2W	U3	1
LM3524D	PWM Controller	U4	1
R1S-2405/HP	DC-DC Conv, Isolated, 24-5V, 1W	U5, U14	2
C3M0280090J	SiC Power MOSFET, 900V, 7A	U6, U9, U10	3
Gen 3 TPT	Tunable PT 30W	U7	1
CDBHM2100L	Schottky Bridge Rectifier	U8	1
LTC6906	Oscillator, 10kHz to 1Mhz Resistor set	U11	1
LTC6994-2	Delay Block	U12	1
Si8620BC-B-IS	Isolation Buffer IC	U13	1